Liquid Transport Pipeline Monitoring Architecture Based on State Estimators for Leak Detection and Location

Javier Augusto Jiménez Cabas

Supervisors: Ph.D. Marco Sanjúan
Ph.D. Lizeth Torres

Department of Mechanical Engineering
Universidad del Norte

This dissertation is submitted for the degree of
Doctor en Ingeniería Mecánica

Universidad del Norte March 2018

To my beloved Valle Pechocha...

Declaration

I hereby declare that except where specific reference is made to the work of others, the contents of this dissertation are original and have not been submitted in whole or in part for consideration for any other degree or qualification in this, or any other university. This dissertation is my own work and contains nothing which is the outcome of work done in collaboration with others, except as specified in the text and Acknowledgements.

Javier Augusto Jiménez Cabas
March 2018

Acknowledgements

Firstly, I would like to express my sincere gratitude to my advisors Dr. Marco Sanjúan and Dr. Lizeth Torres for the continuous support of my Ph.D study and related research, for their patience, motivation, and immense knowledge. Their guidance helped me in all the time of research and writing of this thesis. I could not have imagined having a better advisors and mentors for my Ph.D study.

Besides my advisors, I would like to thank the rest of my thesis committee: Dr. Gildas Besançon, Dr. Carlos Smith, Dr. Antonio Bula and Dr. Lesme Corredor, for their insightful comments and encouragement, but also for the hard question which incented me to widen my research from various perspectives.

My sincere thanks also goes to Dr. Cristina Verde, who provided me an opportunity to join their team as intern, and who gave access to laboratories and research facilities of the Instituto de Ingeniería of the Universidad Autónoma de México. Without they precious support it would not be possible to conduct this research. Also I thank my special friends Michelle del Carmen, Diana María de la Concepción and Ángel in México.

I thank my fellow labmates in for the stimulating discussions and for all the fun we have had in the last five years. In particular, I am grateful to Elena for her support in the improvement of the friction model used in my work.

Last but not the least, I would like to thank my family: my parents and to my brothers and sister for supporting me spiritually throughout writing this thesis and in my life in general.

Abstract

This research presents the implementation of optimization algorithms to build auxiliary signals that can be injected as inputs into a pipeline in order to estimate —by using state observers— physical parameters such as the friction or the velocity of sound in the fluid. For the state estimator design, the parameters to be estimated are incorporated into the state vector of a Liénard-type model of a pipeline such that the observer is constructed from the augmented model. A prescribed observability degree of the augmented model is guaranteed by optimization algorithms by building an optimal input for the identification. The minimization of the input energy is used to define the optimality of the input, whereas the observability Gramian is used to verify the observability.

Besides optimization algorithms, a novel method, based on a Liénard-type model, to diagnose single and sequential leaks in pipelines is proposed. In this case, the Liénard-type model that describes the fluid behavior in a pipeline is given only in terms of the flow rate. This method was conceived to be applied in pipelines solely instrumented with flowmeters or in conjunction with pressure sensors that are temporarily out of service. The design approach starts with the discretization of the Liénard-type model spatial domain into a prescribed number of sections. Such discretization is performed to obtain a lumped model capable of providing a solution (an internal flow rate) for every section. From this lumped model, a set of algebraic equations (known as residuals) are deduced as the difference between the internal discrete flows and the nominal flow (the mean of the flow rate calculated prior to the leak). The residual closest to zero will indicate the section where a leak is occurring. The main contribution of our method is that it only requires flow measurements at the pipeline ends, which leads to cost reductions. Some simulation-based tests in PipelineStudio and, even more importantly, experimental tests illustrating the suitability of the proposed method are shown.

Finally, given the increasing importance of water use efficiency, the above mentioned pipeline leaks diagnosis method is extended to water distribution networks. Water distribution networks around the world are infested with leaks which cause significant losses and

a subsequent suboptimal performance, which in turn aggravates the worldwide imbalance between demand for treated water and available water resources. Some simulation-based tests in PipelineStudio that show the suitability of the proposed method are presented.

Table of contents

List of figures

List of tables

Chapter 1

Introduction

Transport of commodities through pipelines is one of the most used transport mechanisms worldwide, mainly because it allows to transport large volumes in relatively short periods of time. It is estimated that there are more that 3.500.000 [km] of pipelines in about 120 countries of the world [49]. Pipeline and Gas Journal's worldwide survey shows that 134.866 [km] of pipelines are planned and under construction worldwide. Of these, 61.782 [km] include projects in the engineering and design phase and 73.083 [km] in various stages of construction [165]. In South/Central America and Caribbean there are about 2930 [km] of pipeline under construction and 4601 [km] of new and planned pipelines.

Pipeline networks go through neighborhoods and cities, stretch across mountains, deserts, forests, and everywhere in between. They collect crude oil from many remote areas to deliver it to refineries where it is converted into products such as diesel oil, high-octane gasoline, kerosene, heating fuel oils, lubricating oils and liquefied petroleum gas (LPG). However, not only products that come from petroleum are transported through pipelines but also other commodities including water, slurry, sewage, hydrogen and beverages (see Table 1.1).

On the other hand, despite a good maintenance plan for fault prevention, leaks in pipelines are unfortunately very common events that must be early diagnosed to avoid irreparable losses. Leaks in pipelines are mainly caused by aging of the pipes (corrosion), faults in the installation (particularly at construction joints and valves), natural events (earthquakes, hurricanes and tsunamis), pipe segments with imperfections, low points where moisture collects, construction excavations, illegal tapping and terrorist sabotage. Only in the United States during period comprised between 1997 and 2016, 832 serious incidents took place in gas distribution networks, causing 310 fatalities and 1299 injured and causing the loss of millions of dollars in property damage [166].

Table 1.1 Commodities moved in pipelines, [129]

For	Commodities
Refiners	Gasoline, home heating oil, diesel, jet fuel, crude oil
Manufacturers	Natural gas, ethane, ethylene, propylene
Agriculture	Diesel fuel, propane, fertilizer
Transportation	Kerosene, gasoline, diesel fuel, natural gas, aviation gasoline, jet fuel

Table 1.1 shows a list of the most significant leaks in pipelines that have occurred throughout the world. Total losses are around 10000 tons of product (1 ton $\approx$ 1165 liters).

Table 1.2 Pipeline worldwide accidents

Spill	Location	Date	Tons	Reference
Belle Fourche	United States, North Dakota, Billings County	05/05/2016	571	[165]
Fox Creek	Canada, Alberta, Fox Creek	06/10/2016	240	[148]
Colonial	United States, Shelby County, Alabama	12/09/2016	1092	[144]
ConocoPhillips	Canada, Alberta, Grande Cache	09/06/2016	323	[109]
Black Sea	Russia, Tuapse	24/12/2014	unknown	[121]
Trans-Israel	Israel, Eilat	06/12/2014	4300	[11]
Mid-Valley	United States, Louisiana, Mooringsport	13/10/2014	546	[107]
North Dakota	United States, North Dakota, Hiland	21/03/2014	110	[55]
North Dakota	United States, North Dakota, Tioga	25/09/2013	2810	[55]

Thus, how to maintain the integrity of pipelines is an ongoing concern for operators around the world. Aerial surveillance (by helicopters, satellites and drones) are traditional pipeline security measures. There are also on-the-ground actions such as awareness campaigns to educate those alongside pipeline routes, installation of pipeline warning boards and markers and security personnel. Furthermore, although control rooms constantly monitor pipelines

through leak-detection systems, these detected only 19.5% of the 251 spills in the United States between 2010 and 2013 [123]. In fact, most alarms were raised by on-site employees and residents (Table 1.3). Therefore, since protection of pipeline networks is an ongoing concern,

Table 1.3 A review of how hazardous pipeline spill were detected, [123]

How	Number of spills (percentage)
By on-site workers	73 (29.1%)
Local residents	66 (26.3%)
Remote detection	49 (19.5%)
Air and ground patrols	28 (11.2%)
Emergency responders	16 (6.4%)
Others and out-of-service tests	19 (7.6%)

investigations directed to develop reliable early leak detection systems are completely relevant and even more, necessary.

1.1 Leak Detection Systems

Leak detection systems (LDS) are based on a number of different detection principles and cover a wide spectrum of technologies. Many countries formally regulate pipeline operation through official requirements to guaranty a safe operation, especially for pipelines transporting hazardous fluids. Table 1.4 shows some international regulatory standards on pipeline networks operation. These standars not only provide tools that assist pipeline operators in detecting

Table 1.4 International Regulations

Standard	Country	Requirements	Reference
API 1130	USA	Computational pipeline monitoring for liquids	[5]
API 1149	USA	Variable uncertainties in pipelines and their effects on leak detection	[140]
API 1155	USA	Performance criteria for leak detection systems (replaced by API 1130)	[4]
49 CFR 195	USA	Transport of hazardous liquids via pipeline	[43]
CSA Z662	Canada	Oil and gas pipelines	[149]
TRFL	Germany	Technical rule for pipelines	[46]

commodity leaks wich are within the sensitivity of the algorithms but also encourage pipeline

controllers to “go beyond", that is to strive for better utilization of LDS in hazardous products pipelines.

Leak detection systems can be categorized into two major types: internal leak detection systems and external leak detection systems. In external LDS the monitoring of external pipeline parameters is carried out by using field instrumentation (such as acoustic microphones, thermal cameras, fiber-optic cables, infrared radiometers or vapor sensors), while in internal LDS internal pipeline parameters are monitored by using typical pipeline instrumentation (such as pressure, flow or temperature sensors). Fig. 1.1 shows the leak detection approach classification. Notice that LDS can be also classified into two major categories: continuous and non-continuous methods. In practice continuous and non-continuous methods are often used in conjunction.

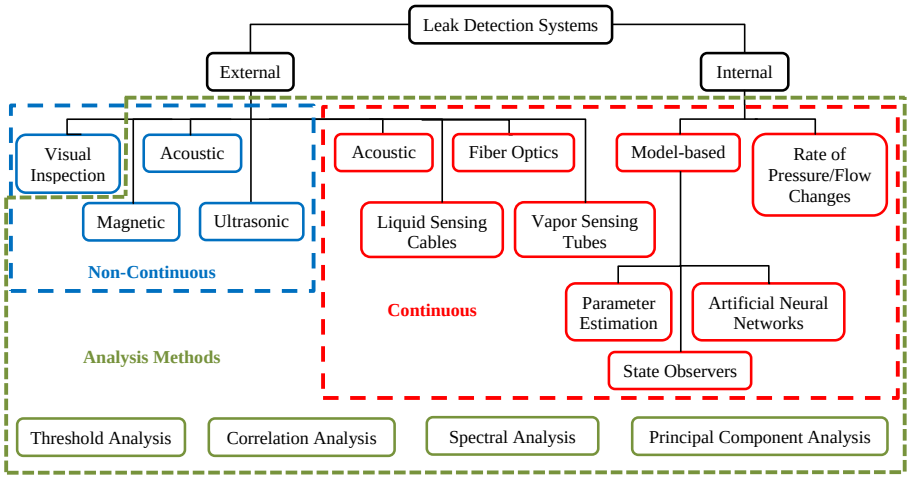

Fig. 1.1 Leak Detection Methods Categorization

1.1.1 External Methods

External methods seek to detect the presence of fluid outside of pipeline. They can in turn be divided into non-continuous and continuous methods. Non-continuous methods can be classified according to the physical principle involved in the leak detection. They include:

- **Visual Inspection Methods:** as part of a periodic pipeline right-of-way patrolling and monitoring program, simple visual inspection becomes a reliable alternative. Inspection can be carried out by walking, driving, flying or by other means. Pipeline surface

conditions on or adjacent to each pipeline must be inspected looking for evidence of leaks and conditions that could lead to a pipeline failure. Clearly, the capability of leak detection dependen on factors such as inspection frequency, inspectors' ability and leak size.

- **Acoustic Leak Detection:** when a leak occurs it produces an acoustic noise, thus, acoustic sensors can be used to track and detect internal noise level and create a baseline with specific characteristic [52, 53, 116]. If the characteristics of the low frequency acoustic signal produced by a leak differs from the baseline, an alarm will be activated. Leak localization is possible thanks to the fact that, near the leak, the received signal is stronger.

- **Magnetic and Ultrasonic Methods:** magnetic and ultrasonic methods are two of the most common leak detection techniques that use smart pigs. In the case of magnetic flux leak detection systems, the pipeline is magnetized through a strong permanent magnet. If a leak happens the magnetic flux lines will change, and these changes are recorded by sensing probes attached to the pig [153, 48]. On the other hand, when the leak detection is based on ultrasonic principles, a ultrasonic pulse is transmitted by the pig into the pipeline wall and it receives the reflected signals. Again, once a leak happens the reflected signals are affected and, based on the running speed of the pig, the leak can be located [169].

Otherwise, due to the cost associated with installing additional sensors along the pipeline, external continuous methods are better suited for shorter pipeline segments. Within this leak detection systems are included:

- **Liquid Sensing Cables:** conductive fluid sensing cable techniques rely on specialized cables buried adjacent to the pipeline. The cables can be electrochemical or fiber optics. Electrochemical cables are designed to reflect changes in their impedance when in contact with hydrocarbons [181, 135].

- **Fiber Optics Cables:** in the fiber optic cables cases, when a leak occurs the substance inside the pipeline gets in touch with fiber cable and this contact affects the temperature of the cable. The leak can be detected by measuring the changes in the temperature of the fiber cable [147, 87, 124, 71]. In many pipelines it has been installed distributed acoustic sensing systems, which are networks of fiber optic-linked sensors placed along a pipeline

that monitor not only the state of the pipeline, but also detect potential threats from tiny cracks, corrosion or metal loss [123].

- **Vapor Sensing Tubes:** vapor sensing tubes based leak detection methods involves the installation of a tube along the entire length of the pipeline. The tube is full of air at atmospheric pressure. When a leak happen the substance inside the pipeline penetrates into the tube. Gas sensors located at the ends of tube shall detect any increase in gas concentration. Moreover, the magnitude of the concentration increase is an indication of the size of the leak [56].

1.1.2 Internal Methods

Internal leak detection systems are the most practical methods for diagnose pipeline leaks from a remote location. Internal methods use instruments to continuously monitor the hydraulic conditions of the system. When measurements deviate from normal operations conditions an alarm will be activated. Measured data quality can affects ability of this methods to detect a leak. Internal leak detection methods include:

- **Rate of Pressure/Flow Change Method:** for this methods the principle is that rapid increase of the input flow, rapid decrease of the output flow, a rapid increase of the difference between them and rapid pressure drops are associated with a leak occurrence [103]. To avoid false alarms, these must be disable for time periods corresponding to operation pipeline transients (such as a pump startup or a change in pressure/flow set point).

- **Model-based Methods:** in this case the leak detection problem is tackled with the aid of mathematical models of the process and its signals. Thus, typically this methods use nonmeasurable quantities which can be obtained by process models and estimation methods. Parameter estimation, state observers and artificial neural networks are some techniques used in model-based leak detection methods.

  - **Parameter Estimation:** parameters of a model are constants or time-varying coefficients in the process which appears in the process model. The process model parameters are mostly related to physical process coefficients. Thus, since a leak can make itself noticeable in some physical process constants, e.g. friction coefficient, is therefore also expressed in the process model parameters. If the physical process

coefficients which can indicate leaks occurrence are not directly measurable, an attempt can be made to determine their changes via the changes in the process model parameters [73].

- **State Observer:** since leaks can be indicated by internal, nonmeasurable process state variables, e.g. pressure head, flow rate, state estimator can be used to reconstruct these state variables from the measurable signals. Observer-based methods require a relatively exact knowledge of the process parameters and the input signals [73, 56].
- **Artificial Neural Networks (ANNs):** ANNs have attributes that make them ideal for processing routine measurements made in pipelines, thus ANNS are used in leak-detection systems, without requiring very high sampling frequencies. Ideally, data measured when there are actual leaks should be used for ANN training. Since such data are rarely available from the field in a comprehensive form, in works as in [10] the data for network training were generated by a computer code expressly developed for simulating flow in pipelines with and without leaks.

On the other hand, among the first principles used to build up the models stand out:

- **Mass Balance Based Method:** it is based on the principle of conservation of mass, which states that mass in a closed system remains constant and is not changed by processes within the system. Thus, if a pipeline is considered to be a closed system, the difference between inlet and outlet mass flows in a leak-free pipeline should be equal zero. In practice, by measuring input and output flow rates a leak is detected if the difference between inflow and outflow measurement exceed predefined threshold. The main two weakness of the mass balance method are: 1) the long detection times (several tens of minutes) necessaries to avoid false alarms, which are due to the assumption of steady state and 2) the leak location is unknown [91].
- **Continuity, Momentum and Energy Equations Based Method:** this leak detection technique is based on pipeline hydraulic model constructed by using the principles conservation of mass, conservation of momentum, and conservation of energy [16]. The occurrence of a leak is detected by comparing measured and estimated values. To implement these leak detection systems flow rate and pressure measurements at both ends of the pipeline are necessary. Leak detection and location are possible in this cases [157, 172, 159]. Moreover, a literature review revealed

an investigative trends on leak detection system based on state observer algorithms designed from fluid mathematical models (continuity, momentum and energy equations) expressed in state-space representation [156–158, 160, 15, 172, 174]. In next section a brief literature review related to state observers in leak detection systems is presented.

Model-based methods are popular among the researchers due to the cost effectiveness and advances in microcomputer technology and computational techniques, which permit the effective implementation of this methods.

Several approach can be used to analyze the data collected/generated by any of the leak detection methods presented above. Some of them are threshold analysis [73], correlation analysis [68, 79], spectral analysis [146], principal component analysis [132], among others.

1.2 State-observer-based Leak Detection Systems: Literature Review 2010–2017

To improve the security in pipeline systems operations several model-based methodologies for leak diagnose have been developed in the last few years, many of which use state estimators. Several kinds of state estimators such as, among others, Kalman filters, Luenberger-type observers, high gain observers and sliding mode observers have been used for leak detection. This review is intended to summarize the current research and development about state-observer-based leak detection systems for liquid pipelines during the seven-year period from January 2010 to September 2017. For comparison of some methodologies for leak detection based on state observers, published prior to January 2010, see, e.g., [173, 7]. For a comprehensive review of leak diagnose methods in oil and gas pipelines in recent years, see [90].

1.2.1 Extended Luenberger Observer

In [8, 130] a lumped parameter (discretized) version of momentum and continuity equations are used to design a nonlinear Luenberger-type observer, which is used in detection and isolation algorithms. In both cases friction factor is estimated by using an adaptive scheme proposed in [86]. In [8] a single leak detection and isolation algorithm implemented on a digital signal processor system is presented. While in [130] an algorithm to achieve the isolation of two non-concurrent water leaks is presented. Moreover, in [44] various friction models for the leak

detection system based on nonlinear observer are analyzed. The results strongly recommended do not use a constant friction model. In [18] the effect of the instrumentation used at the ends of the pipeline is considered in the finite-difference modeling for pipelines dynamics. The proposed model is used to design a fault detection and isolation system based on a high gain observer [54], and it enables the detection of possible faults in the instrumentation in addition to leaks.

1.2.2 Adaptive State Observer

Meanwhile, mass and momentum conservation principles are used tor formulate a adaptive observer in [1]. This adaptive observer is the core of a leak detection system in which are only necessary measurements at both end of the pipeline (inlet flow rate and outlet pressure). The proposed approach carries out leak detection, leak location and leak size estimation.

1.2.3 Sliding Mode Method

Furthermore, sliding mode methods have been widely used in control and observation systems design of dynamic systems basically due to their finite time convergence and robustness [89]. In sliding mode observers a sliding operator (e.g. a sign function) depending on the output error provides the sliding motion [35], and in turn guarantees insensitiveness to some forms of noise [180]. In [120] an observer based on robust sliding mode differentiators is proposed as the core of a leak detection and isolation algorithm. In the proposed methodology it is necessary to transform the system in a special case of triangular form based on the Lie derivatives of the system output to estimate the states. Finite time convergence of the observer is guaranteed. In [122] a multi-leak diagnose system based on sliding mode observer scheme is presented. The key of the proposed approach is the estimation of pressures at the leak points through successive estimations of internal states, which is necessary because fluid model of a pipeline with only pressures and flows measurements at the ends does not satisfy the sliding mode observer conditions for leak diagnose. Besides, authors in [47] compare two leak diagnose approach, one is based on a sliding mode observer and the other is an algebraic method obtained from the pipeline model in steady state. Two algorithms were tested in real time scenarios and better results were obtained with the algebraic algorithm. In [26] two algorithm are proposed, the fist one is based on a first order sliding mode observer and the second one is a super-twisting algorithm. Both algorithm look for estimating the position and pressure of a leak in a water plastic pipeline. Proposed algorithm only use measures of flow and pressure at the ends of

a pipeline and they were validated in a pipeline prototype. Meanwhile, [36] an algorithm to diagnose a leak in a plastic water pipeline taking under consideration temperature variations is presented. The proposed algorithm is based on a model that includes temperature dependence in some parameters (e.g. equivalent length and friction factor), as well as an exact differentiation method which is based on so-called higher-order sliding modes.

1.2.4 Nonlinear Recursive Observer

Moreover, in [104] a diagnosis approach that carries out detection of leaks, partially closed in-line valves and partial blockages by means of pressure head measurements is presented. The proposed method is based on the stochastic successive linear estimator (SLE) algorithm developed in [170], which considers the estimation improvement through the iterative solution of the governing flow equations and updating the covariance and cross-covariance matrices of transmissivity and hydraulic head fields. In [105] the SLE algorithm is extended to enable the leak and faults location. The SLE algorithm is also used to estimate diameter distribution of partial blocked pipelines in [106]. The proposed methodology exploits the diameter measurements along the pipe and the pressure measurements to provide 1) the diameter distribution associated to a partial blockage and 2) the error of that estimation.

1.2.5 Kalman Filter, Extended Kalman Filter and Adaptive Kalman Filter

The Kalman filter and its the nonlinear version the so-called Extended Kalman Filter (EKF) have been used in leak diagnose systems to estimate parameters as friction factor in addition to leak coefficients. In such as methods, a estimation error (difference between measured output and the observer output) is used to detect a leak occurrences. In [118] a leak detection and isolation algorithm based on a EKF is proposed and tested on a plastic pipeline prototype. The friction factor is calculated through the so-called Swamee-Jain equation, [151]. In [126] a burst detection methodology is presented. Proposed approach is based on a Kalman filter to detect pipe bursts with distributed noisy flow data. The performance of various burst detection metrics is evaluated under different conditions by using artificial generated burst events. Meanwhile, in [31] an adaptive Kalman filter is used for detecting bursts and leaks in water distribution systems. The effect of sampling interval is analyzed and an algorithm that calculate sampling interval depending on the normalized residuals of flow after filtering is presented. In [131, 37] an EKF is used as state estimator in a leak detection and isolation system. In these work

variations associated to temperature in parameters as friction factor, density and kinematic viscosity are compensated through temperature measurement. In [119] a two-stages leak isolation methodology is proposed. First, a EKF is used to estimate the equivalent straight length (ESL) of the pipeline. Once the leak is detected, an algebraic observer (with the ESL value fixed by the previous observer) is used to estimate the leak position. The Swamee-Jain equation, [151], is used to calculate the friction factor.

1.2.6 High Gain Observer

In [162] nonlinear observers are presented as tools for the diagnose of pipelines. Two different scenarios are considered: a single-leak diagnose scenario and a similar situation but with friction estimation in addition. In the first case a classical high gain observer is used, while in the second case an Extended Kalman Filter is proposed. While in [163] scheme based on high-gain observers is proposed to detect and locate leaks in subterranean pipelines of liquefied petroleum gas (LPG).

1.2.7 Exponential Observer

In [161] the fluid flow in a pipeline is represented as a nonlinear model of so-called Liénard-type [61]. Besides in [155] in a more complete derivation of spatio-temporal Liénard-type models for expressing the dynamical behavior of a fluid transmission line is presented. The benefits of Liénard-type models is their suitable structure for the design of state observers, which can be used leak diagnosis systems. In both works Liénard model-based exponential observers are used to estimate parameters of a pipeline such as the friction factor, the equivalent length and the wave speed. On the other hand and unlike the other cases mentioned so far in [142] the problem of observability of the pipeline system is faced. In this work a algorithm to build an optimal input for a state affine system which guarantees a pre-specified degree of observability is proposed. Optimality is defined with respect to the minimization of the input energy, and observability through a lower bound for the observability Gramian. The proposed method is illustrated through simulation by an application example corresponding to a problem of leak detection in pipelines. It is worth address that a constant friction factor is assumed in all cases.

1.3 Scope and Emphasis

The scope for this thesis will be the design of a liquid pipeline monitoring system that incorporates state estimators for iteratively identifying physical parameters as well as early detection and tracing of leaks. Since space-time nonlinear partial differential equations (the momentum and continuity equations) governs the dynamics of the flow of a slightly compressible fluid in a horizontal pipeline, it is necessary to build auxiliary input signals to excite the system that guarantee observability (it is important to address that for nonlinear systems observability is in general determined locally around a given point and may depend on the applied input). The methodologies proposed for parameters identification and leak diagnose are model-based approaches that relies on Liénard-type representation of pipelines, varying friction factor and flow and/or pressure measurements at both ends of pipeline.

1.4 Outline of the Thesis

Chapter 2 first will be dedicated to the mathematical modeling of the dynamics of the fluid in a pipeline. Chapter 3 will be dedicated to a recall on state space models and state estimation. Chapter 4 will present an algorithm to build an auxiliary signal that guarantees the identification of the parameters of a pipeline by using state observers based on Liénard-type models. Chapter 5 will be dedicated to a novel method, based on a Liénard-type model, to diagnose single and sequential leaks in pipelines. The Liénard-type model describes the fluid behavior in a pipeline and is given only in terms of the flow rate. Chapter 6 will extend the method presented in Chapter 5 to leak diagnose in water distribution networks. Conclusion and discussion of the results and suggestions for further work are found in Chapter 7.

Chapter 2

Pipeline Modeling

2.1 Introduction

The transient flow in closed conduits is described by continuity and momentum equations (some authors use a simplified form of the momentum equations, the equation of motion or the dynamic equation). These equations are the mathematical statements of two fundamental physical principles upon which all of fluid dynamics is based: 1) mass conservation and 2) Newton's second law. Since the velocity and pressure during transient flow are functions of time as well as distance these equations are a set of partial differential equations. Since no analytical solution of these equations is known yet numerical approaches must be used instead.

In this chapter, the continuity and momentum equations are used to derived a mathematical model that describes the dynamics of the fluid in a horizontal pipeline. The proposed models can be used for different purposes, however in this work they will be used in observer-based leak diagnosis schemes.

The chapter is organized as follows: in Section 2.2 continuity and momentum equations are used to develop a nonlinear model with distributed parameters for a pipeline, a simplified version of this model is then presented and various models used to calculate the friction factor are listed. In Section 2.3, Liénard-type models for a pipeline are introduced.

2.2 Fluid Dynamics Equations

2.2.1 Nonlinear Pipeline Model with Distributed Parameters

Let us now consider a pipeline of length L [m], constant inside diameter ϕ [m] and inclined an angle α [rad] with respect to a horizontal plane as that showed in Fig. 2.1. To facilitate

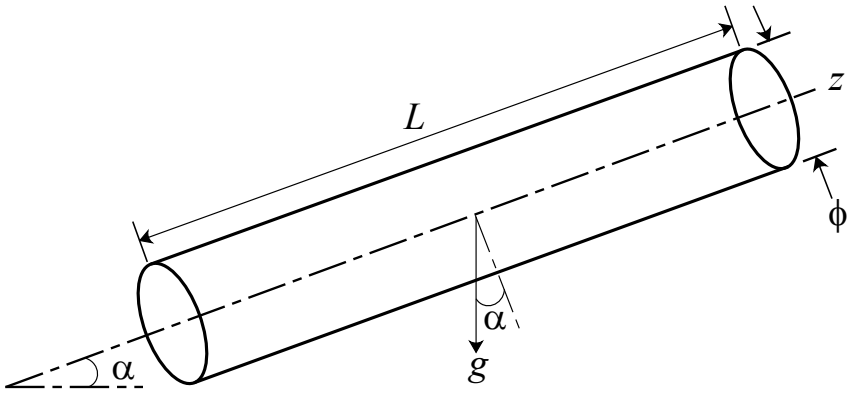

Fig. 2.1 Diagram of a Pipeline Section

understanding the following assumptions for the derivation of a mathematical model of the flow through pipelines are made, [183]:

1. Compressible Fluid. Resulting in an unsteady flow. This yields the finite velocity of sound
$$b^2 = \frac{\partial p}{\partial \rho} \tag{2.1}$$
2. Viscous flow. Viscosity causes shear stresses in a moving fluid.
3. Isothermal flow. Temperature changes due to pressure changes and friction effects can be neglected. Furthermore, the temperature T along the pipeline is considered constant.
4. One-dimensional flow. Pipeline characteristics (as velocity v and pressure p) depend only on the z-axis laid along the pipeline.

The equation of continuity in cylindrical coordinates can be written as follows [19]:

$$\frac{\partial \rho}{\partial t} + \frac{1}{r}\frac{\partial (\rho r v_r)}{\partial r} + \frac{1}{r}\frac{\partial (\rho v_\theta)}{\partial \theta} + \frac{\partial (\rho v_z)}{\partial z} = 0, \tag{2.2}$$

where for simplicity of notation we drop the temporal and spatial dependence of mass density $\rho(t,r,\theta,z)$ [kg/m^3] and velocity components $v_r(t,r,\theta,z)$, $v_\theta(t,r,\theta,z)$ and $v_z(t,r,\theta,z)$ [m/s]. For the one-dimensional case, that is assumption 4, (2.2) which yields

$$\frac{\partial \rho(t,z)}{\partial t} + \frac{\partial(\rho(t,z)v_z(t,r,z))}{\partial z} = 0. \tag{2.3}$$

Substituting (2.1) into (2.3) gives

$$\frac{\partial p(t,z)}{\partial t} + \rho(t,z)b^2\frac{\partial v_z(t,r,z)}{\partial z} + v_z(t,r,z)\frac{\partial p(t,z)}{\partial z} = 0 \tag{2.4}$$

with pressure $p(t,z)$ [Pa] and speed of sound in the fluid b [m/s].

In an actual pipeline the flow shows different nonuniform velocity profiles, therefore the mean velocity will be used for $v_z(t,r,z)$ in (2.4). Mean velocity is calculated as follows

$$\overline{v}(t,z) = \frac{1}{A_r}\int_A v_z(t,r,z)dA = \frac{2}{R^2}\int_0^R v_z(t,r,z)dr \tag{2.5}$$

with cross-sectional area of the pipeline A_r [m^2] and pipeline radius $R = \phi/2$ [m]. Taking into account the volumetric flow rate $Q(t,z) = A_r\overline{v}(t,z)$ [m^3/s] together with (2.4) lead to

$$\frac{\partial p(t,z)}{\partial t} + \frac{\rho(t,z)b^2}{A_r}\frac{\partial Q(t,z)}{\partial z} + \frac{Q(t,z)}{A_r}\frac{\partial p(t,z)}{\partial z} = 0. \tag{2.6}$$

Let us now consider the z-component of the equation of motion in cylindrical coordinates given by, [19]:

$$\rho\left(\frac{\partial v_z}{\partial t} + v_r\frac{\partial v_z}{\partial r} + \frac{v_\theta}{r}\frac{\partial v_z}{\partial \theta} + v_z\frac{\partial v_z}{\partial z}\right) = -\frac{\partial p}{\partial z} + \left[\frac{1}{r}\frac{\partial(r\tau_{rz})}{\partial r} + \frac{1}{r}\frac{\partial \tau_{\theta z}}{\partial \theta} + \frac{\partial \tau_{zz}}{\partial z}\right] + \rho g_z \tag{2.7}$$

with gravitational force per unit volume along z-axis g_z [N/m^3] and shear stresses $\tau_{rz}(t,r,\theta,z)$, $\tau_{\theta z}(t,r,\theta,z)$ and $\tau_{zz}(t,r,\theta,z)$. Notice that τ_{ij} is the force in the j direction on a unit area perpendicular to the i direction. For the one-dimensional case, assumption 4, (2.7) yields

$$\rho\left(\frac{\partial \overline{v}(t,z)}{\partial t} + \overline{v}(t,z)\frac{\partial \overline{v}(t,z)}{\partial z}\right) = -\frac{\partial p(t,z)}{\partial z} + \frac{\partial \tau_{zz}(t,z)}{\partial z} - \rho(t,z)g\sin(\alpha), \tag{2.8}$$

where mean velocity $\overline{v}(t,z)$ has been used for $v_z(t,r,z)$ and the Newton's Law of Viscosity in (2.9) has been considered [19]

$$\begin{aligned}\tau_{r\theta} &= \tau_{\theta r} = -\mu\left[r\frac{\partial}{\partial r}\left(\frac{v_\theta}{r}\right)+\frac{1}{r}\frac{\partial v_r}{\partial r}\right]\\ \tau_{\theta z} &= \tau_{\theta z} = -\mu\left[\frac{1}{r}\frac{\partial v_z}{\partial \theta}+\frac{\partial v_\theta}{\partial z}\right]\\ \tau_{zr} &= \tau_{rz} = -\mu\left[\frac{\partial v_r}{\partial z}+\frac{\partial v_z}{\partial r}\right]\end{aligned}, \tag{2.9}$$

with dynamic viscosity μ [Pa·s].

Pressure loss due to friction rely on the shear stress term $\partial\tau_{zz}(t,z)/z$ in (2.8). Thus, the Darcy-Weisbach friction equation, which relates the friction losses along a given length of pipe to the average velocity of the fluid flow [27, 183], can be used for computing wall shear stress term as follows

$$\frac{\partial\tau_{zz}(t,z)}{\partial z} = -\rho(t,z)\frac{f(\overline{v})\overline{v}(t,z)\left|\overline{v}(t,z)\right|}{2\phi}, \tag{2.10}$$

where $f(\overline{v})$ is the dimensionless Darcy-Weisbach friction factor which depends on the Raynolds number which in turn depends on the flow rate. Notice that it has been written $\overline{v}^2(t,z)$ as $\overline{v}(t,z)\left|\overline{v}(t,z)\right|$ to allow for the reverse flow. Considering the volumetric flow rate together with (2.8) lead to

$$\frac{\partial Q(t,z)}{\partial t}+\frac{Q(t,z)}{A}\frac{\partial Q(t,z)}{\partial z}+\frac{A_r}{\rho(t,z)}\frac{\partial p(t,z)}{\partial z}+\frac{f(Q)Q(t,z)\left|Q(t,z)\right|}{2\phi A_r}+gA_r\sin(\alpha)=0, \tag{2.11}$$

Therefore, the set of hyperbolic partial differential equations (2.6) and (2.11) describe unsteady, nonuniform flow of a slightly compressible fluid in an elastic conduit. In these equations the independent variables are distance z and time t, while the dependent variables are pressure p and flow rate Q.

2.2.2 Simplified Equations

In most of the engineering applications, the convective terms, $Q(\partial p/\partial z)$ and $Q(\partial Q/\partial z)$ are small as compared to the other terms and may be neglected [27]. This considerably simplifies the analysis without significantly affecting the accuracy of the computed results. Thus, dropping these terms from equations (2.6) and (2.11), we obtain

$$\frac{\partial p(t,z)}{\partial t}+\frac{\rho(t,z)b^2}{A_r}\frac{\partial Q(t,z)}{\partial z}=0 \tag{2.12}$$

$$\frac{\partial Q(t,z)}{\partial t}+\frac{A_r}{\rho(t,z)}\frac{\partial p(t,z)}{\partial z}+\frac{f(Q)Q(t,z)\,|Q(t,z)|}{2\phi A_r}+gA_r\sin(\alpha)=0, \tag{2.13}$$

It is common in hydraulic engineering to compute pressures in the pipeline in terms of the piezometric head, H. The gauge pressure may be written as

$$p=\rho g(H-h_0) \tag{2.14}$$

where h_0 is elevation of the pipe centerline above the specified datum. Notice that for a horizontal pipeline $\partial p/\partial t=\rho g(\partial H/\partial t)$ and $\partial p/\partial z=\rho g(\partial H/\partial z)$. By substituting these relationships into (2.12) and (2.13), we obtain

$$\frac{\partial H(t,z)}{\partial t}+\frac{b^2}{gA_r}\frac{\partial Q(t,z)}{\partial z}=0 \tag{2.15}$$

$$\frac{\partial Q(t,z)}{\partial t}+gA_r\frac{\partial H(t,z)}{\partial z}+\frac{f(Q)}{2\phi A_r}Q(t,z)\,|Q(t,z)|=0, \tag{2.16}$$

2.2.3 Friction Loss Models

Pressure drop estimation due to the flow friction in pipelines can be considered as a crucial task in the solution of turbulent flow problems. In a fully developed steady flow in a straight pipe with uniform inner diameter ϕ and flowing full, the Darcy-Weisbach equation is considered appropriate to determine head loss due to viscous effects in closed pipelines. Darcy-Weisbach equation has been defined as follows [184]:

$$h_f=f\frac{L\bar{v}^2}{2g\phi} \tag{2.17}$$

where h_f is the frictional pressure loss [m], f is the Darcy-Weisbach friction factor and $\bar{v}$ is the mean flow velocity [m/s], which can be experimentally measured as the volumetric flow rate Q per unit cross-sectional area A_r.

The friction factor is a function of the Reynolds number of the flow Re and the relative roughness ε/ϕ, which is the ratio of the mean height of roughness ε of the pipe to the pipe diameter ϕ. The relation among f, the Reynolds number and the relative roughness is experimentally determined and plotted in Fig. 2.2, which is called the Moody diagram or Moody chart. It is one of the most widely accepted and used charts in engineering. Although it is developed for circular pipes, it can also be used for non-circular pipes by replacing the diameter by the hydraulic diameter.

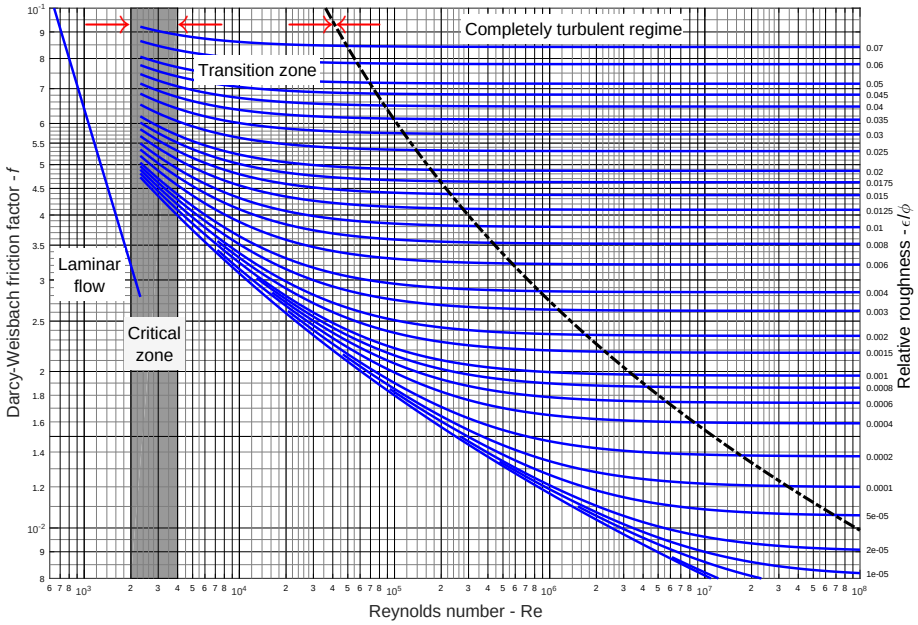

Fig. 2.2 Moody Diagram

The Moody chart can be divided into three regimes of flow: laminar, transition and turbulent. For the laminar flow regime (Re $<\sim$ 2040), roughness has no discernible effect, and the Darcy–Weisbach friction factor f can be calculated as $f = 64/\mathrm{Re}$. On the transition zone, where the flow varies between laminar and complete turbulent, as well as for the turbulent flow regime the relationship between the friction factor f, the Reynolds number Re, and the relative roughness ε/ϕ is more complex. However, notice that at large values of Reynolds number and for a fixed value of relative roughness the friction factor becomes independent of the Reynolds number (complete turbulence zone in Fig. 2.2). An expression for calculating the friction factor for transition and complete turbulent flow, in smooth as well as rough pipes, which agree well with Fig. 2.2 is the relation known as the Colebrook equation given by

$$\frac{1}{\sqrt{f}} = -2log_{10}\left(\frac{\varepsilon}{3.71\phi} + \frac{2.51}{\mathrm{Re}\sqrt{f}}\right), \tag{2.18}$$

where $\mathrm{Re}(z,t) = Q(z,t)\phi/\nu A_r$ is the Reynolds number, ν is the kinematic viscosity [m^2/s] and ε is the pipe's effective roughness height [m]. However, since the Colebrook equation Eq. (2.18) is implicit with respect to f it has to be solved by using iterative methods which causes serious difficulties in repetitive calculations of the friction factor such as those encountered in leak diagnostic algorithms. Because of this reason, over the time a large number of studies developed

several explicit approximations to the implicit Colebrook equation, for a comprehensive review in recent years see [20, 57, 67].

2.3 Liénard-Type Models

Among dynamical systems and differential equations, *Liénard system* is a second order differential equation, named after the French physicist Alfred-Marie Liénard [161]. Due to Liénard equations can be used to model oscillating circuits they were intensely studied during the development of radio and vacuum tube technology [186]. In 1920 a Dutch engineer working for Philips Company, Balthasar Van der Pol, studied a differential equation which describes the circuit of a vacuum tube, the Van der Pol oscillator, one of the most widely used models of nonlinear self-oscillation, is named after him. In 2928 Van del Pol modeled the electric activity of the heart rate, [167]. In the early sixties authors in [51, 117] used the Van der Pol equation to model action potentials of neurons. In seismology, the Van der Pol equation has been used to model the interaction of two plates in a geological fault [25].

2.3.1 Liénard Equation

The French physicist and engineer, Liénard proposed the following generalization of the Van der Pol equation

$$\ddot{x}(t) + F_0(x(t))\dot{x}(t) + G_0(x(t)) = 0 \tag{2.19}$$

where $\dot{x}(t) = dx(t)/dt$, $\ddot{x}(t) = d^2x(t)/dt^2$ for given functions F_0, G_0 and a scalar (unknown) variable $x(t)$. By considering the state variables

$$\begin{aligned} x_1(t) &= x(t) \\ x_2(t) &= \dot{x}(t), \end{aligned} \tag{2.20}$$

the Liénard equation can be rewritten as a set of two first-order differential equations in terms of the state variables x_1 and x_2 as follows:

$$\begin{aligned} \dot{x}_1(t) &= x_2(t) \\ \dot{x}_2(t) &= -F_0(x_1(t))x_2(t) - G_0(x_1(t)) \\ y(t) &= x_1(t), \end{aligned} \tag{2.21}$$

Table 2.1 Approximation to the Colebrook's Equation, [57]

Equation	Range	Authors Year	Ref.
$f = 0.0055\left[1+\left(20000\left(\frac{\varepsilon}{\phi}\right)+\frac{10^6}{\mathrm{Re}}\right)^{\frac{1}{3}}\right]$	$\mathrm{Re} = 4000-5\times10^8$ $\varepsilon = 0-0.01$	Moody 1947	[114]
$f = 0.11\left[\left(\frac{\varepsilon}{\phi}\right)+\frac{68}{\mathrm{Re}}\right]^{\frac{1}{4}}$	$\mathrm{Re} = 10^4-10^6$ ε = not specified	Altshuler 1952	[101]
$f = 0.53\left(\frac{\varepsilon}{\phi}\right)+0.094\left(\frac{\varepsilon}{\phi}\right)^{0.225}+V$ $V = 88\left(\frac{\varepsilon}{\phi}\right)^{0.44}\mathrm{Re}^{-1.62\left(\frac{\varepsilon}{\phi}\right)^{0.134}}$	$\mathrm{Re} = 4000-5\times10^7$ $\varepsilon = 0.00001-0.04$	Wood 1966	[178]
$f = \left[-2\log\left(\frac{\varepsilon}{3.7\phi}+\frac{7}{\mathrm{Re}^{0.9}}\right)\right]^{-2}$	Not specified	Churchill 1973	[32]
$f = \left[1.14-2\log\left(\frac{\varepsilon}{\phi}+\frac{21.25}{\mathrm{Re}^{0.9}}\right)\right]^{-2}$	$\mathrm{Re} = 5000-10^7$ $\varepsilon = 0.00004-0.05$	Jain 1976	[76]
$f = \left[-2\log\left(\frac{\varepsilon}{3.7\phi}+\frac{5.74}{\mathrm{Re}^{0.9}}\right)\right]^{-2}$	$\mathrm{Re} = 5000-10^8$ $\varepsilon = 0.000001-0.05$	Swamee, Jain 1976	[152]
$f = \left\{-2\log\left[\frac{\varepsilon}{37.065\phi}-\frac{5.0452}{\mathrm{Re}}V\right]\right\}^{-2}$ $V = \log\left(\frac{1}{2.8257}\left(\frac{\varepsilon}{\phi}\right)^{1.1098}+\frac{5.8506}{\mathrm{Re}^{0.891}}\right)$	$\mathrm{Re} = 4000-4\times10^8$ ε =not specified	Chen 1979	[28]
$f = \left[-1.8\log\left(\frac{0.135\varepsilon}{\phi}+\frac{6.5}{\mathrm{Re}}\right)\right]^{-2}$	$\mathrm{Re} = 4000-4\times10^8$ $\varepsilon = 0-0.05$	Round 1980	[139]
$f = \left\{-2\log\left[\frac{\varepsilon}{3.7\phi}-\frac{5.02}{\mathrm{Re}}V\right]\right\}^{-2}$ $V = \log\left(\frac{\varepsilon}{\phi}-\frac{5.02}{\mathrm{Re}}\log\left(\frac{\varepsilon}{3.7\phi}+\frac{13}{\mathrm{Re}}\right)\right)$	$\mathrm{Re} = 4000-10^8$ $\varepsilon = 0.00004-0.05$	Zigrang, Sylvester 1982	[189]
$f = \left[-1.8\log\left(\left(\frac{\varepsilon}{3.7\phi}\right)^{1.11}+\frac{6.9}{\mathrm{Re}}\right)\right]^{-2}$	$\mathrm{Re} = 4000-10^8$ $\varepsilon = 0.000001-0.05$	Haaland 1983	[63]
$A = 0.11\left(\frac{\varepsilon}{\phi}+\frac{68}{\mathrm{Re}}\right)^{\frac{1}{4}}$ If $A \geq 0.018$ then $f = A$ and if $A < 0.018$ then $f = 0.0028+0.85A$	$\mathrm{Re} = 4000-10^8$ $\varepsilon = 0-0.05$	Tsal 1989	[164]
$f = \left[-2\log\left(\frac{\varepsilon}{3.7\phi}+\frac{95}{\mathrm{Re}^{0.983}}-\frac{96.82}{\mathrm{Re}}\right)\right]^{-2}$	$\mathrm{Re} = 4000-10^8$ $\varepsilon = 0-0.05$	Manadili 1997	[102]
$f = \left\{-2\log\left[\frac{\varepsilon}{37.065\phi}-\frac{5.0272}{\mathrm{Re}}log\left(\frac{\varepsilon}{3.827\phi}-V\right)\right]\right\}^{-2}$ $V = \frac{4.567}{\mathrm{Re}}\log\left(\left(\frac{\varepsilon}{\phi}\right)^{0.9924}+\left(\frac{5.3326}{208.82+\mathrm{Re}}\right)^{0.9345}\right)$	$\mathrm{Re} = 3000-1.5\times10^8$ $\varepsilon = 0-0.05$	Romeo, Royo, Monzon 2002	[138]
$f = \left[-2\log\left(\frac{\varepsilon}{3.71\phi}+\frac{2.18V}{\mathrm{Re}}\right)\right]^{-2}$ $V = \ln\frac{\mathrm{Re}}{1.816\ln\left(\frac{1.1\mathrm{Re}}{\ln(1+1.1\mathrm{Re})}\right)}$	Not specified	Brkić 2011	[20]
$f = \left[-2\log\left(\frac{\varepsilon}{3.71\phi}+10^{-0.4343V}\right)\right]^{-2}$ $V = \ln\frac{\mathrm{Re}}{1.816\ln\left(\frac{1.1\mathrm{Re}}{\ln(1+1.1\mathrm{Re})}\right)}$	Not specified	Brkić 2011	[20]

Since in the case in which the model (2.21) is going to be used in an observer-based algorithm it is necessary to define the measured output, the output equation $y(t) = x_1(t)$ has been added in (2.21). This means that only the first state is measured, however notice that the function $F_0(x_1(t))$ is *affine* to the unmeasured state $x_2(t)$, which makes it difficult the design of a estimator. In this case a more appropriate state variables definition is

$$\begin{aligned} \zeta_1(t) = &\quad x(t) \\ \zeta_2(t) = &\quad \dot{x}(t) + F(x(t)) \end{aligned} \tag{2.22}$$

with $F(x) = \int_0^x F_0(\sigma)\, d\sigma$. By considering this we can rewrite (2.19) in a state-space form as follows:

$$\begin{aligned} \dot{\zeta}_1(t) = &\quad \zeta_2(t) - F(\zeta_1(t)) \\ \dot{\zeta}_2(t) = &\quad -G_0(\zeta_1(t)) \\ y(t) = &\quad \zeta_1(t), \end{aligned} \tag{2.23}$$

Representation (2.23) is called the Liénard form, and since now nonlinear functions are decoupled from the unmeasured state $\zeta_2(t)$, it facilitates the estimation.

Let us now assume that the functions F and G_0 can be linearly parameterized with respect to some parameter vectors θ_1 and θ_2 respectively, that is

$$\begin{aligned} \dot{\zeta}_1(t) = &\quad \zeta_2(t) - \tilde{F}^T(\zeta_1(t))\theta_1 \\ \dot{\zeta}_2(t) = &\quad -\tilde{G}_0^T(\zeta_1(t))\theta_2 \\ y(t) = &\quad \zeta_1(t), \end{aligned} \tag{2.24}$$

where $\tilde{F}^T(\zeta_1(t))$ and $\tilde{G}_0^T(\zeta_1(t))$ are nonlinear function vectors. The Liénard system in (2.24) can be rewritten in matrix form as follows [14]:

$$\begin{aligned} \dot{\zeta}(t) &= A_o \zeta(t) + \Phi(u(t), y(t))\,\theta + \varphi(u(t), y(t)) \\ y(t) &= C_o(t) \end{aligned} \tag{2.25}$$

with $A_o = \begin{bmatrix} 0 & 1 \\ 0 & 0 \end{bmatrix}$, $C_0 = [\ 1 \quad 0\ ]$, $\Phi(y(t)) = \begin{bmatrix} \tilde{F}^T(y(t)) \\ \tilde{G}_0^T(y(t)) \end{bmatrix}$, $\theta = [\theta_1 \theta_2]$ and a non-parametrized function $\varphi((u(t), y(t))$ which depend exclusively on the inputs and outputs of the system. In consideration of the augmented state vector $\xi(t) = [\ \zeta(t) \quad \theta\ ]^T$, (2.25) can be

rewritten as follows:

$$\begin{aligned}\dot{\xi}(t) &= \underbrace{\begin{bmatrix} A_o & \Phi(u(t),y(t)) \\ 0 & 0 \end{bmatrix}}_{A(u(t),y(t))} \xi(t) + \underbrace{\begin{bmatrix} \varphi(u(t),y(t)) \\ 0 \end{bmatrix}}_{B(u(t),y(t))} \\ y(t) &= \underbrace{\begin{bmatrix} C_o & 0 \end{bmatrix}}_{C} \xi(t).\end{aligned} \tag{2.26}$$

2.3.2 Liénard-Type Models for Pipelines

As we showed in section 2.2, by assuming that convective changes in velocity are negligible and that the cross section area is constant, the momentum and continuity equations governing the dynamics of the fluid in a horizontal pipeline can be expressed as in (2.15) and (2.16), and written here again

$$\frac{\partial H(t,z)}{\partial t} + \frac{b^2}{gA_r}\frac{\partial Q(t,z)}{\partial z} = 0, \tag{2.27}$$

$$\frac{\partial Q(t,z)}{\partial t} + gA_r\frac{\partial H(t,z)}{\partial z} + \frac{f(Q)}{2\phi A_r}Q(t,z)\,|Q(t,z)| = 0. \tag{2.28}$$

where $(z,t) \in (0,L)\times(0,\infty)$ gathers the space [m] and time [s] coordinates respectively, L is the length of the pipe [m], $H(z,t)$ is the pressure head [m], $Q(z,t)$ is the flow rate [m^3/s], b is the velocity of sound in the fluid [m/s], g is the gravitational acceleration [m/s^2], A_r is the cross-sectional area of the pipe [m^2], ϕ is the inside diameter of the pipe [m] and $f(Q(z,t))$ is the Darcy-Weisbach friction factor which depends on the Raynolds number which in turn depends on the flow rate.

Notice that to fully define solutions of (2.27) and (2.28), two of the following Dirichlet conditions must be imposed at the boundaries of the pipeline: (i) upstream pressure head, $H(0,t) = H_{in}(t)$, (ii) downstream pressure head, $H(L,t) = H_{out}(t)$, (iii) upstream flow rate, $Q(0,t) = Q_{in}(t)$ and (iv) downstream flow rate, $Q(L,t) = Q_{out}(t)$.

Flow-based Liénard Form

A representation only in terms of the flow rate can be obtained from (2.28) and (2.27), first, by differentiating (2.27) with respect to z as follows

$$\frac{\partial^2 H(t,z)}{\partial z \partial t} = -\frac{b^2}{gA_r}\frac{\partial^2 Q(t,z)}{\partial z^2} = 0. \tag{2.29}$$

Then, by differentiating (2.28) with respect to t, we get

$$\begin{array}{c} \frac{\partial^2 Q(t,z)}{\partial t^2} + gA_r \frac{\partial^2 H(t,z)}{\partial t \partial z} + \frac{\partial}{\partial t}\left(\frac{f(Q)}{2\phi A_r} Q(t,z)\,|Q(t,z)|\right) = 0 \\ \frac{\partial^2 Q(t,z)}{\partial t^2} + gA_r \frac{\partial^2 H(t,z)}{\partial t \partial z} + \frac{f(Q)}{2\phi A_r}\frac{\partial}{\partial t}\left(Q(t,z)\,|Q(t,z)|\right) + Q(t,z)\,|Q(t,z)|\,\frac{\partial}{\partial t}\left(\frac{f(Q)}{2\phi A_r}\right) = 0. \end{array} \tag{2.30}$$

Let us now evaluate $\frac{\partial}{\partial t}\left(Q(t,z)\,|Q(t,z)|\right)$ as follows:

$$\begin{aligned} \frac{\partial}{\partial t}\left(Q(t,z)\,|Q(t,z)|\right) &= |Q(t,z)|\,\frac{\partial Q(t,z)}{\partial t} + Q(t,z)\frac{\partial |Q(t,z)|}{\partial t} \\ &= |Q(t,z)|\,\frac{\partial Q(t,z)}{\partial t} + Q(t,z)\frac{Q(t,z)}{|Q(t,z)|}\frac{\partial Q(t,z)}{\partial t} \\ &= |Q(t,z)|\,\frac{\partial Q(t,z)}{\partial t} + Q(t,z)\mathrm{sgn}\left(Q(t,z)\right)\frac{\partial Q(t,z)}{\partial t} \\ &= |Q(t,z)|\,\frac{\partial Q(t,z)}{\partial t} + |Q(t,z)|\,\frac{\partial Q(t,z)}{\partial t} = 2\,|Q(t,z)|\,\frac{\partial Q(t,z)}{\partial t}. \end{aligned} \tag{2.31}$$

Substituting (2.31) in (2.30)

$$\begin{array}{c} \frac{\partial^2 Q(t,z)}{\partial t^2} + gA_r \frac{\partial^2 H(t,z)}{\partial t \partial z} + \frac{f(Q)}{\phi A_r}\,|Q(t,z)|\,\frac{\partial Q(t,z)}{\partial t} + \frac{Q(t,z)|Q(t,z)|}{2\phi A_r}\frac{\partial f(Q)}{\partial Q}\frac{\partial Q(t,z)}{\partial t} = 0 \\ \frac{\partial^2 Q(t,z)}{\partial t^2} + gA_r \frac{\partial^2 H(t,z)}{\partial t \partial z} + \frac{|Q(t,z)|}{\phi A_r}\left[f(Q) + \frac{Q(t,z)}{2}\frac{\partial f(Q)}{\partial Q}\right]\frac{\partial Q(t,z)}{\partial t} = 0. \end{array} \tag{2.32}$$

By combining (2.32) and (2.29), we finally obtain:

$$\frac{\partial^2 Q(t,z)}{\partial t^2} + \frac{|Q(t,z)|}{\phi A_r}\left[f(Q) + \frac{Q(t,z)}{2}\frac{\partial f(Q)}{\partial Q}\right]\frac{\partial Q(t,z)}{\partial t} - b^2\frac{\partial^2 Q(t,z)}{\partial z^2} = 0, \tag{2.33}$$

which has the form of (2.19) with

$$\begin{aligned} F_0(Q(t,z)) &= \frac{|Q(t,z)|}{\phi A_r}\left[f(Q) + \frac{Q(t,z)}{2}\frac{\partial f(Q)}{\partial Q}\right] \\ G_0(Q(t,z)) &= -b^2\frac{\partial^2 Q(t,z)}{\partial z^2}. \end{aligned} \tag{2.34}$$

Therefore, by considering the state variables definition in (2.22), that is $Q^a(t,z) = Q(t,z)$ and $Q^b(t,z) = \partial Q(t,z)/\partial t + F(x(t))$, (2.33) can be rewrite in a state-space form as follows:

$$\begin{aligned} \frac{\partial Q^a(z,t)}{\partial t} &= Q^b(z,t) - F(Q^a(z,t)) \\ \frac{\partial Q^b(z,t)}{\partial t} &= b^2\frac{\partial^2 Q^a(z,t)}{\partial^2 z} \end{aligned} \tag{2.35}$$

where $F\left(Q^a(z,t)\right) = \int_0^{Q^a(z,t)} F_0\left(\sigma\right) d\sigma$ and $F_0(\sigma)$ is given by the first equation in (2.34).

Hybrid Liénard Form (flow rate and pressure head)

Let us now assume that the flow rate is driven by pressure heads at the ends of the pipeline. Notice that by differentiating the continuity equation (2.27) with respect to z we have

$$\frac{\partial^2 Q(t,z)}{\partial z^2} = -\frac{gA_r}{b^2}\frac{\partial \dot{H}(t,z)}{\partial z} \tag{2.36}$$

with $\dot{H}(t,z) = \partial \dot{H}(t,z)/\partial t$. Combining (2.36) and (2.35) subsequently yields:

$$\begin{array}{ll} \frac{\partial Q^a(z,t)}{\partial t} & = Q^b(z,t) - F(Q^a(z,t)) \\ \frac{\partial Q^b(z,t)}{\partial t} & = -gA_r\frac{\partial \dot{H}(t,z)}{\partial z} \end{array}, \tag{2.37}$$

which is given in terms of the flow rate and pressure derivatives.

Spatial Discrete Models

By using the finite difference method, a spatial discrete version of (2.35) can be expressed by

$$\begin{array}{ll} \dot{Q}_i^a(t) & = Q_i^b(t) - F\left(Q_i^a(t)\right), \quad i = 1,...,n_\ell \\ \dot{Q}_i{}^b(t) & = b^2\left[\frac{Q_{i-1}^a(t) - 2Q_i^a(t) + Q_{i+1}^a(t)}{(\Delta z_i)^2}\right] \end{array}, \tag{2.38}$$

where Δz_i is the spatial step, n_ℓ is the total number of discretization levels. Furthermore, if Eq. (2.37) is discretized in space, we get the following ODE system:

$$\begin{array}{ll} \dot{Q}_i^a(t) & = Q_i^b(z,t) - F(Q_i^a(t)), \quad i = 1,...,n_\ell \\ \dot{Q}_i{}^b(t) & = gA_r\left[\frac{\dot{H}_{i-1}(t) - \dot{H}_{i+1}(t)}{2\Delta z_i}\right] \end{array}, \tag{2.39}$$

It is important to state that the finite-difference schemes (2.38) and (2.39) are stable if $\triangle z_i \geqslant b\triangle t$, this condition is called the Courant-Friedrich-Lewy (CFL) stability condition [27]. Additionally notice that if the flow rate is measured at three positions corresponding to indexes $i-1, i, i+1$ (see Fig. 2.3), model (2.38) is of the form (2.25), which is suitable for an observer-based estimation of the parameter b^2. If instead derivatives of pressure heads can be available at two positions of indexes $i+1, i$, model (2.39) can be used for estimating $1/\Delta z$.

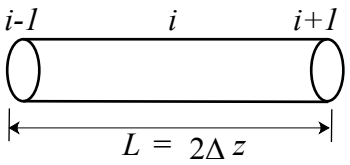

Fig. 2.3 Spatial Discretization of a Pipeline Section

Friction Model Selected

Notice that Liénard-type models (2.38) and (2.39) involve the calculation of $F\left(Q^a(z,t)\right)$, which depending on the model used to calculate the friction factor can results in a pipeline model mathematically unmanageable. Thus, the selection of the friction model to be used implies to face a trade-off between math complexity and accuracy. Among the explicit approximations to the Colebrook equation available, in the present work it was chosen to compute the friction factor by the power-law type equation proposed by Wood in [178] as follows:

$$f(\mathrm{Re}) = f(Q(z,t)) = 0.53\left(\frac{\varepsilon}{\phi}\right) + 0.094\left(\frac{\varepsilon}{\phi}\right)^{0.225} + 88\left(\frac{\varepsilon}{\phi}\right)^{0.44}\mathrm{Re}^{-V}, \tag{2.40}$$

where $V = 1.62\left(\frac{\varepsilon}{\phi}\right)^{0.134}$. It is important to address that the estimated error of Wood approximation can reach a 49.51% in the range $10^4 < \mathrm{Re} < 10^8$ and $1\times10^{-7} < \frac{\varepsilon}{\phi} < 0.05$ (see Fig. 2.4 (a)). To improve the approximation performance new coefficients for the Wood model were calculated by using nlinfit iterative reweighted least squares algorithm in MATLAB®. The improved Wood approximation is shown in Fig. (2.41).

$$f(\mathrm{Re}) = f(Q(z,t)) = 0.4133\left(\frac{\varepsilon}{\phi}\right) + 0.1110\left(\frac{\varepsilon}{\phi}\right)^{0.2598} + 42.6463\left(\frac{\varepsilon}{\phi}\right)^{0.3273}\mathrm{Re}^{-V}, \tag{2.41}$$

where $V = 1.3624\left(\frac{\varepsilon}{\phi}\right)^{0.1124}$. The maximum error is reduced to 11.67% as can be see in Fig. 2.4 (b). Although this error is greater than that obtained with other approximation [20], the convenience of using Wood equation will be understood soon.

Therefore, if the Darcy-Weisbach friction factor is assumed to be constant, $F\left(Q^a(z,t)\right)$ in (2.38) and (2.39) is given by

$$F\left(Q^a(z,t)\right) = \frac{f}{2\phi A_r} Q^a(z,t)\left|Q^a(z,t)\right|, \tag{2.42}$$

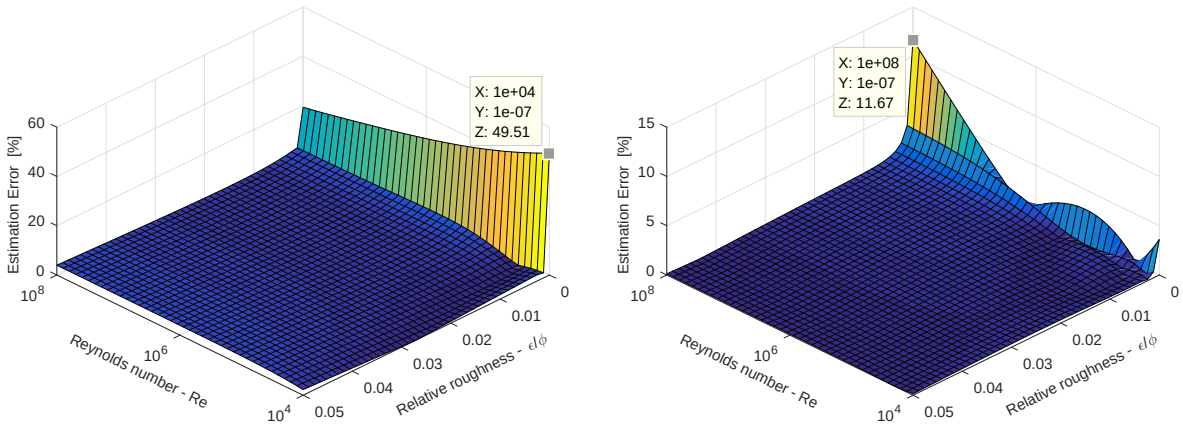

(a) Original Approximation (b) Improved Approximation

Fig. 2.4 Estimated Error of Wood Approximations

and if a varying friction factor calculated through (2.41) is considered, $F\left(Q^a(z,t)\right)$ is given by

$$F\left(Q^a(z,t)\right) = \frac{Q^a(z,t)|Q^a(z,t)|\left(410(\frac{\varepsilon}{\phi}) + 111\left(\frac{\varepsilon}{\phi}\right)^{\frac{13}{50}}\right)}{2000A_r\phi} + \frac{43Q^a(z,t)|Q^a(z,t)|\left(\frac{\varepsilon}{\phi}\right)^{\frac{33}{100}}}{2A_r\phi^{(1+\kappa)}\left(\frac{Q^a(z,t)}{A\upsilon}\right)^{\kappa}}, \tag{2.43}$$

with $\kappa = \frac{34\left(\frac{\varepsilon}{\phi}\right)^{\frac{14}{125}}}{25}$.

It is worth to state that to the best of the our knowledge, this is the first work in which a varying friction factor is taken into account in the formulation of a Liénard-type model for pipelines.

Chapter 3

State Estimation

3.1 Introduction

A state-space representation of a physical system is a mathematical model expressed by first-order differential equations that relates a set of input, output and state variables. The most general state-space representation is written in the following form [15]:

$$\begin{aligned} \dot{x}(t) &= f(x(t),u(t),t) \\ y(t) &= h(x(t),u(t),t) \end{aligned} . \tag{3.1}$$

where $x(t) \in X \subset \mathbb{R}^n$ denotes the state vector, $u(t) \in U \subset \mathbb{R}^p$ the control input vector and $y(t) \in Y \subset \mathbb{R}^q$ the measured output. The input function $u(\cdot)$ is assumed to be bounded and measurable in a set $\mathscr{U}$, and functions f and h to be C^∞ with respect to their arguments.

"State variables" refers to the smallest possible subset of system variables, that together with the input signals and the equations describing the dynamics, will provide the future state and output of the system [125, 42]. By "state space" it should be understood an Euclidean space in which the state variables are the variables on the axes. Within that space the state of the system can be represented as a vector. Also known as the "time-domain approach", the state-space representation provides a compact way to model and analyze systems with multiple inputs and outputs. The transfer function representation for a system with p inputs and q outputs would be a $q \times p$ matrix of Laplace transforms. Unlike the frequency domain approach, the use of the state-space representation is not limited to linear systems with zero initial conditions.

State Space Model is used in many different areas, however, in many real-world systems not all states are available for online measurement due to the high price of sensors [41, 77, 45].

Therefore, measuring the missing states or variables can result expensive and time consuming due the high cost of installation of these devices and the significant technical standard requirements [59, 72]. Consequently, devices called observers or state estimators have been developed to estimate the missing variables and to reduce the usage of high-priced sensors [41, 42]. Thus, the state estimation problem can be interpreted as estimating the states x of a dynamical system described by the system of first-order differential equation in (3.1), given the inputs u and the measurements y.

The solution for this problem was first given by Weiner, Kalman and Luenberger [177, 82, 97, 98], and over the years many authors have worked on the development of state estimators for linear and nonlinear systems looking for guarantee the requirements of high accuracy, low cost and good prediction performances. In fact, many observers today are simply modifications and extended versions of the classical Luenberger observer and Kalman filter. Although the main field of application of observers has been for the operation of control system in which the full information of the system's states is not available, researchers have also developed state estimators to tackle problems such as disturbances, faults and leaks diagnosis [3, 16].

This chapter is organized as follows. Section 3.2 presents state estimators classification, whereas Section 3.3 is dedicated to a review on the observability condition and observer formulation.

3.2 State Estimators Classification

Based on an extensive literature review of the recent observers applications authors in [3] differentiate six major classes in which state estimators can be classified (Table 3.1): Luenberger-based observers, finite-dimensional system observers, Bayesian estimators, disturbances and fault detection observers, artificial intelligence-based observers and hybrid observers.

- **Luenberger-based Observers:** this class groups together all of the observers designed based on the Luenberger observer methodology. Extended versions of the classical Luenberger observer [187], adaptive state observer [17] and sliding mode observer [59] are examples of observers falling into this class. These types of observers are suitable for less complex linear systems [9].

- **Finite-dimensional System Observers:** observers grouped in this class are designed for systems whose dynamics are described by ordinary differential equations (ODEs). Reduced order [34], high gain [12, 163], exponential [85] and interval observers [108]

Table 3.1 State Estimator Classification, [3]

Class	Specific observer
Luenberger-based observers	1. Extended Luenberger observer 2. Sliding mode observer (SMO) 3. Adaptive state observer 4. High-gain observer 5. Zeitz nonlinear observer 6. Discrete-time nonlinear recursive observer 7. Geometric observer 8. Backstepping observer
Finite-dimensional system observers	1. Reduced-order observer 2. Low-order observer 3. High gain observer 4. Asymptotic observer 5. Exponential observer 6. Integral observer 7. Interval observer
Bayesian estimators	1. Particle filter 2. Extended Kalman filter (EKF) 3. Unscented Kalman filter 4. Ensemble Kalman filter 5. Steady state Kalman filter 6. Adaptive fading Kalman filtering 7. Moving horizon estimator 8. Generic observer 9. Specific observer
Disturbance and fault detection observers	1. Disturbance observer 2. Modified disturbance observer 3. Fractional-order disturbance observer 4. Bode-ideal cut-off observer 5. Unknown input observer 6. Nonlinear unknown input observer 7. Extended unknown input observer 8. Modified proportional observer
Artificial intelligence-based observers	1. Fuzzy Kalman filter 2. Augmented fuzzy Kalman filter 3. Differential neural network observer 4. EKF with neural network model
Hybrid observers	1. Extended Luenberger-asymptotic observer 2. Proportional-integral observer 3. Proportional-SMO 4. Continuous-discrete observer 5. Continuous-discreteinterval observer 6. Continuous-discrete-EKF 7. High-gain continuous-discrete

are included in this class. These state estimators suit systems with less kinetic information. Asymptotic/exponential and interval observers can also be extended to infinite dimensional systems [40].

- **Bayesian Estimators:** observers within this class are characterized by a probability distribution estimation of state variables [30]. Extended Kalman filter [69], moving horizon estimators [134] and adaptive fading Kalman filter [179] are examples of Bayesian estimators. These consistent and versatile estimators are highly appropriate for fast estimation [127].

- **Disturbance and Fault Detection Observers:** since both disturbance and fault detection observers are mostly used to estimate irregularities in the system, they are included in the same category. Unknown input observer [29], Bode's ideal cut-off filter [100] and fractional-order disturbances observer [99] fall into this class. Observers belonging to this class are mostly appropriated for estimating faults and disturbances, which allows for early warning.

- **Artificial Intelligence-based Observers:** these observers are based on artificial intelligence techniques as fuzzy logic, artificial neural networks and genetic algorithms. These widely utilized estimators are suitable for systems with incomplete model structure and information. Fuzzy Kalman filter [6] and differential neural network observer [95] are some examples of artificial intelligence-based observers.

- **Hybrid Observers:** these observers result from the combination of more than one observer to improve the estimation in certain systems. The combination allow to overcome the limitations of a particular single observer, however the selection of an appropriate combination may be time consuming [58]. Examples Hybrid observers types are the high-gain continuous-discrete observer [2], proportional sliding modes observer [94] and extended Luenberger-asymptotic observer [72].

3.3 Observability and Observer Formulation

3.3.1 State-space Representations

Although the general form of the state-space representation is the shown in 3.1, others more specific forms are typically used for state estimator design. Among which we have:

- **State-affine Systems:**

$$f(x,u) = A(u)x + B(u), \quad h(x) = C(u)x + D(u) \tag{3.2}$$

- **Control-affine Systems:**

$$f(x,u) = f_0(x) + g(x)u \tag{3.3}$$

- **Linear Time-Varying (LTV) Systems:**

$$f(t,x,u) = A(t)x + B(t)u, \quad h(t,x,u) = C(t)x + D(t)u \tag{3.4}$$

- **Linear Time-Invariant (LTI) Systems:**

$$f(x,u) = Ax + Bu, \quad h(x,u) = Cx + Du \tag{3.5}$$

3.3.2 Observer, Observability and Regularly Persistent Input

State Observer

Given a system described by equations (3.1), the role of an observer consists of estimating the current state $x(t)$ of the system from the knowledge of its inputs $u(t)$ and its outputs $y(t)$. Such a system can be defined as follows [15]:

Definition 3.3.1 (State Observer)**.** An observer for (3.1) is therefore an auxiliary dynamic system whose inputs are the inputs/outputs of (3.1), and the outputs the estimated states $\hat{x}(t)$. Such a system can be represented generally as follows

$$\begin{aligned} \dot{X}(t) &= F(X(t), u(t), y(t), t) \\ \hat{x}(t) &= H(X(t), u(t), y(t), t) \end{aligned}$$

such that:

(i) $\hat{x}(0) = x(0) \Longrightarrow \hat{x}(t) = x(t), \forall t \geq 0$

(ii) $\|\hat{x}(t) - x(t)\| \to 0$ as $t \to \infty$;

If (ii) holds for any $x(0)$, $\hat{x}(0)$, the observer is global.
If (ii) holds with exponential convergence, the observer is exponential.
If (ii) holds with a convergence rate which can be tuned, the observer is tunable.

Geometric Conditions of Observability

Before designing a observer it is important to consider the observability condition of the system because observers can only be designed for observable systems. For stationary linear systems, observability depends exclusively on of the mathematical description of the system and it is also sufficient for guarantee the existence of an observer with global convergence, exponential and arbitrarily fast. For nonlinear systems, the problem is complicated by fact that the observability also depends on the input applied. Relying on the work of ([15]), we define the observability from the notion of indistinguishability.

Definition 3.3.2 (Indistinguishability)**.** The $(x_0, x_0') \in \mathbb{R}^n \times \mathbb{R}^n$ is indistinguishable for u if

$$\forall u \in \mathscr{U}, \forall t \geq 0, h(\mathscr{X}_u(t, x_0)) = h(\mathscr{X}_u(t, x_0')).$$

A state x is indistinguishable from x_0 if the pair (x, x_0) is indistinguishable.

From this definition, we can define the observability.

Definition 3.3.3 (Observability)**.** The system (3.1) is said to be observable if it does not admit an indistinguishable pair.

This definition is quite global, and even too general for practical use. This brings us to consider a weaker notion of observability:

Definition 3.3.4 (Weak observability)**.** The system (3.1) is said to be weakly observable if there exists a neighborhood W of any x such that there is no indistinguishable state from x in W.

This definition does not take into account the cases where the trajectories have go to far from W before one can distinguish between two states of W. In order to prevent this situation, a more local definition can be given:

Definition 3.3.5 (Local Weak Observability)**.** The system (3.1) is said to be locally weakly observable if there exists a neighborhood W of any x such that for any neighborhood V of x contained in W, there is no indistinguishable state from x in V when considering time intervals for which trajectories remain in V.

This means in others words that we can distinguish every state from its neighbors without "going too far". This notion is more interesting in practice, and also since it presents the advantage of admitting some some 'rank condition' characterization. Such condition is based on the notion of observation space which corresponds to the space of all observable states:

Definition 3.3.6 (Observation Space)**.** The observation space for a system (3.1) is defined as the smallest real vector space (denoted by $\mathscr{O}(h)$) of C^∞ functions containing the components of h and closed under Lie derivation along $f_u := f(.,u)$ for any constant $u \in \mathbb{R}^m$ (namely such that for any $\varphi \in \mathscr{O}(h)$, where $L_{f_u}\varphi(x) = \frac{\partial \varphi}{\partial x} f(x,u)$).

Definition 3.3.7 (Observability Rank Condition)**.** The system (3.1) is said to satisfy the observability rank condition if:

$$\forall x, \dim d\mathscr{O}(h)|_x = n$$

where $\dim d\mathscr{O}(h)|_x$ is the set of $d\varphi$ with $\varphi \in \mathscr{O}(h)$.

From this we have [65]:

Theorem 1. The system (3.1) satisfying the observability rank condition at x_0 is locally weakly observable at x_0.
More generally the system (3.1) satisfying the observability rank condition is locally weakly observable.
Conversely, a system (3.1) locally weakly observable satisfies the observability rank condition in an open dense subset of X.

Moreover, there is an equivalence between the rank condition for observability and the Kalman rank condition used for linear time-invariant systems.

Theorem 2. For a system of the form (3.5):

- The observability rank condition is equivalent to $\texttt{rank}\mathscr{O}_m = n$, with $\mathscr{O}_m$ the so-called observability matrix defined by

$$\mathscr{O}_m = \begin{bmatrix} C & CA & CA^2 & \dots & CA^{n-1} \end{bmatrix}^T$$

- The observability rank condition is equivalent to the observability of the system.

Notice that this condition is sufficient for the design of an observer for (3.5) (even necessary and sufficient for the design of an tunable observer). However, in general, the observability rank condition is not enough for a possible observer design: this is due to the fact that in general, observability depends on the inputs. This means that the purpose of observer design requires a look at the inputs [15].

Analytic Conditions for Observability

Since the conditions presented above are not sufficient for an observer's synthesis, additional input conditions must be provided.

Definition 3.3.8 (Universal Inputs)**.** An input $u : [0,T] \to U$ is said to be universal for system (3.1) on $[0,T]$ if $\forall x_0 \neq x_0', \exists \tau \geq 0$ such that $h(\mathscr{X}_u(\tau, x_0)) \neq h(\mathscr{X}_u(\tau, x_0'))$. An input u is a singular input if it is not universal.

When there is no singular entry among the set of allowable inputs U, then any pair of initial states are distinguishable. This property is called U-uniform observability.

Definition 3.3.9 (Uniformly Observable Systems)**.** A system is uniformly observable (UO) if every input is universal.

This property means that observability is independent of the inputs, as in the case of LTI systems, and thus can allow an observer design also independent of the inputs. For not uniformly observable systems, possible observers will depend on the inputs, and not all inputs will be admissible. It is not enough to restrict the set of inputs to universal ones, as in the case of uniformly observable systems (for which all inputs are universal). Universality must be guaranteed over the time, namely must be persistent. In order to characterize this persistency, notice first the following property [15]:

Proposition 1. An input u is a universal input on $[0,t]$ for system (3.1) if and only if $\int_0^t \|h(\mathscr{X}_u(\tau, x_0)) - h(\mathscr{X}_u(\tau, x_0'))\|^2 d\tau > 0$ for all $x_0 \neq x_0'$.

This can be easily checked from definition 3.3.8. Then we can define persistency as follows:

Definition 3.3.10 (Persistent Inputs)**.** An input u is a persistent input for a system (3.1) if

$$\exists t_0, T : \forall t \geq t_0, \forall x_t \neq x_t',$$
$$\int_t^{t+T} \|h(\mathscr{X}_u(\tau, x_0)) - h(\mathscr{X}_u(\tau, x_0'))\|^2 d\tau > 0$$

This definition guarantees observability over a given time interval. However this does not prevent observability from possibly vanishing as time goes to infinity. To avoid this, we must guarantee the observability with a regular persistence:

Definition 3.3.11 (Regularly Persistent Inputs)**.** An input u is a regularly persistent input for a system (3.1) if:

$$\exists t_0, T : \forall t \geq t_0, \forall x_{t-T} \neq x'_{t-T},$$
$$\int_{t-T}^{t} \|h(\mathscr{X}_u(\tau, x_{t-T})) - h(\mathscr{X}_u(\tau, x'_{t-T}))\|^2 d\tau \geq \beta(\|x_{t-T} - x'_{t-T}\|)$$

for some class $\mathscr{K}$ function β.

From these definitions of persistency and regular persistency, we can recover the usual definitions already available for state affine systems [65].

Proposition 2. For state affine systems, regularly persistent inputs are inputs u such that:

$$\int_{t-T}^{t} \Phi_u^T(\tau, t-T) C^T C \Phi_u(\tau, t-T) d\tau \geq \alpha I_d > 0 \quad \forall t \geq t_0 \tag{3.6}$$

with $\Phi_u(\tau, t)$ the transition matrix classically defined by:

$$\frac{d\Phi_u(\tau,t)}{d\tau} = A(u(\tau))\Phi_u(\tau), \quad \Phi_u(t,t) = Id,$$

The term to the left of (3.6) corresponds to the *observability Gramian*, classically defined for LTV systems.

Now we know that regular persistence is the property we need for state reconstruction, but it depends on the time needed to obtain sufficient information. If one is interested in a short-time estimate, one will need a stronger property of observability. This can be stated as follows:

Definition 3.3.12 (Locally Regular Inputs)**.** An input u is a locally regular input for a system (3.1) if:

$$\exists T_0, \alpha : \forall T \leq T_0, \forall t \geq T, \forall x_{t-T} \neq x'_{t-T},$$
$$\int_{t-T}^{t} \|h(\mathscr{X}_u(\tau, x_{t-T})) - h(\mathscr{X}_u(\tau, x'_{t-T}))\|^2 d\tau \geq \beta(\|x_{t-T} - x'_{t-T}\|, \frac{1}{T})$$

for some class $\mathscr{K}$ function β.

3.3.3 Model Under Consideration

This section presents a brief description of the observability characterization of a class of state affine controlled systems (3.2), of interest in this work, which can be rewritten as follows:

$$\begin{aligned} \dot{x}(t) &= A_c(u(t), y(t))\, x(t) + B_c(u(t), y(t)), \\ y(t) &= C_c x(t) \end{aligned} \tag{3.7}$$

where $x(t) \in \mathbb{R}^n$ denotes the state vector, $u(t) \in \mathbb{R}^p$ the control input vector and $y(t) \in \mathbb{R}^q$ the measured output. The nonlinear system (3.7) can be discretized through a single matrix exponential as follows [168]:

$$\begin{bmatrix} A_k & B_k \\ 0 & I \end{bmatrix} = \exp\left(T_s \begin{bmatrix} A_c(u_k, y_k) & B_c(u_k, y_k) \\ 0 & 0 \end{bmatrix} \right),$$

where k is any sampling instant, $u_k \equiv u(kT_s)$, $y_k \equiv y(kT_s)$, T_s is the sampling time and 0 and I stand for null and identity matrices of appropriate dimensions.

According to Ţiclea and Besançon [154], given the initial condition $x(0)$ and the input function, the observation problem of (3.7) can be reduced to the observation of the linear time-varying system

$$\begin{aligned} x_{k+1} &= A_k x_k + B_k \\ y_k &= C_k x_k \end{aligned} \tag{3.8}$$

where x_k denotes the state vector, u_k the control input vector and y_k the measured output at time k. It is worth noting that in general system (3.8) is *not uniformly observable* (definition 3.3.9), i.e. it may admit inputs for which observability is lost. Its observability property can yet be characterized through a discrete version of the *observability Gramian* (3.6), the so called discrete *observability Gramian*, defined for system (3.8) by

$$\Gamma(k, \sigma) = \sum_{l=k-\sigma}^{k} \Phi(l,k)^T C_l^T C_l \Phi(l,k) \tag{3.9}$$

where σ is the length of the Gramian window and

$$\Phi(k, k_0) = A_k A_{k-1} \cdots A_{k_0} = \prod_{p=k_0}^{k} A_p$$

is the state transition matrix. System (3.8) is said to be observable if $\Gamma(k,\sigma)$ is a positive definite matrix, therefore the lowest eigenvalue of Γ can then be used to define a *degree of observability*.

As a result, a *regularly persistent input* for the observability of (3.8) can be defined as done in [154]:

Definition 3.3.13. An input sequence u_k is a *regularly persistent input* for (3.8) if, for any initial condition x_0, the induced linear time-varying representation (3.8) is *completely uniformly observable*, that is, it satisfies the following property.

There exists a fixed natural number σ such that at any sampling instant k we have

$$\Gamma(k,\sigma) - \alpha I > 0, \tag{3.10}$$

where I stands for the identity matrix.

3.3.4 Observer Formulation

For a dynamical system described by (3.8), and assuming that the input sequence u_k is regularly persistent and makes A_k invertible, an appropriate observer is a globally exponentially convergent observer that is given by [16]

$$\begin{aligned} \hat{x}_{k|k} &= \hat{x}_{k|k-1} - K_k\left(C\hat{x}_{k|k-1} - y_k\right) \\ \hat{x}_{k+1|k} &= A_k\hat{x}_{k|k} + B_k \\ P_{k+1|k} &= \gamma^{-1}A_k\left(P_{k|k-1} - K_kCP_{k|k-1}\right)A_k \end{aligned} \tag{3.11}$$

with

$$\begin{aligned} K_k &= P_{k|k-1}C^T\left(CP_{k|k-1}C^T + R\right)^{-1} \\ P_{0|-1} &= P_{0|-1}^T > 0,\ R = R^T > 0 \text{ and } 0 < \gamma < 1. \end{aligned}$$

Notice that the convergence rate can here be tuned via parameter γ, with the property that the smaller it is, the faster the observer will converge [154].

Chapter 4

Input Synthesis for Observer-Based Parameter Identification in Pipelines

4.1 Introduction

Pipelines give an efficient way to transport fluids and are widely used in various industries for that reason. As in many other processes, parameters driving their dynamics can change significantly from their design values because of the aging deterioration, the installation process or the manufacturing execution. Hence, in order to design algorithms based on first principles model of the pipeline such as leak detection and isolation systems (as in [38, 64, 172, 174, 188, 150] for a few examples), monitoring systems (as in [160, 64]), control laws for the optimal transmission and distribution of the products (as in [128, 190, 62, 60, 66] for instance); it is necessary to develop techniques for the continuous updating of the pipeline parameters.

The updating of parameters in a process model is a task known as *parameter identification*, and many methodologies for such a task have been developed over time; see [74, 145], among many. For the particular case of parameter *identification in pipelines*, some approaches can be found in [182, 185], each one with advantages and disadvantages according to the characteristics of the problem.

In the recent work of [161], a parameter identification methodology based on *state observers* and *Liénard-type models* was introduced, and a validation of such a methodology with experimental data was proposed in [155]. In the present chapter, we reconsider this approach, with significant improvement for its implementation, as summarized hereafter.

The methodology is based on the conversion of hyperbolic partial differential equations that represent the fluid dynamics in a pipeline to Liénard-type equations by considering a varying friction factor as it was presented in Section (2.3). To the best of the our knowledge, this is the first work in which a varying friction factor is takes into account in the formulation of a Liénard-type model for pipelines. The benefits of Liénard-type models is their suitable structure for the design of state observers, which can also be used for parameter estimation. The convergence of such observers is guaranteed under a specific excitation condition in the inputs, which means that appropriate signals should be applied (see Definition 3.3.13). Even though in some (simple) cases such inputs can be found analytically, in general their selection is an open problem, and a commonly used alternative is to heuristically look for a solution. In fact, the design of an adequate input is known to be crucial in the field of identification, and there is extensive literature on optimal input design from the 1960s [93, 88, 110]: see for instance [111] for linear systems, [133] for distributed systems, [81] for nonlinear systems, [143, 78, 96] for specific applications, or [23] for fault detection.

In the present chapter, the constructive approach recently presented in [142], and more specifically dedicated to *observability* guarantee by input optimization, is adopted and updated. In other words, we here propose to build an auxiliary signal that guarantees the identification of the parameters of a pipeline by using state observers based on Liénard-type models. Observability is characterized through the so-called observability Gramian (3.9), which is in short a measure of the energy in the output signal, [142]. The lowest eigenvalue of this Gramian defines a degree of observability .

The organization of the chapter is as follows. Section 4.2 recalls the optimization algorithm proposed in [142] for the design of optimal inputs and presents a new algorithm based on it. Section 4.3 presents some simulation and experimental tests to show the input design procedure as well as the estimation of some parameters by using the synthesized inputs. Finally, Section 4.4 concludes this chapter.

4.2 Input Optimization Algorithms

In this work the pipeline dynamics are modeled through the flow-based and hybrid Liénard models given in (2.38) and (2.39), and reproduced here in (4.1) and (4.2)

$$\begin{array}{ll} \dot{Q}_i^a(t) & = Q_i^b(t) - F\left(Q_i^a(t)\right), \quad i = 1, ..., n_\ell \\ \dot{Q}_i{}^b(t) & = b^2 \left[\frac{Q_{i-1}^a(t) - 2Q_i^a(t) + Q_{i+1}^a(t)}{(\Delta z_i)^2}\right] \end{array}, \tag{4.1}$$

$$\begin{array}{ll} \dot{Q}_i^a(t) & = Q_i^b(z,t) - F(Q_i^a(t)), \quad i = 1,...,n_\ell \\ \dot{Q}_i{}^b(t) & = gA_r \left[\frac{\dot{H}_{i-1}(t) - \dot{H}_{i+1}(t)}{2\Delta z_i} \right] \end{array} . \tag{4.2}$$

To guarantee the convergence of observers of the form (3.11) for estimation problems in (4.1) or (4.2), finding an appropriate regularly persistent input is a general and open problem, but in [142] an off-line optimization algorithm was proposed to obtain a periodic persistent input sequence for a given system over a time window of N steps. The optimization problem under consideration can be summarized as follows:

$$\begin{array}{c} \min\limits_{u_k} \sum_{k=0}^{N-1} \left(u_{ref} - u_k\right)^2 \\ \Gamma\left(U_{k+i}, N\right) - \alpha I >, \; 0 \leq i \leq N-1 \\ U_k = \left[\begin{array}{ccccc} u_0 & u_1 & \cdots & u_{N-2} & u_{N-1} \end{array} \right] \\ u^{\min} < u_k < u^{\max}, \; 0 \leq k \leq N-1 \\ \Delta u^{\min} < |u_{k+1} - u_k| < \Delta u^{\max}, \; 0 \leq k \leq N-2 \\ \Delta u^{\min} < |u_0 - u_{k+1}| < \Delta u^{\max}, \end{array} \tag{4.3}$$

where $\Gamma\left(U_{k+i}, N\right)$ represents the observability Gramian over the time window $[0, N-1]$ with input sequence u_k. Since the input sequence is periodic

$$U_{k+N-1} = \left[\begin{array}{ccccc} u_{N-1} & u_0 & \cdots & u_{N-3} & u_{N-2} \end{array} \right],$$

N should be larger than or equal to the system dimension, u_{ref} is a reference signal, $u^{\min}$ and $u^{\max}$ are admissible minimum and maximum values for each element of the input sequence u_k, and $\Delta u^{\min}$ and $\Delta u^{\max}$ are admissible minimum and maximum values for the difference between two consecutive elements of the sequence. Notice that as compared with the original algorithm of [142], a minimum absolute difference $\Delta u^{\min}$ is here included to guarantee that the actuator resolution limitation is respected. In other words, there is a limitation in the smallest increment or step that can be taken or seen by the device that generates the physical input.

The algorithm looks for the persistent input with minimal energy by considering the energy of the difference between the reference signal u_{ref} and the additional persistent input u_k. It was illustrated in [142] in a problem of leak estimation. In the present chapter, examples of applications for parameters' identification in models (4.1) and (4.2) will be given.

Notice that in the case of model (4.2) the inputs are the time derivatives of pressure heads which can reduce to $u^1(t) = \dot{H}_{in}(t)$ and $u^2(t) = \dot{H}_{out}(t)$ when considering $\triangle z = L$. Because of

this, some additional modifications of the algorithm given by (4.3) are needed as follows:

$$\begin{gathered}
\min_{u_k} \sum_{k=0}^{N-1} \left(u_{ref} - u_k^1\right)^2 \\
\Gamma\left(dU_{k+i}^1, N\right) - \alpha I > 0,\ 0 \le i \le N-1 \\
dU_k^1 = \left[\begin{array}{cccc} \frac{u_1^1 - u_0^1}{\Delta t} & \frac{u_2^1 - u_1^1}{\Delta t} & \cdots & \frac{u_{N-1}^1 - u_{N-2}^1}{\Delta t} \quad \frac{u_0^1 - u_{N-1}^1}{\Delta t} \end{array} \right] \\
U^2(k) = f\left(U^1(k)\right),\ 0 \le k \le N-1 \\
u^{\min} < u_k^1 < u^{\max},\ 0 \le k \le N-1 \\
\Delta u^{\min} < \left|u_{k+1}^1 - u_k^1\right| < \Delta u^{\max},\ 0 \le k \le N-2 \\
\Delta u^{\min} < \left|u_{N-1}^1 - u_0^1\right| < \Delta u^{\max},
\end{gathered} \tag{4.4}$$

where $\Gamma\left(dU_{k+i}^1, N\right)$ stands for the observability Gramian over the time window $[0, N-1]$ with input sequence derivative dU_k^1 . Since the input sequence dU_k^1 is periodic

$$dU_{k+N-1}^1 = \left[\begin{array}{cccc} \frac{u_0^1 - u_{N-1}^1}{\Delta t} & \frac{u_1^1 - u_0^1}{\Delta t} & \cdots & \frac{u_{N-3}^1 - u_{N-2}^1}{\Delta t} \end{array} \right],$$

N should be larger than the system dimension, u_{ref} is a reference signal for the input sequence U_k^1, $u^{\min}$ and $u^{\max}$ are the minimum and maximum values for each element of the sequence U_k^1, and $\Delta u^{\min}$ and $\Delta u^{\max}$ are the minimum and maximum values for the difference between two consecutive elements of the sequence U_k^1.

The proposed algorithm works on the input sequence U_k^1, but at each iteration the derivative of that sequence is approximated by using forward finite differences to calculate the observability Gramians Γ. Additionally, by considering that the two inputs, u_k^1 and u_k^2, are not independent, it was necessary to find an expression for relating them: $u_k^2 = f\left(u_k^1\right)$. Since in pipeline systems the flow is usually forced by upstream pumping, $H_{in}(t)$ was considered the independent variable. For simplicity, a steady-state gain was employed, thereby $u_k^2 = f\left(u_k^1\right) = K^{21} u_k^1$.

Since in algorithm (4.3), the input needs to be defined at any time (for the observer application purposes [142]), the sequence u_k^1 calculated through the algorithm must be repeated as many times as necessary. The $N-1$ Gramian constraints guarantee that the observability condition (3.10) holds at any shifted time.

4.3 Application Results

Let us present here two examples of the application of the above input optimization for observer-based parameter identification in pipelines: the first in simulation, which considers model (4.1)

and algorithm (4.3), and the second, with real experiments, which considers model (4.2) and algorithm (4.4). In both examples results obtained by considering constant friction factor (2.42) and varying (2.43) friction factors are presented. We highlight the fact that in all the cases it was verified that the *regularly persistent inputs* calculated were independent of the initial conditions $\hat{x}_0$. Additionally, in this section the exponential forgetting factor observer (3.11) was used for the corresponding nonlinear estimation problem. In both examples, the discretization sampling time was $T_s = 0.002$ [s].

4.3.1 Simulation Tests

In the system under consideration, the pipeline is assumed to be connected to a pump that provides the upstream pressure head $H_{in}(t)$, while the downstream pressure head is considered to be constant $H_{out}(t) = H_{out}$ (see Fig. 4.1). In addition, Table 4.1 provides the list of parameters

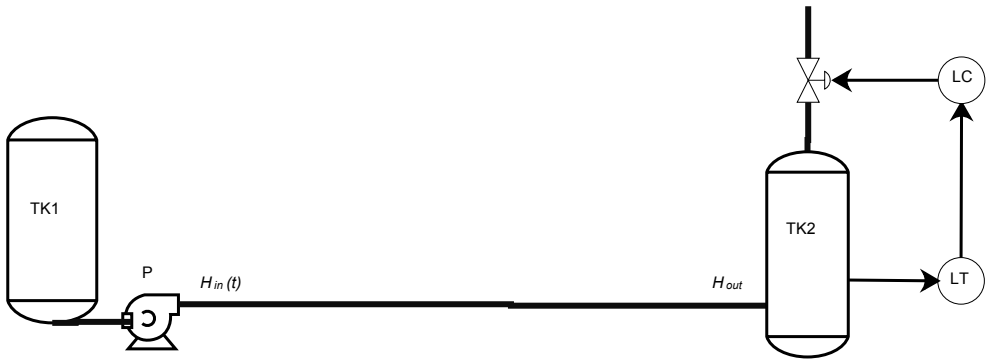

Fig. 4.1 Pipeline System P&ID

considered here for the pipeline model. In order to compare results, those data were taken from [161], but here the friction is assumed not constant and is calculated through (2.18) by using an iterative solution scheme.

Constant Friction Factor: Estimation of the Friction Factor and the Wave Speed

In this case Liénard form (4.1) and (2.42) are considered, with the simplest discretization ($n_\ell = 1$) corresponding to $\triangle z = L$, $Q^a_{i-1}(t) = Q(0,t)$, $Q^a_{i+1}(t) = Q(L,t)$ and $Q^a_i(t)$ being some intermediate measured flow rate. When parameters f, b are unknown, an augmented system (as

Table 4.1 Physical parameters

Symbol	Value	Units	Description
g	9.81	m/s^2	Gravitational acceleration
L	200.16	m	Pipeline length
ϕ	0.1016	m	Pipeline diameter
b	1284	m/s	Wave speed in the fluid
υ	8.94×10^{-7}	m^2/s	Kinematic viscosity
ε	0.5×10^{-3}	m	Roughness height

in (2.26)) from (4.1) would be

$$\dot{x}(t) = \begin{bmatrix} 0 & 1 & -\frac{y(t)|y(t)|}{2\phi A_r} & 0 \\ 0 & 0 & 0 & \rho(t) \\ 0 & 0 & 0 & 0 \\ 0 & 0 & 0 & 0 \end{bmatrix} x(t) \tag{4.5}$$

where $\rho(t) = \frac{Q(L,t)-2y(t)+Q(0,t)}{(\Delta z)^2}$ and $x(t) = \begin{bmatrix} Q_i^a(t) & Q_i^b(t) & f & b^2 \end{bmatrix}^T$.

The followings settings were considered for the simulation [161].

- The downstream pressure head was set to $H_{out}(t) = 5.7$ [m]
- The observer was set with $R = 1$, $\lambda = 0.998$, $P_{0|-1} = I$, and initial condition $\hat{x}_0 = \begin{bmatrix} 0.01913 & 0.01913 & 0.02 & 112871 \end{bmatrix}^T$

It is important to state that the parameters with which the observer was set, as well as the parameters employed for the optimal persistent input calculation (see Table 4.2) were defined by applying a sequential quadratic programming optimization technique using the fmincon function of MATLAB®.

Table 4.2 Parameter for H_{in} sequence calculation for f and b estimation

Symbol	Value	Units	Symbol	Value	Units
u_{min}	17	m	T_{in}	1.5	s
u_{max}	20	m	α	0.018	
Δu_{min}	0.8	m	N	10	
Δu_{max}	1.2	m	u_{ref}	18	m

Fig. 4.2 illustrates the optimal persistent $H_{in}(t)$ sequence obtained and used in the simulation, which is repeated over time. Each step of this sequence corresponds to a time period of $T_{in} = 1.5\ (s)$.

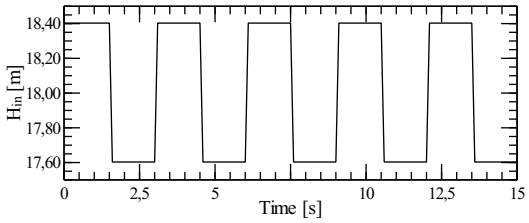

Fig. 4.2 Optimal Regularly Persistent $H_{in}(t)$ Sequence for f and b Estimation

In Fig. 4.3, estimation results obtained with the optimal persistent input calculated here are compared with results obtained by using an additional sine-like input signal. This sine-like signal is labeled as "sin" and it corresponds to the input signal proposed in [161], i.e. $H_{in}(t) = 18 + 0.9\sin(t)$ [m]. Reported results present the simultaneous estimation of the friction factor and wave speed, both without and with measurement noise.

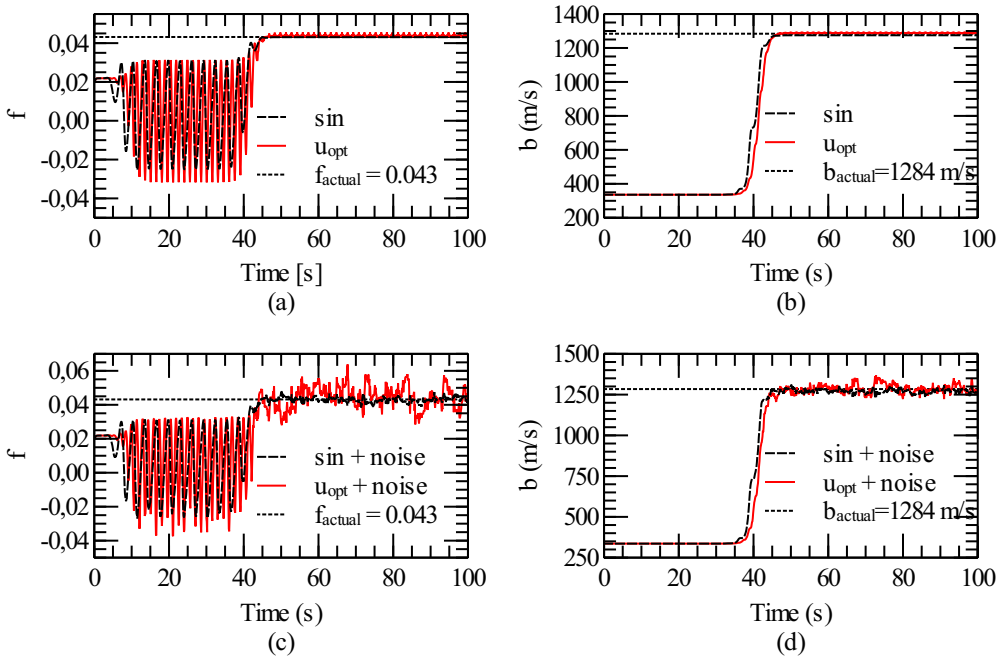

Fig. 4.3 Friction Coefficient and Wave Speed Estimation

From Fig. 4.3, one can see how the estimation indeed performed well in all the cases. The mean value, standard deviation and percentage estimation error of the estimations at steady state are used as performance indexes. Table 4.3 summarizes the energy of each input signal considered as well as the values of the performance indexes obtained. Results show that higher energy inputs show better estimation accuracy; however, the performance of the optimal persistent input is good enough (maximum estimation error less that 3%). The performance is even better if we consider the fact that a pulse signal, as shown in Fig. 4.2, is generated more easily in a control unit i.e., a PLC, than a sinusoidal one.

Table 4.3 Performance indexes in f and b estimation

Signal	E	$\bar{\hat{f}}$	$\sigma_{\hat{f}}$	$e_{\hat{f}}$		$\bar{\hat{b}}$	$\sigma_{\hat{b}}$	$e_{\hat{b}}$
u_{opt}	16	0.0438	6.9×10^{-4}	1.478		1287.1	6.43	0.244
u_{opt} + w$_n$	16	0.0444	6.5×10^{-3}	2.856		1283.9	28.075	4.8×10^{-3}
sin	40.68	0.0431	7.4×10^{-5}	0.25		1274.4	1.509	0.744
sin + w$_n$	40.68	0.043	1.5×10^{-3}	0.479		1270.8	12.641	1.0288

Varying Friction Factor: Estimation of the Wave Speed

Now Liénard form (4.2) and (2.43) are considered, with the simplest discretization ($n_\ell = 1$) corresponding to $\triangle z = L$, $Q^a_{i-1}(t) = Q(0,t)$, $Q^a_{i+1}(t) = Q(L,t)$ and $Q^a_i(t)$ being some intermediate measured flow rate. When the parameter b is unknown, an augmented system (as in (2.26)) from (4.2) would be

$$\dot{x}(t) = \begin{bmatrix} 0 & 1 & 0 \\ 0 & 0 & \rho(t) \\ 0 & 0 & 0 \end{bmatrix} x(t) + \begin{bmatrix} -F(y(t)) \\ 0 \\ 0 \end{bmatrix} \tag{4.6}$$

where $\rho(t) = \frac{Q(L,t)-2y(t)+Q(0,t)}{(\Delta z)^2}$, $y(t) = Q^a_i(t)$ is some intermediate measured flow rate and $x(t) = \begin{bmatrix} Q^a_i(t) & Q^b_i(t) & b^2 \end{bmatrix}^T$.

The followings settings were considered for the simulation [161].

- The downstream pressure head was set to $H_{out}(t) = 5.7$ [m]
- The observer was set with $R = 1$, $\lambda = 0.998$, $P_{0|-1} = I$, and initial condition $\hat{x}_0 = \begin{bmatrix} 0.01913 & 0.01913 & 112871 \end{bmatrix}^T$

It is important to state that the parameters with which the observer was set, as well as the parameters employed for the optimal persistent input calculation (see Table 4.4) were defined by applying optimization techniques using fmincon function of MATLAB®.

Table 4.4 Parameter for H_{in} sequence calculation for b estimation

Symbol	Value	Units	Symbol	Value	Units
u_{min}	17	m	T_{in}	1.5	s
u_{max}	20	m	α	0.018	
Δu_{min}	0.8	m	N	3	
Δu_{max}	1.2	m	u_{ref}	18	m

Fig. 4.4 illustrates the optimal persistent $H_{in}(t)$ sequence obtained and used in the simulation, which is repeated over time. Each step of this sequence corresponds to a time period of $T_{in} = 1.5$ [s].

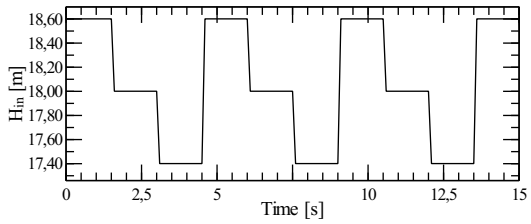

Fig. 4.4 Optimal Regularly Persistent $H_{in}(t)$ Sequence for b Estimation

In Fig. 4.5, estimation results obtained with the optimal persistent input calculated here are compared with results obtained by using the sine-like input signals proposed in [161], i.e. $H_{in}(t) = 18 + 0.9\sin(t)$ [m]. Reported results present the wave speed estimation, both without and with measurement noise.

From Fig. 4.5, one can see how the estimation indeed performed well in all the cases. The mean value, standard deviation and percentage estimation error of the estimations at steady state are used as performance indexes. Table 4.5 summarizes the energy of each input signal considered as well as the values of the performance indexes obtained. Results show that a better performance is obtained with the optimal persistent input although this has a lower energy.

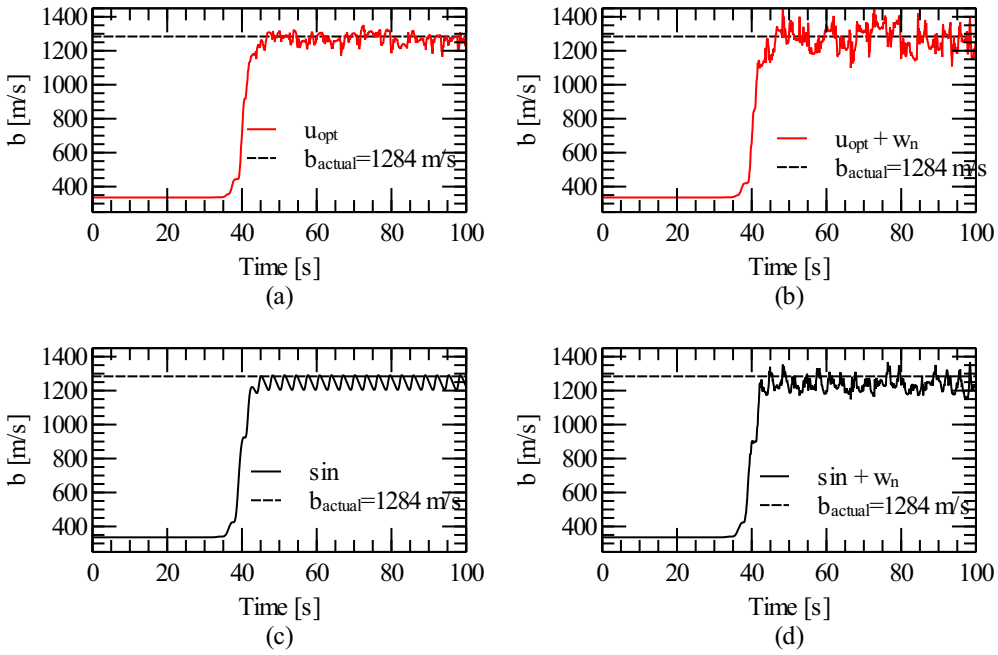

Fig. 4.5 Wave Speed Estimation

Table 4.5 Performance indexes in b estimation

Signal	E	$\hat{\bar{b}}$	$\sigma_{\hat{b}}$	$e_{\hat{b}}$
u_{opt}	24.12	1283.7	17.162	0.025
u_{opt} + w$_n$	24.12	1270	66.48	1.091
sin	40.68	1248	29.614	2.803
sin + w$_n$	40.68	1237.7	42.188	3.607

4.3.2 Experimental Tests

In this section, the estimation of parameters as friction factor and equivalent length[1] of a pipeline is performed by using only one boundary flow measurement ($Q(0,t)$) in addition to the knowledge of boundary pressure heads H_{in}, H_{out}. This is similar to a case considered in [155], but here by using an optimal regularly persistent input calculated through algorithm (4.4).

A prototype built in the Hydrodynamic Laboratory of the UNAM Engineering Institute is considered here (see Fig. 4.6). The prototype is equipped, among other, with

[1]Equivalent length is defined as the pressure drop due to the duct or pipe fittings, or other obstruction to the flow, expressed in number of length units (meter or feet) of a straight pipeline of the same diameter that would cause the same pressure drop.

- A 7.5 HP centrifugal pump (P1), which provides the energy needed to recirculate the water from a reservoir (TK1) through a galvanized steel pipeline of 0.1016 [m] of diameter and 169.43 [m] of length.
- A Mitsubishi variable-frequency drive (VFD) which controls the rotational speed of the pump motor by a variation of the AC frequency in a range from 0 to 60 [Hz].
- Six taps (V1 to V6) to simulate leaks.
- Eight intermediate pressure measurement points (PT2 to PT9).
- Flow and pressure sensors installed at both ends of the pipeline (FT1, PT1, FT3 and PT10), as well as a flow sensor to measure the flow through tap 4 (FT2).
- A recycling system for leak water composed of a tank (TK2) and a centrifugal pump (P2).

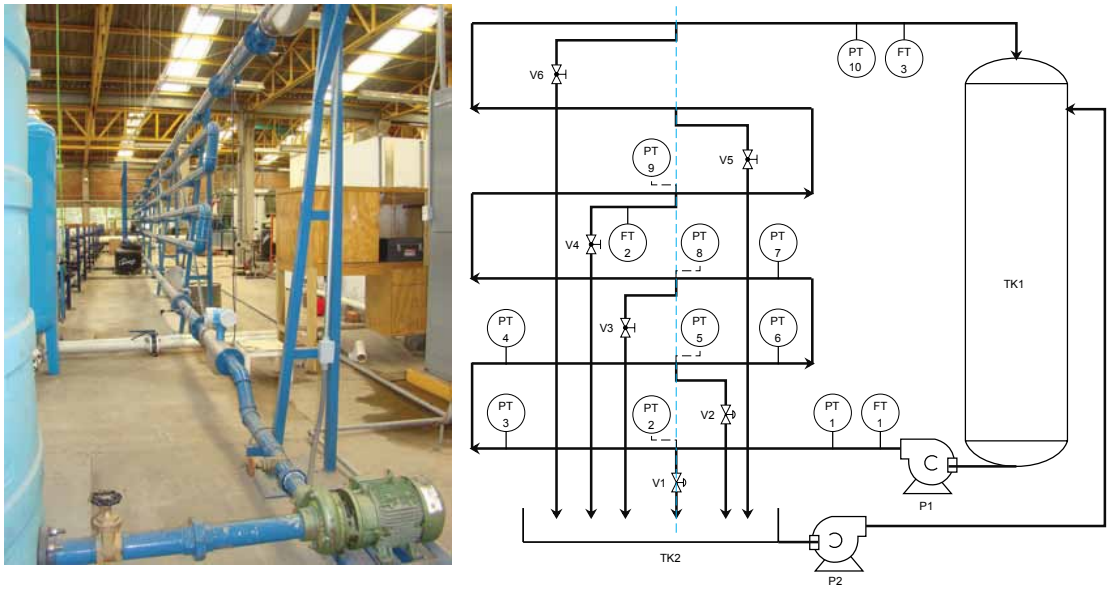

Fig. 4.6 Pipeline Prototype P&ID

In addition, Table 4.6 provides the list of parameters considered here for the pipeline model.

Table 4.6 Pipeline Prototype Physical Parameters

Symbol	Value	Units	Description
g	9.81	m/s^2	Gravitational acceleration
L	169.43	m	Pipeline length
ϕ	0.1016	m	Pipeline diameter
υ	8.94×10^{-7}	m^2/s	Kinematic viscosity
ε	0.7×10^{-3}	m	Roughness height

Constant Friction Factor: Estimation of the Friction Factor and the Equivalent Length

In this case, model (4.2) and (2.42) are considered, with $H_i = H_{in}$ and $H_{i+1} = H_{out}$. When parameters f and L_{eq} are unknown system (4.2) can be extended into:

$$\dot{x}(t) = \begin{bmatrix} 0 & 1 & -\frac{\xi_1(t)|\xi_1(t)|}{2\phi A_r} & 0 \\ 0 & 0 & 0 & \rho(t) \\ 0 & 0 & 0 & 0 \\ 0 & 0 & 0 & 0 \end{bmatrix} x(t) \tag{4.7}$$

where $\rho(t) = a_1\left(\dot{H}_{in}(t) - \dot{H}_{out}(t)\right)$, $y(t) = Q^a_{in}(t)$ and $\xi(t) = \begin{bmatrix} Q^a_{in}(t) & Q^b_{in}(t) & f & \frac{1}{L_{eq}} \end{bmatrix}^T$. Here the spatial step Δz in (4.2) has been replaced by equivalent length L_{eq}. The observer is here tuned with $R = 0.98$, $\lambda = 0.25$, $P_{0|-1} = I$ and initial condition $\hat{x}_0 = \begin{bmatrix} 0.01913 & 0.01913 & 0.07 & 1/300 \end{bmatrix}^T$. The parameters involved in the input calculation are listed in Table 4.7.

Table 4.7 Parameter for H_{in} sequence calculation for L_{eq} estimation

Symbol	Value	Units	Symbol	Value	Units
u_{min}	17	m	T_{in}	6	s
u_{max}	20	m	α	0.00018	
Δu_{min}	1	m	N	6	
Δu_{max}	0.5	m	K^{21}	0.19426	
			u_{ref}	18	m

The sequence obtained by using the algorithm (4.4) was

$$u^1_k = H^{u_{opt}}_{in} = \begin{bmatrix} 18.0309 & 18.6251 & 18.0157 & 18.6233 & 18.6309 & 18.0251 \end{bmatrix} \text{[m]} \tag{4.8}$$

where the time period is $T_{in} = 6(s)$. To experimentally generate this pressure sequence, the pump controller was set up with the sequence

$$VFD_k^{u_{opt}} = [56.7191 \quad 57.7095 \quad 56.6937 \quad 57.7064 \quad 57.7191 \quad 56.7095] \text{ [Hz]}. \tag{4.9}$$

In Fig. 4.7 (a) through (c), the resulting pressure heads $(H_{in}^{u_{opt}}(t), H_{out}^{u_{opt}}(t))$ and the corresponding flow rate $(Q_{in}^{u_{opt}}(t))$ measurements are displayed, respectively.

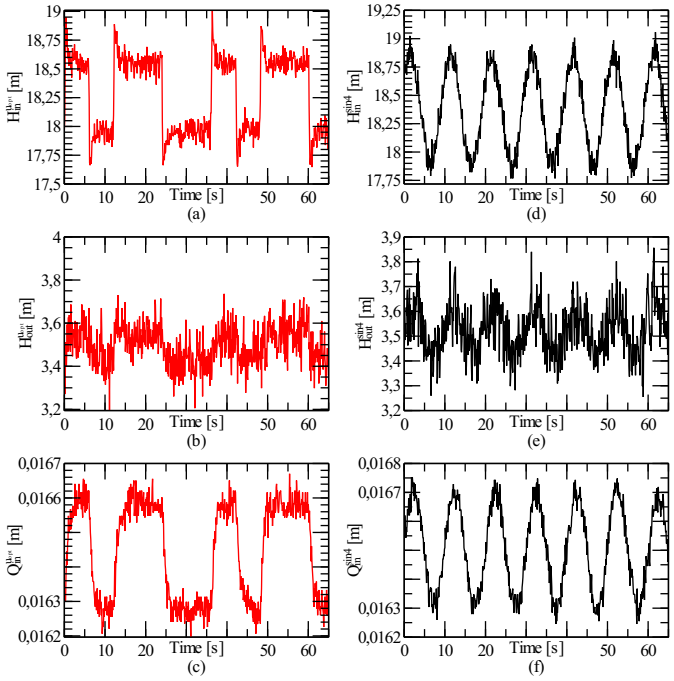

Fig. 4.7 Optimal Regularly Persistent $H_{in}(t)$ (a)-(d), $H_{out}(t)$ (b)-(c) for f and Leq Estimation, Together with Corresponding Input Flows (c)-(f)

In addition, simply to compare results, the estimation was also carried out by using a sine-like pressure signal. It was experimentally determined that sinusoids with frequencies greater than 0.01 [Hz] cannot be generated by the pump because of bandwidth limitation. Thus, for a given frequency of 0.01 [Hz], the lowest energy signal with which the estimation performed well is the following:

$$VFD^{sin4}(t) = 57.5 + 0.75\sin(0.0628t) \text{ [Hz]}, \tag{4.10}$$

and the corresponding upstream and downstream pressure heads $(H_{in}^{sin4}(t), H_{out}^{sin4}(t))$ and input flow rates $(Q_{in}^{sin4}(t))$ are illustrated in Fig. 4.7 (d) - (f) respectively.

Fig. 4.8 shows the related friction coefficient and equivalent length estimation results by using both the optimal regularly persistent input and the sine-like input. The mean value, standard deviation and percentage estimation error of the estimations at steady state are used as performance indexes. Table 4.8 summarizes the energy of each input signal considered as well as the values of the performance indexes obtained. Results show that higher energy inputs show better estimation accuracy; however, the performance of the optimal persistent input ($u_{opt}^{R_\alpha=3\times10^{-5}}$) is good enough (maximum estimation error less that 8% for friction factor and around 2%) for equivalent length.

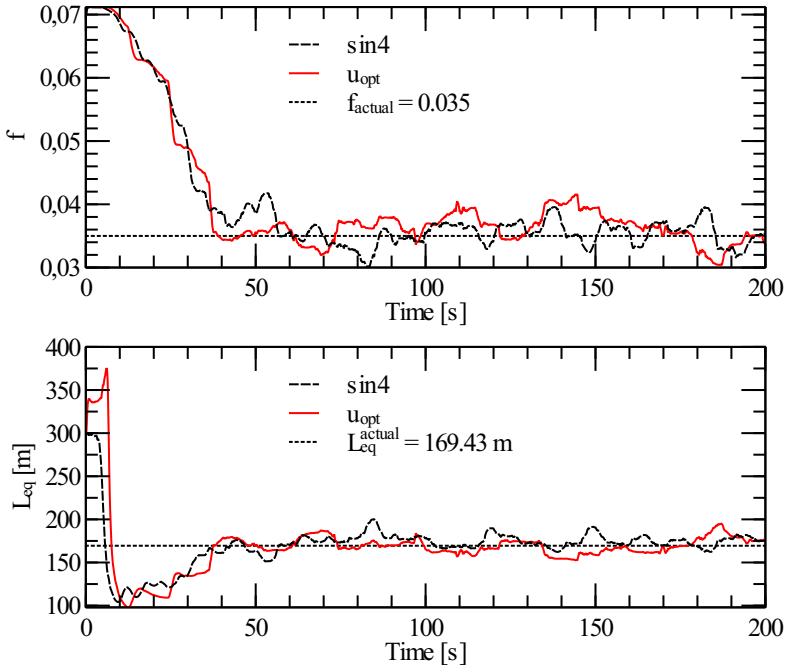

Fig. 4.8 Friction Coefficient and Equivalent Length Estimation

Table 4.8 Performance indexes in f and L_{eq} estimation

Signal	E	$\bar{\hat{f}}$	$\sigma_{\hat{f}}$	$e_{\hat{f}}$		$\bar{\hat{L}}_{eq}$	$\sigma_{\hat{L}_{eq}}$	$e_{\hat{L}_{eq}}$
$u_{opt}^{R_\alpha=3\times10^{-5}}$	21.64	0.0376	5.3×10^{-3}	7.406		165.85	15.084	2.111
sin	24.03	0.0371	5.3×10^{-3}	6.070		170.72	13.693	0.764
$u_{opt}^{R_\alpha=3}$	332.7	0.0354	7.5×10^{-4}	1.1687		167.06	2.862	1.401

The effect of the algorithm parameters, the observability degree α and the Gramian window N on the observer performance is presented in Fig. 4.9. The ratio $R_\alpha = \frac{\alpha}{N}$ was increased from

3×10^{-5} to 3. Performance indexes for the input signal $u_{opt}^{R_\alpha=3}$ (last row of Table 4.8) clearly reveal how increasing R_α produces an improvement of the estimation accuracy; however, the price to be paid is an increment in the input energy.

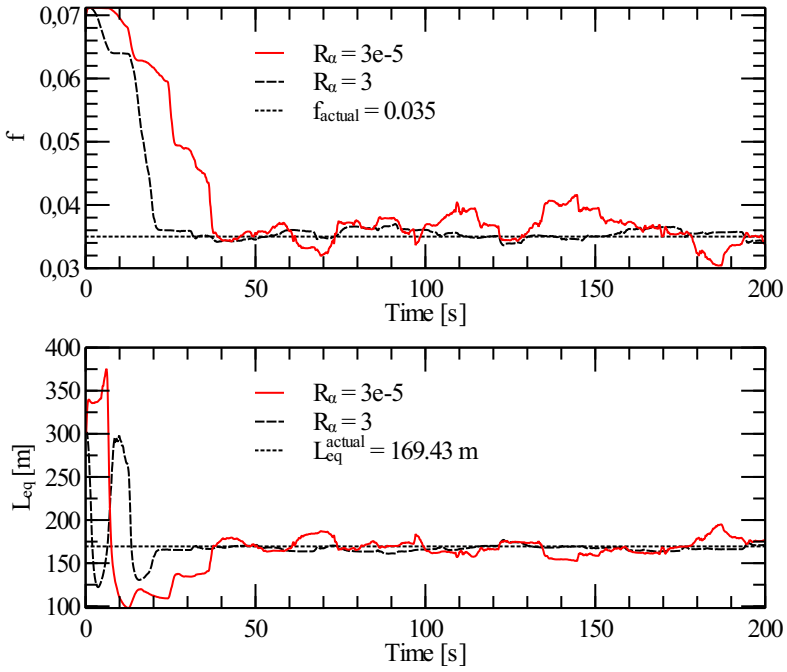

Fig. 4.9 Friction Coefficient and Equivalent Length Estimation for $R_\alpha = 3$ and $R_\alpha = 3 \times 10^{-5}$

Varying Friction Factor: Estimation of the Equivalent Length

In this case, model (4.2) is considered, with $H_i = H_{in}$ and $H_{i+1} = H_{out}$. When the parameter L_{eq} is unknown system (4.2) can be extended into [155]:

$$\dot{x}(t) = \begin{bmatrix} 0 & 1 & 0 \\ 0 & 0 & \rho(t) \\ 0 & 0 & 0 \end{bmatrix} x(t) + \begin{bmatrix} -F(y(t)) \\ 0 \\ 0 \end{bmatrix} \tag{4.11}$$

where $\rho(t) = a_1 \left(\dot{H}_{in}(t) - \dot{H}_{out}(t)\right)$, $y(t) = Q_{in}^a(t)$ and $x(t) = \begin{bmatrix} Q_{in}^a(t) & Q_{in}^b(t) & \frac{1}{L_{eq}} \end{bmatrix}^T$. Here the spatial step Δz in (4.2) has been replaced by equivalent length L_{eq}. The observer is here tuned with $R = 1$, $\lambda = 0.9997$, $P_{0|-1} = I$ and initial condition $\hat{x}_0 = \begin{bmatrix} 0.01913 & 0.01913 & 1/300 \end{bmatrix}^T$. The parameters involved in the input calculation are listed in Table 4.7.

The sequence obtained by using the algorithm (4.4) was that showed in (4.8). And to compare results, the estimation was also carried out by using the sine-like pressure signal in (4.10).

Fig. 4.10 shows the related equivalent length estimation results by using both the optimal regularly persistent input and the sine-like input. The mean value, standard deviation and percentage estimation error of the estimations at steady state are used as performance indexes. Table 4.9 shows that a better performance is obtained with the optimal persistent input, and one must remark that the energy of the sine-like input is higher than the energy of the calculated optimal regularly persistent input ($u_{opt}^{R_\alpha=3\times10^{-5}}$).

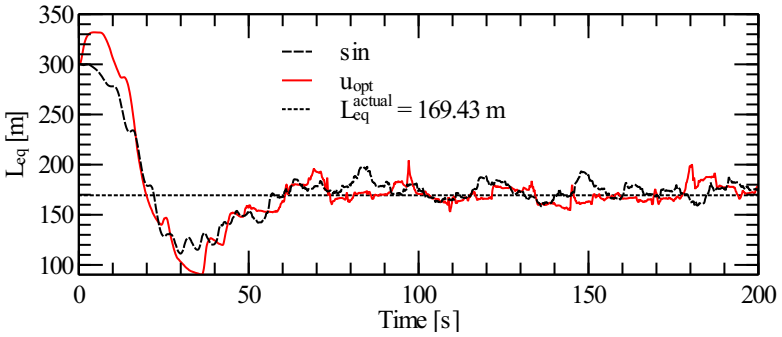

Fig. 4.10 Equivalent Length Estimation

Table 4.9 Performance indexes in L_{eq} estimation

Signal	E	$\hat{L}_{eq}$	$\sigma_{\hat{L}_{eq}}$	$e_{\hat{L}_{eq}}$
$u_{opt}^{R_\alpha=3\times10^{-5}}$	21.64	175.31	3.624	3.473
sin	24.03	176.56	5.162	4.210
$u_{opt}^{R_\alpha=3}$	332.7	169.89	1.468	0.272

The effect of the algorithm parameters, the observability degree α and the Gramian window N on the observer performance is presented in Fig. 4.11. Performance indexes for the input signal $u_{opt}^{R_\alpha=3}$ (last row of Table 4.9) clearly reveal how increasing R_α produces an improvement of the estimation accuracy; however, the price to be paid is an increment in the input energy.

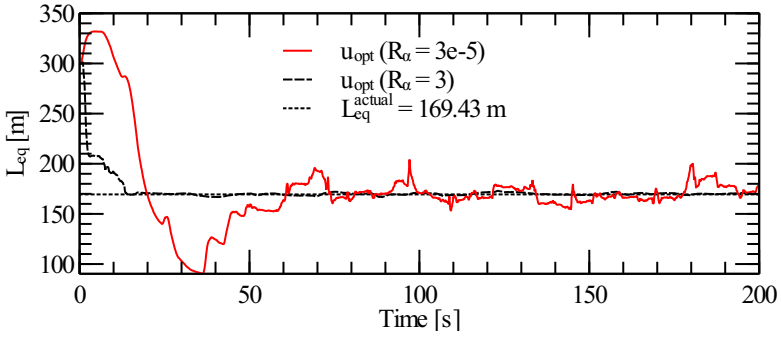

Fig. 4.11 Equivalent Length Estimation for $R_\alpha = 3$ and $R_\alpha = 3 \times 10^{-5}$

4.4 Conclusions

In this chapter, optimization algorithms for calculating *regularly persistent inputs* for state affine systems have been considered and illustrated in a parameter identification issue. Two representations of pipeline dynamics under the form of Liénard-like systems and by considering of a varying friction factor have been used in formulating identification problems as observers. Such observers have been used to estimate the wave speed and the equivalent length of a pipeline. The approach both for input constraints and parameters' estimation has been validated through simulation results as well as experimental tests.

Chapter 5

Leaks Diagnosis in Pipelines by Using Only Flow Rate Measurements

5.1 Introduction

Pipeline networks are the most efficient mode of transportation for fluid products as gasoline, diesel, jet fuel, home heating oil, raw natural gas liquids, among others. As a long-distance transport mean, pipelines have to fulfill high demands of safety and reliability. However, despite a good maintenance plan for fault prevention, leaks in pipelines are unfortunately very common events that must be early diagnosed to avoid irretrievable losses. In this regard, the main objective of leak diagnosis systems (LDS) is to detect and localize leaks with a small error and minimum instrumentation.

According to the American Petroleum Institute [5], LDS can be externally based LDS or internally based LDS. The first ones use a specific set of field instrumentation (e.g. sensing cables [141, 113, 137], acoustic sensors [112], laser sensors [24], vapor sensors [136], fiber-optic cables [147], infrared radiometers or thermal cameras [83]) to monitor external pipeline parameters. While the latter use field instrumentation (e.g. flow or pressure sensors [171, 157]) to monitor internal pipeline parameters.

Because of the high costs associated to installing and maintaining sensors and communication equipment for the entire length of the pipeline, external methods are typically used only in very especial cases. On the other hand, internal methods are constituted as most practical to early and reliably diagnose significant leaks from a remote location. Among the internal methods, one finds the methods based on mathematical models ([13, 175, 80]) and the methods

based on the analysis of a pressure wave traveling along the pipeline ([21, 50, 33]). While model-based methods typically use pressure and flow rate measurements, the methods based on the analysis of a pressure wave only use pressure measurements to perform the diagnosis. Nevertheless, the main drawback of methods that analyze the pressure is the need of disturbing the fluid in order to generate a pressure transient (wave). This procedure is usually done by opening or closing a valve.

Despite of this disadvantage, methods based on pressure wave result attractive because it is always preferable to use the fewest number of sensors for performing the diagnosis. Bearing this in mind, in this chapter it is proposed a method to diagnose (i.e. to detect and locate) pipeline leaks by only using flow rate sensors, which does not require generating disturbances in the fluid transportation process. To the best of the our knowledge, this is the first work that proposes a diagnosis approaches with these characteristics to detect and locate leaks. Usually, flow rates have only been employed to compute a mass balance that allows the leak detection but not the leak location ([91, 92]).

The proposed method is based on a lumped version of a Liénard-type model given in terms of the flow rate, the so-called flow-based Liénard form presented in (2.38). This model is implemented in Matlab® by considering as boundary conditions the inlet and oulet flow rates of the supervised pipeline. To be more specific, since in (2.38) the pipeline is space discretized into space steps (sections), the lumped model will provide a numerical solution: an internal discrete flow for each section. If the pipeline is free of leaks, the discrete flow rates provided by the model will be equal, otherwise the leak flow rate (the outflow) will be distributed along the discrete space of the pipeline. If the discrete flow rates, calculated by the model after the leak, are subtracted from the nominal flow (the pipeline flow rate without leaks), residuals corresponding to each section will be then obtained. The residual close to zero will indicate the section where the leak is occurring. Indispensable requirements for the operation of the method are both the knowledge of the nominal flow as well as fixed pressures at the pipeline ends.

For online implementation the proposed method incorporates a *principal component analysis* PCA stage to detect a leak occurrence. PCA is a dimensionality reduction technique commonly used for fault detection that uses a linear orthogonal transformation to produces a set of values of linearly uncorrelated variables called principal components, from a given set of observations of possibly correlated variables [132].

The main contribution of our method is that requires only flow measurements at the pipeline ends and that a varying friction factor is considered. Some simulation-based tests in PipeluineStudio® and experimental tests in a lab pipeline illustrating the suitability of our

method are shown at the end of this chapter. This chapter is organized as follows. Section 5.2 presents the core of the diagnosis methodology which comprises the elements of the considered model. Section 5.3 describes the proposed diagnostic method. Section 5.4 presents some simulation and experimental test results and Section 5.5 presents the corresponding conclusions.

5.2 System Model

The pipeline model considered here is mainly based on the flow-based form given in (2.38) and reproduced here in (5.1)

$$\begin{array}{ll} \dot{Q}_i^a(t) & = Q_i^b(t) - F\left(Q_i^a(t)\right), \quad i = 1,...,n_\ell \\ \dot{Q}_i{}^b(t) & = b^2\left[\frac{Q_{i-1}^a(t) - 2Q_i^a(t) + Q_{i+1}^a(t)}{(\Delta z_i)^2}\right] \end{array}, \tag{5.1}$$

where Δz_i is the spatial step, n_ℓ is the total number of internal discrete flows and $F(Q_i^a(t))$ is given in (2.43), that is

$$F\left(Q^a(z,t)\right) = \frac{Q^a(z,t)|Q^a(z,t)|\left(410(\frac{\varepsilon}{\phi}) + 111\left(\frac{\varepsilon}{\phi}\right)^{\frac{13}{50}}\right)}{2000A_r\phi} + \frac{43Q(z,t)|Q^a(z,t)|\left(\frac{\varepsilon}{\phi}\right)^{\frac{33}{100}}}{2A_r\phi^{(1+\kappa)}\left(\frac{Q}{A\upsilon}\right)^{\kappa}}, \tag{5.2}$$

with $\kappa = \frac{34\left(\frac{\varepsilon}{\phi}\right)^{\frac{14}{125}}}{25}$.

To find a numerical solution for (5.1), $Q_{in}(t)$ and $Q_{out}(t)$ are used as boundary conditions. Thereby, one can rewrite system (5.1) as follows.

$$\begin{aligned}
\dot{Q}_1^a(t) &= Q_1^b(t) - F\left(Q_1^a(t)\right) \\
\dot{Q}_1{}^b(t) &= b^2\left[\frac{Q_{in}(t) - 2Q_1^a(t) + Q_2^a(t)}{(\Delta z_1)^2}\right] \\
\dot{Q}_2^a(t) &= Q_2^b(t) - F\left(Q_2^a(t)\right) \\
\dot{Q}_2{}^b(t) &= b^2\left[\frac{Q_1(t) - 2Q_2^a(t) + Q_3^a(t)}{(\Delta z_2)^2}\right] \\
&\vdots \\
\dot{Q}_{n_\ell}^a(t) &= Q_{n_\ell}^b(t) - F\left(Q_{n_\ell}^a(t)\right) \\
\dot{Q}_{n_\ell}^b(t) &= b^2\left[\frac{Q_{n_\ell-1}(t) - 2Q_{n_\ell}^a(t) + Q_{out}(t)}{(\Delta z_{n_\ell})^2}\right]
\end{aligned} \tag{5.3}$$

where the spatial step can be computed as $\Delta z_i = L/N_\ell$ with $N_\ell = n_\ell + 1$ as the total number of space steps (sections). For example, if the total number of discrete flows is fixed as $n_\ell = 4$ for a pipeline with length $L = 500$ [m], then the total number of sections (space steps) is $N_\ell = 5$ and $\Delta z_i = 100$ [m]. Check Fig. 5.1 for a better conceptualization. Notice that $Q_i^a(t)$ is the internal discrete flow of section i.

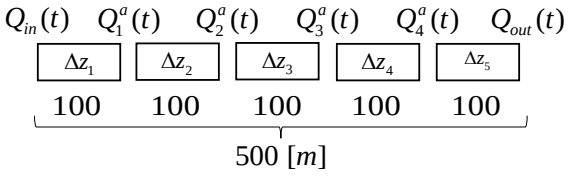

Fig. 5.1 Space Discretization Scheme

5.3 Methodology

The strategy of our methodology incorporates a *principal component analysis* PCA stage to detect a leak occurrence. PCA is a dimensionality reduction technique commonly used for fault detection that uses a linear orthogonal transformation to produces a set of values of linearly

uncorrelated variables called principal components, from a given set of observations of possibly correlated variables [132]. Conventional PCA is shortly presented below.

5.3.1 Principal Component Analysis

Data corresponding to process normal operation are arranged in a matrix $X^{\rho} \in \mathbb{R}^{n \times m}$, where each of the m columns represent a process variable being measured and each of the n rows represents a different sample. It is important to address that variables with missing signal problems or with null variance must be excluded from matrix X^{ρ}.

Since the range of values of raw data may vary widely, it is very important to perform a data normalization (scaling) to standardize the range of the variables considered. Scaling is performed as follows:

$$X = (X^{\rho} - I_n \mu)\Sigma^{-1} \tag{5.4}$$

where $\mu = \frac{1}{n}(X^{\rho})^T I_n$ is a vector containing the means of the m variables in X^{ρ}, $I_n = \begin{bmatrix} 1 & 1 & \cdots & 1 \end{bmatrix} \in \mathbb{R}^n$ and $\Sigma = \text{diag}(\sigma_1, \sigma_2, \cdots, \sigma_m)$ is a diagonal matrix containing the standard deviations of the m variables in X^{ρ}.

Once the data are normalized spectral decomposition of the covariance matrix $S = \frac{1}{n-1}X^T X$ is calculated as follows:

$$S = V \Lambda V^T \tag{5.5}$$

where Λ^T is a $m \times m$ diagonal matrix containing the non-negative real eigenvalues arranged in descending order along its main diagonal, and V is a $m \times m$ matrix containing the corresponding eigenvectors. After that the statistics T^2 and Q are calculated as follows [75, 70]:

$$T^2 = \chi^T P \Gamma_a^{-2} P^T \chi \tag{5.6}$$

$$Q = \chi^T (1 - PP^T)\chi,\ \chi \in \mathbb{R}^{1 \times m} \tag{5.7}$$

where a is the number of principal components selected by using *parallel analysis* as dimensional reduction technique [191, 132], $P \in \mathbb{R}^{m \times a}$ is the so called *loading matrix* which contain the first a column of V, the matrix $\Gamma_a \in \mathbb{R}^{a \times a}$ is composed of the first a rows ans columns of Γ, which in turn is a $m \times m$ matrix such that $\Lambda = \Gamma^T \Gamma$.

For a better understanding a block diagram of the PCA algorithm is showed in Fig. 5.2. Notice that principal component analysis cab be divided in two stages: an offline stage and an online stage.

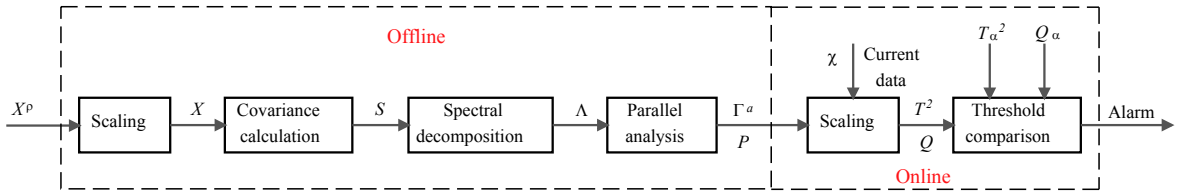

Fig. 5.2 Principal Components Analysis Diagram

5.3.2 Methodology Description

For a better conceptualization Fig. 5.3 shows a flow diagram of the proposed methodology. The proposed approach relies on model (5.3), which is implemented in Matlab® and has as inputs the flow rates measured at the ends of the supervised pipeline, $Q_{in}(t)$ and $Q_{out}(t)$, which in fact, as mentioned before, are the boundary conditions required for the solution of model (5.3). Since the unidimensional space is discretized into space steps (sections) of equal size, model (5.3) shall compute internal discrete flow rates corresponding to each section. If the pipeline is free of leaks, the discrete flow rates provided by the model will be equal, otherwise the leak outflow will be distributed along the discrete space of the pipeline.

If the internal discrete flows, calculated by the model after the leak, are subtracted from the mean nominal flow $\overline{Q}_0$ (the mean flow rate of the pipeline without leaks), residuals corresponding to each section will be then obtained as follows:

$$r_i(t) = \overline{Q}_0 - Q_{\bar{\imath}}^a(t), \forall i = 1,2,...,n_\ell, \;\; \forall \bar{\imath} = n_\ell, n_{\ell-1}, ..., 2, 1. \tag{5.8}$$

where i is the index to enumerate the residuals, $\bar{\imath}$ is the index for the countdown of the flows and n_ℓ is the total number of residuals that matches with the total number of discrete flow rates calculated by the Liénard-type model (5.3).

Residual are used to feed a principal component analysis algorithm to detect a leak occurrence. Whenever a leak is detected, the section where the leak occurs is determined as follows: for a given section $i = j$, the mean value of the residuals $i = j$ will have the following behavior

$$\overline{r}_i(t)|_{i=j} \begin{cases} > 0, & \text{if there is a leak downstream of } \Delta z_j; \\ = 0, & \text{if there is a leak in section } \Delta z_j; \\ < 0, & \text{if there is a leak upstream of } \Delta z_j. \end{cases}$$

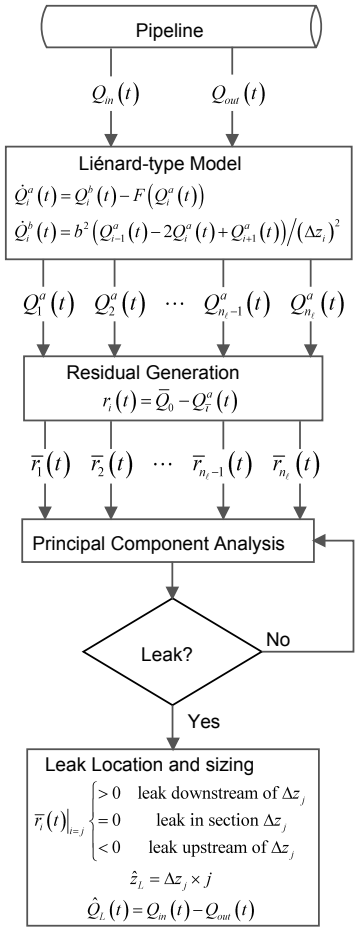

Fig. 5.3 Methodology Flow Diagram

Remark 1: Notice that last section has not assigned a residual since the flow in this section is the downstream boundary condition $Q_{out}(t)$ of model (5.3) and not an internal discrete flow computed by model (5.3).

Remark 2: As a consequence, if a leak is placed in the last section, all the residuals will be then positive.

Remark 3: If the position of the leak does not match with the limits of each section, then $\bar{r}_j \approx 0$.

Resuming the explanation of our methodology, the position of the single leak can be computed by using the following equation:

$$\hat{z}_L = \Delta z_j \times j. \tag{5.9}$$

where j is the section number where the leak happens and Δz_j is the section size, which in fact is the same than the rest of sections ($\Delta z_j = \Delta z_i$). Thus, $\hat{z}_L \to z_L$ inasmuch $\Delta z_i \to 0$. The magnitude of a single leak (the leak outflow) can be calculated by means of the mass balance

$$\hat{Q}_L(t) = Q_{in}(t) - Q_{out}(t). \tag{5.10}$$

In case of sequential leaks, the leak outflow computed by (5.10) will increase with the addition of the outflow of each sequential leak. Each leak flow can be calculated by using the following equation:

$$\hat{Q}_{eq}(t) = \sum_{\kappa=1}^{M} \hat{Q}_{L_\kappa}(t), \tag{5.11}$$

where $\hat{Q}_{eq}$ is the *equivalent flow*, which is the total flow lost due to the leaks, $\hat{Q}_{L_\kappa}$ is the flow lost due to the κ-th sequential leak, which is located at the position $\hat{z}_{L_\kappa}$ and M is the total number of sequential leaks.

In case of sequential leaks, the residual close to zero will indicate the section involving the *equivalent position*. Hence, the leak position of the κ-th sequential leak can be obtained through the following equation:

$$\hat{z}_{eq} = \frac{\sum_{\kappa=1}^{M} \hat{Q}_{L_k}(t)\hat{z}_{L_\kappa}}{\hat{Q}_{eq}(t)}, \tag{5.12}$$

5.4 Application Results

Two scenarios regarding the application of the proposed method algorithms are presented. The first one is simulation based, while in the second one real data obtained from a laboratory pipeline are used.

5.4.1 Simulation Test

In this section some simulation-test results are presented. In the first test three cases of single leaks are treated. The second test presents the performance of our proposed leak diagnosis method to detect sequential leaks. In all cases a pipeline transporting water at 30°C is considered. The pipeline behavior was recreated with the commercial software PipelineStudio® from Energy Solutions, by considering as boundary conditions the upstream and downstream pressure heads

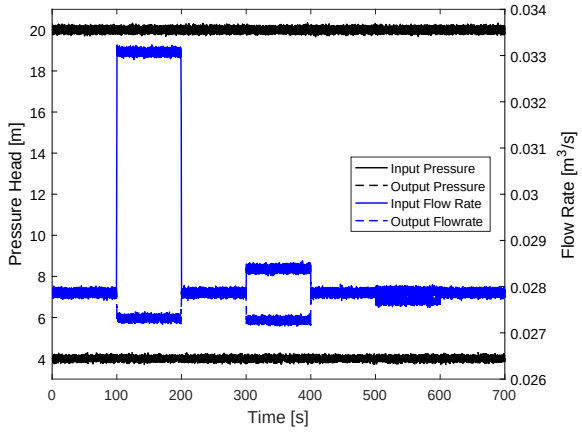

Fig. 5.4 Simulation Test 1 - Pressures and Flow Rates at the Pipeline Ends

$H_{in}(t)$ and $H_{out}(t)$. Thus, this simulator provides the boundary flow rates to be injected to the Liénard model (5.3), in order to compute the discrete flows for the residual generation.

Test 1

In this case a three independent single leaks scenario is considered for a pipeline with the characteristic shown in Table 5.1. The three independent single leak were induced at $z_{L_1} = 15$ [m] (leak 1), $z_{L_2} = 90$ [m] (leak 2) and $z_{L_3} = 146$ [m] (leak 3). The leaks were activated at the instants $t_{L_1}^{on} = 100$ [s], $t_{L_2}^{on} = 300$ [s] and $t_{L_3}^{on} = 500$ [s] and each one had a duration of 100 [s]. The mean values of the boundary conditions considered were $H_{in}(t) = 20$ [m] and $H_{out}(t) = 4$ [m]. Fig. 5.4 shows upstream and downstream pressure heads injected to the PipelineStudio® simulator and the flow rates provided by this for the leaks scenario considered. Notice that the mean nominal flow obtained was about $\overline{Q}_0 = 0.0279$ [m^3/s].

Table 5.1 Physical parameters

Symbol	Value	Units	Description
g	9.81	m/s^2	Gravitational acceleration
L	170	m	Pipeline length
ϕ	0.1016	m	Pipeline diameter
ε	1.083×10^{-3}	m	Mean height of roughness
ν	7.9822×10^{-7}	m^2/s	Kinematic viscosity

On the other hand, the Liénard-type model (5.3) was programmed in Matlab® by fixing a space step (section size) $\Delta z_i = L/N_\ell = 170/21 = 8.1$ [m]. Since $N_\ell = 21$, 20 internal flow are calculated (i.e. $n_\ell = 20$), thereby 20 residuals can be calculated ($r_1(t)$, $r_2(t)$, ..., $r_{20}(t)$). Fig. 5.5 (a) shows the discrete flows computed by the Liénard-type model and Fig. 5.5 (b) shows the residuals calculated through (5.8) (with $\overline{Q}_0 = 0.0279$ [m^3/s]) for each of the leaks considered. The effects of the leak on the synthetic flows is clearly observed (once a leak occurs the leak outflow is distributed as several leaks in each discretization node). Fig. 5.5 (c) shows the response of Hotelling's statistic and the results of leak position and leak flow rate estimations are showed in Fig. 5.5 (d).

The residuals with mean value closer to zero were $r_2(t)$, $r_{12}(t)$ and $r_{19}(t)$ for the leaks 1, 2 and 3 respectively. The leak positions were estimated through (5.9). Table 5.2 summarizes the estimated leak positions $\hat{z}_L$ and the estimation errors obtained for each one of three leaks considered. The estimation errors were calculated as $e = 100\left|\frac{z_L - \hat{z}_L}{L}\right|$. It is important to address that the minimal leak detectable corresponds to a flow rate of 2×10^{-4} [m^3/s] (leak 3), which is equivalent to a 0.72% of the nominal flow .

Table 5.2 Simulation Test - Single Leaks Diagnosis Results

z_L [m]	$\hat{z}_L$ [m]	Error [%]
15	15.45	0.27
90	92.73	1.6
146	146.82	0.48

Test 2

In this case a two sequential leaks scenario is considered for a pipeline with the characteristic showed in Table 5.3. The two sequential leaks were induced at position $z_{L_1} = 12.87$ [m] and $z_{L_2} = 25.3$ [m], at the instants $t_{L_1} = 100$ [s] and $t_{L_2} = 150$ [s]. The mean values of the boundary conditions considered were $H_{in}(t) = 4.18$ [m] and $H_{out}(t) = 0.73$ [m]. Fig. 5.6 (a) shows upstream and downstream pressure heads injected to the PipelineStudio® simulator and the flow rates provided by this for the two sequential leaks considered, and Fig. 5.6 (b) shows the response of Hotelling's statistic.

For this test the Liénard-type model (5.3) was programmed in Matlab® by fixing a space step (section size) $\Delta z_i = L/N_\ell = 57.76/21 = 2.75$ [m]. Since $N_\ell = 21$, 20 internal flow are calculated (i.e. $n_\ell = 20$), thereby 20 residuals can be calculated ($r_1(t)$, $r_2(t)$, ..., $r_{20}(t)$). The

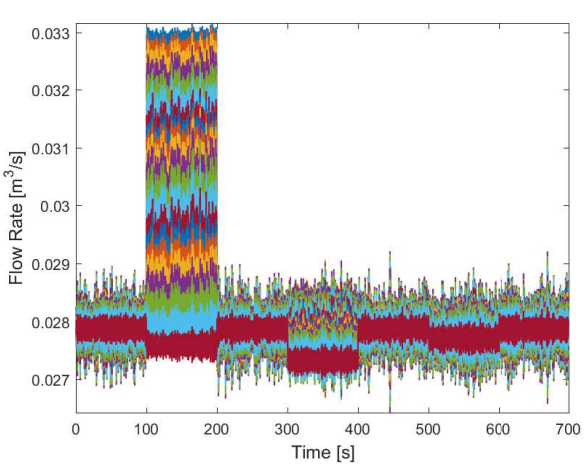

(a) Discrete flows

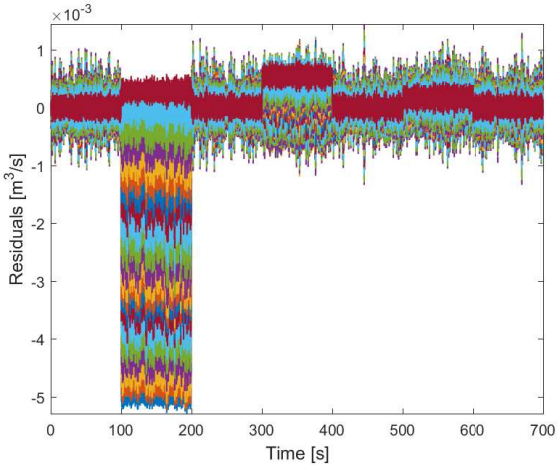

(b) Residuals

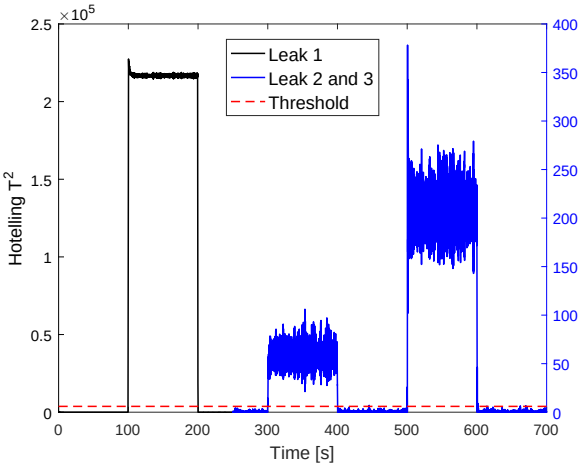

(c) Hotelling's T^2 statistic

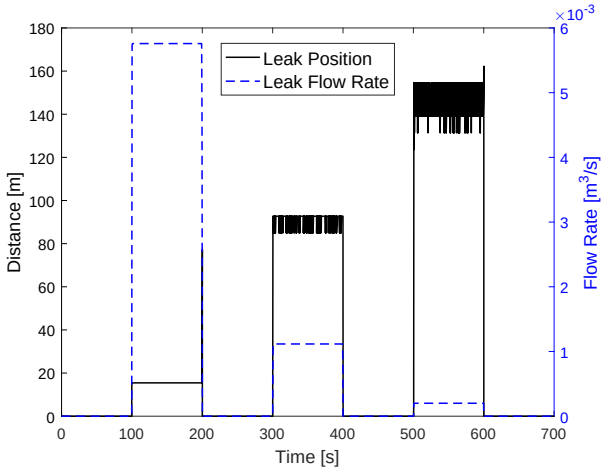

(d) Estimation of Leak Position and Leak Flow Rate

Fig. 5.5 Simulation Test 1 - Results

discrete flows computed by the Liénard-type model are shown in Fig. 5.7 (a), and the residuals in Fig. 5.7 (b). Equation (5.10) can be used to compute the outflow of the first leak and the total outflow (if applied once the second leak occurs). We obtain then $\hat{Q}_{L_1} = 5.3 \times 10^{-4}$ [m^3/s] and $\hat{Q}_{eq} = 9.4 \times 10^{-4}$ [m^3/s]. By using then (5.11), we obtain $\hat{Q}_{L_2} = 4.1 \times 10^{-4}$ [m^3/s]. It can be verified that the residual with mean value closer to zero is $r_5(t)$ before the second leak and $r_7(t)$ after it (see Fig. 5.7 (b). This means that $\hat{z}_{L_1} = \Delta z_i \times 5 = 13.75$ [m] and the *equivalent leak* is $z_{eq} = \Delta z_i \times 7 = 19.25$ [m]. By using then (5.12), the position of the second leak can be determined: $\hat{z}_{L_2} = 26.36$ [m]. The error with respect to the *real* position is due to the discretization space step. To obtain better results Δz_i should be smaller. Table 5.4 summarizes

Table 5.3 Physical parameters

Symbol	Value	Units	Description
g	9.81	m/s^2	Gravitational acceleration
L	57.76	m	Pipeline length
ϕ	0.052	m	Pipeline diameter
ε	1.654×10^{-5}	m	Mean height of roughness
ν	8.0066×10^{-7}	m^2/s	Kinematic viscosity

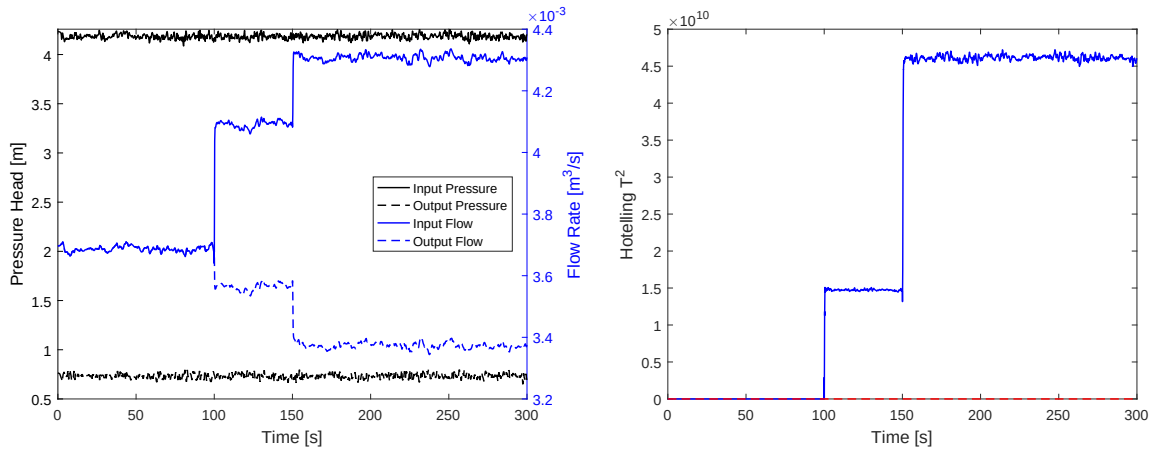

(a) Simulation Test 2 - Pressures and flow rates

(b) Hotelling's T^2 statistic

Fig. 5.6 Simulation Test 2 - Boundary Conditions and T^2 Statistic

the estimated leak positions $\hat{z}_L$ and the estimation errors obtained in this case. The estimation errors were calculated as $e = 100 \left| \frac{z_L - \hat{z}_L}{L} \right|$.

Table 5.4 Simulation Test - Sequential Leaks Diagnosis Results

z_L [m]	$\hat{z}_L$ [m]	Error [%]
12.87	13.75	1.55
25.3	26.36	1.87

5.4.2 Experimental Test

In this section some experimental test results are presented. The diagnosis of two single leaks is performed. Flow rates measurements at the ends of a pipeline prototype built in Instituto Tecnológico de Tuxtla Gutiérrez are used as boundary condition to the Liénard-type model

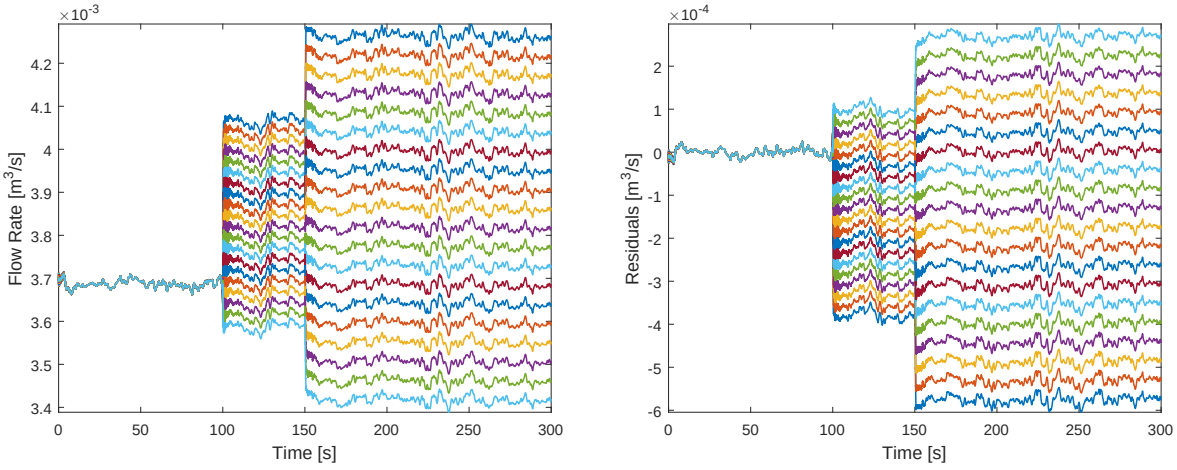

(a) Discrete flows (b) Residuals

Fig. 5.7 Simulation Test 2 - Discrete Flows and Residuals

(5.3). Table 5.3 provides the list of model parameters considered. The prototype considered here (Fig. 5.8) is equipped with:

- A 5 HP centrifugal pump, which provides the energy needed to recirculate the water from a reservoir through a PVC pipeline of 0.052 [m] of diameter and 57.76 [m] of length.
- A Siemens Micromaster 420 variable-frequency drive which controls the rotational speed of the pump motor by a variation of the AC frequency in a range from 0 to 60 [Hz].
- Four valves to emulate leaks.
- Flow and pressure sensors installed at both ends of the pipeline.

Then, in this case two independent single leak cases were induced at $z_{L_1} = 12.87$ [m] (leak 1) and $z_{L_2} = 25.3$ [m] (leak 2). The leaks were activated at the instant $t_{L_1}^{on} = 115$ [s] and $t_{L_2}^{on} = 120$ [s] respectively. Fig. 5.9 (a) and Fig. 5.9 (b) show upstream and downstream pressure heads and input and output flow rates for both leak 1 and leak 2 respectively.

Notice that the mean nominal flows obtained were about 4.85×10^{-3} [m^3/s] and 4.68×10^{-3} [m^3/s] for leaks 1 and 2 respectively. For these flow rates (taking into account the pipeline characteristic in Table 5.1) the nominal friction factor was calculated by using an iterative solution scheme for (2.18), obtaining $\overline{f}_{L_1} = 0.01849$ and $\overline{f}_{L_2} = 0.01858$.

Similarly to the simulation tests, the Liénard-type model (5.3) was programmed in Matlab® by fixing a space step (section size) $\Delta z_i = L/N_\ell = 57.76/22 = 2.63$ [m]. Since $N_\ell = 20$, 21

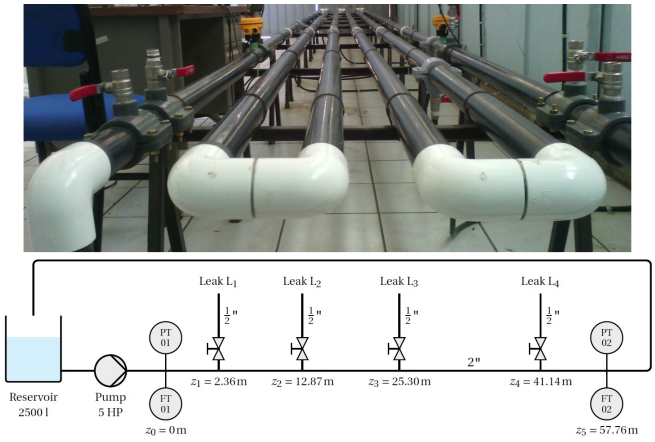

Fig. 5.8 Pipeline Prototype

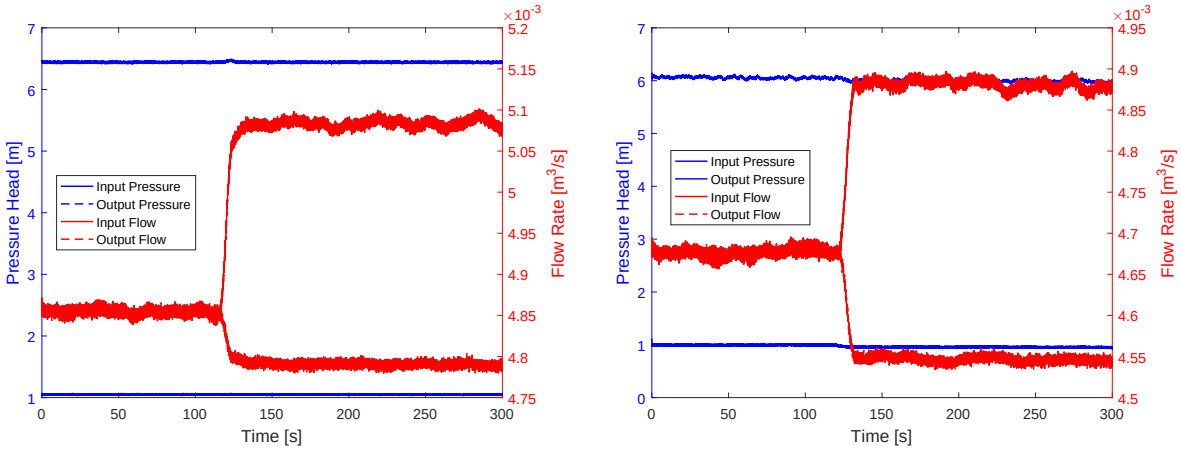

(a) Leak 1 (b) Leak 2

Fig. 5.9 Experimental Test - Pressures and Flow Rates at the Pipeline Ends

internal flow are calculated (i.e. $n_\ell = 21$), thereby 21 residuals can be calculated ($r_1(t)$, $r_2(t)$, ..., $r_{21}(t)$). Fig. 5.10 (a) and Fig. 5.10 (b) show the residuals calculated through (5.8) for the leaks 1 and 2 respectively. Again, the effects of the leak on the synthetic flows is clearly observed (once a leak occurs the leak outflow is distributed as several leaks in each discretization node).

The residuals with mean value closer to zero were $r_5(t)$ and $r_9(t)$ for the leaks 1 and 2 respectively. The leak positions were estimated through (5.9). Table 5.5 summarizes the estimated leak positions $\hat{z}_L$ and the estimation errors obtained for each one of two leaks considered. Notice that the estimation errors is calculated as $e = 100\left|\frac{z_L - \hat{z}_L}{L}\right|$.

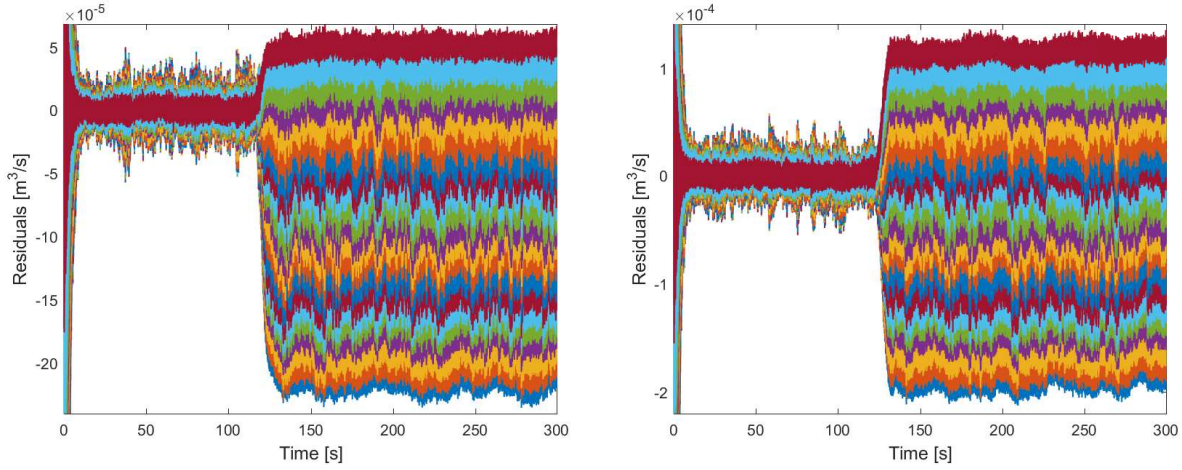

(a) Leak 1 (b) Leak 2

Fig. 5.10 Experimental Test - Residuals

Table 5.5 Experimental Test Single Leaks Diagnosis Results

z_L [m]	$\hat{z}_L$ [m]	Error [%]
12.87	13.13	0.45
25.3	23.63	2.89

5.5 Conclusions

In this chapter, we have presented a novel approach to identify single and sequential leaks. In order to avoid the necessity of using pressure measurements, a representation of the pipeline dynamics under the form of a flow rate Liénard-type model has been considered for the formulation of the proposed method. The approach has been validated through simulation results as well as experimental tests. Provided simulations and, even more importantly, experimental tests illustrated the good leak position estimation results obtained with the proposed methodology. The main drawback of our method is that a better precision in the leak position estimation requires an increasing of the model resolution (that is a reduction of the step used in the spatial discretization) which in turn means an increment of the order of the model (a greater number of equations). However with the current computational resources, this disadvantage can easily be overcome.

Chapter 6

Approach to Diagnose Leaks in Water Distribution Networks Using Only Flow Rate Measurements

6.1 Introduction

Because of population growth and the associated urbanization, to provide an adequate water supply is becoming increasingly challenging in many countries around the world. There is a worldwide significant trend in population migrating to cities. The United Nations annual report on urbanization [39], shows that in 2014 the 54% of the world's population lived in cities. In 1990, only 43% of the world lived in urban areas and it is expected to reach 66% by 2050. Taking as a guide goals 3 (halve the proportion of the population without sustainable access to safe drinking water and basic sanitation) and 7 (ensure environmental sustainability) of the United Nations Millennium Development [22], there has been a paradigm shift in the way water losses are managed. Now-days, on the supply side, water suppliers have the responsibility to manage water efficiently by reducing water losses from distribution system.

Despite the above the amount of wasted treated water is very high. The mean rates of unaccounted-for water are estimated about 40% in developing and underdeveloped countries (Africa, Asia, Latin America and the Caribbean) and about 15% in United States [176]. Actually, according to [84]: "Every year, more than 32×10^9 [m^3] of treated water physically leak(s) from urban water supply systems around the world, while 16×10^9 [m^3] are delivered to customers for zero revenue". These loss in distribution networks are basically due to: overflowing service

reservoirs, illegal connections and leaking pipes (valves and joints) [115]. Associated to the loss of treated water, there are collateral losses among which are energy required to treat the water and energy necessary to compensate the pressure drops due to leaks. Moreover, there are risks associated to leaks such as landslides, contaminant infiltration into water distribution systems, property damage, among others.

Taking into account the above-mentioned, in this chapter the method presented in Chapter 5 to diagnose leaks in pipelines by only using flow rate sensors is extended to water distribution networks. The proposed method is based on modeling the water distribution network by using the flow-based Liénard form presented in (2.38). Inlet and oulet flow rates of each pipe branch are used as boundary conditions in the implementation of the network model in Matlab®. The numerical solution of this model will provide for each space section its internal discrete flow. For pipe branches free of leaks their discrete flow rates will be equals along each branch i.e. for all space sections of the branch. In the case of a leak occurrence, the outflow of the leak will be distributed along the discrete spaces of the pipe branch affected by the leak. For each space section the residuals can be calculated by subtracting the discrete flow rates from the pipe branch flow rate without leaks (the nominal flow). The residual corresponding to the section where the leak is occurring will be that close to zero.

In the present chapter the behavior of a water distribution network was recreated with the commercial software PipelineStudio® from Energy Solutions. Single and sequential leak scenarios were considered. The paper is organized as follows. Section 6.2 presents the considered model. Section 6.3 describes the proposed diagnostic method. Section 6.4 presents some simulation test results and Section 6.5 presents the corresponding conclusions.

6.2 System Model

For modeling a pipeline network, each branch is modeled based on the flow-based form given in (2.38) and reproduced here in (6.1)

$$\begin{array}{ll} \dot{Q}_i^a(t) & = Q_i^b(t) - F\left(Q_i^a(t)\right), \quad i = 1,...,n_\ell \\ \dot{Q}_i{}^b(t) & = b^2\left[\frac{Q_{i-1}^a(t) - 2Q_i^a(t) + Q_{i+1}^a(t)}{(\Delta z_i)^2}\right] \end{array}, \tag{6.1}$$

where Δz_i is the spatial step, n_ℓ is the total number of internal discrete flows and $F(Q_i^a(t))$ is given in (2.43), that is

$$F\left(Q^a(z,t)\right) = \frac{Q^a(z,t)|Q^a(z,t)|\left(410(\frac{\varepsilon}{\phi}) + 111\left(\frac{\varepsilon}{\phi}\right)^{\frac{13}{50}}\right)}{2000A_r\phi} + \frac{43Q(z,t)|Q^a(z,t)|\left(\frac{\varepsilon}{\phi}\right)^{\frac{33}{100}}}{2A_r\phi^{(1+\kappa)}\left(\frac{Q}{A\upsilon}\right)^{\kappa}}, \quad (6.2)$$

with $\kappa = \frac{34\left(\frac{\varepsilon}{\phi}\right)^{\frac{14}{125}}}{25}$.

Therefore, by considering equations (6.1) for each pipe branch, a model could be developed for a pipeline network system by using the Kirchhoff's first laws. Kirchhoff's current law was originally introduced for the flow of electric charges in electrical networks. Kirchhoff's law state that the algebraic sum of flows in a network meeting at a point is zero, i.e. the sum of flows flowing into that node is equal to the sum of flows flowing out of that node. This law could be written as following equation:

$$\sum_{i=1}^{n_b} Q_i^a(t) = 0 \quad (6.3)$$

where n_b is the total number of branches with flows flowing towards or away from the node and the flow rate $Q_i^a(t)$ is positive for flows entering the node and is negative for flows leaving out from the node.

Thereby, one can rewrite (6.1) for a pipeline network as follows:

$$
\begin{aligned}
\dot{Q}_i^{a_1}(t) &= Q_i^{b_1}(t) - F\left(Q_i^{a_1}(t)\right), \quad i = 1,...,n_\ell^1 \\
\dot{Q}_i^{b_1}(t) &= b_1^2 \left[\frac{Q_{i-1}^{a_1}(t) - 2Q_i^{a_1}(t) + Q_{i+1}^{a_1}(t)}{\left(\Delta z_i^1\right)^2} \right] \\
\dot{Q}_i^{a_2}(t) &= Q_i^{b_2}(t) - F\left(Q_i^{a_2}(t)\right), \quad i = 1,...,n_\ell^2 \\
\dot{Q}_i^{b_2}(t) &= b_2^2 \left[\frac{Q_{i-1}^{a_2}(t) - 2Q_i^{a_2}(t) + Q_{i+1}^{a_2}(t)}{\left(\Delta z_i^2\right)^2} \right] \\
&\vdots \\
\dot{Q}_i^{a_p}(t) &= Q_i^{b_p}(t) - F\left(Q_i^{a_p}(t)\right), \quad i = 1,...,n_\ell^p \\
\dot{Q}_i^{b_p}(t) &= b_p^2 \left[\frac{Q_{i-1}^{a_p}(t) - 2Q_i^{a_p}(t) + Q_{i+1}^{a_p}(t)}{\left(\Delta z_i^p\right)^2} \right]
\end{aligned}
\tag{6.4}
$$

where the spatial step for the pipe branch p in the network can be computed as $\Delta z_i^p = L^p / N_\ell^p$ with $N_\ell^p = n_\ell^p + 1$ as the total number of space steps (sections). For example, if the total number of discrete flows is fixed as $n_\ell^p = 4$ for a pipeline branch with length $L^p = 500$ [m], then the total number of sections (space steps) is $N_\ell^p = 5$ and $\Delta z_i^p = 100$ [m]. Check Fig. 6.1 for a better conceptualization. Notice that $Q_i^{a_p}(t)$ is the internal discrete flow of section i.

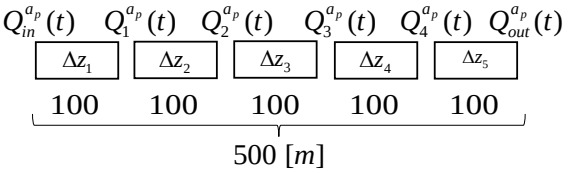

Fig. 6.1 Space Discretization Scheme for Pipe Branch p

6.3 Methodology

The strategy of the methodology here proposed is a reformulation of the approach presented Chapter 5 to use it in water distribution networks. For a better conceptualization Fig. 6.2 shows a flow diagram of the proposed methodology. The proposed approach relies on model (6.4), which is implemented in Matlab® and has as inputs the flow rates measured at the ends of

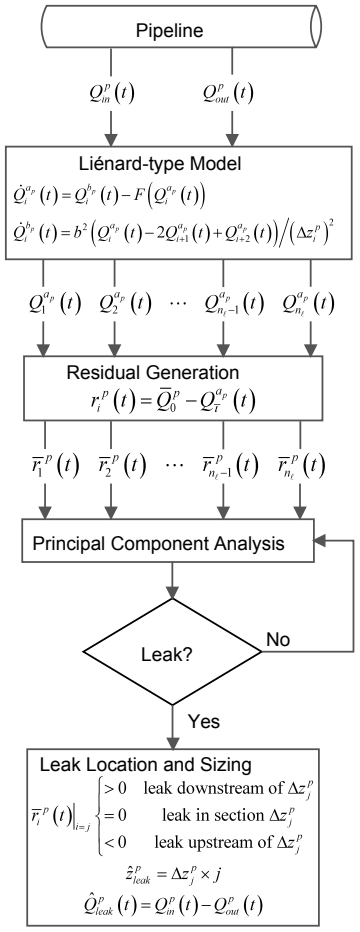

Fig. 6.2 Methodology Flow Diagram

the supervised pipeline branch, $Q_{in}^p(t)$ and $Q_{out}^p(t)$, which in fact, as mentioned before, are the boundary conditions required for the solution of model (6.4).

Since the unidimensional space is discretized into space steps (sections) of equal size, model (6.4) shall compute internal discrete flow rates corresponding to each section. If the pipeline branch is free of leaks, the discrete flow rates provided by the model will be equal, otherwise the leak outflow will be distributed along the discrete space of the pipeline branch.

If the internal discrete flows, calculated by the model after the leak, are subtracted from the mean nominal flow $\overline{Q}_0^p$ (the mean flow rate of the pipeline branch p without leaks), residuals corresponding to each section will be then obtained as follows:

$$r_i^p(t) = \overline{Q}_0^p - Q_{\bar{i}}^{a_p}(t), \forall i = 1,2,...,n_\ell^p, \ \ \forall \bar{i} = n_\ell^p, n_{\ell-1}^p, ..., 2, 1. \tag{6.5}$$

where i is the index to enumerate the residuals, $\bar{\imath}$ is the index for the countdown of the flows and n_ℓ^p is the total number of residuals that matches with the total number of discrete flow rates calculated by the Liénard-type model (6.4).

Depending on the behavior of the discrete flow rates calculated by the Liénard-type model, for a given section $i = j$, the mean value of the residuals $i = j$ will have the following behavior:

$$\bar{r}_i^p(t)|_{i=j} \begin{cases} > 0, & \text{if there is a leak downstream of } \Delta z_j^p; \\ = 0, & \text{if there is a leak in section } \Delta z_j^p; \\ < 0, & \text{if there is a leak upstream of } \Delta z_j^p. \end{cases}$$

Remark 1: Notice that last section has not assigned a residual since the flow in this section is the downstream boundary condition $Q_{out}^p(t)$ of model (6.4) and not an internal discrete flow computed by model (6.4).

Remark 2: As a consequence, if a leak is placed in the last section, all the residuals will be then positive.

Remark 3: If the position of the leak does not match with the limits of each section, then $\bar{r}_j^p \approx 0$.

Resuming the explanation of our methodology, the position of the single leak can be computed by using the following equation:

$$\hat{z}_{leak} = \Delta z_j^p \times j. \tag{6.6}$$

where j is the section number where the leak happens and Δz_j^p is the section size, which in fact is the same than the rest of sections ($\Delta z_j^p = \Delta z_i^p$). Thus, $\hat{z}_{leak} \to z_{leak}$ inasmuch $\Delta z_i^p \to 0$.

The magnitude of a single leak (the leak outflow) can be calculated by means of the mass balance

$$\hat{Q}_{leak}^p(t) = Q_{in}^p(t) - Q_{out}^p(t). \tag{6.7}$$

In case of sequential leaks, the leak outflow computed by (6.7) will increase with the addition of the outflow of each sequential leak. Each leak flow can be calculated by using the following equation:

$$\hat{Q}_{eq}^p(t) = \sum_{\kappa=1}^{M^p} \hat{Q}_{L_\kappa}^p(t), \tag{6.8}$$

where $\hat{Q}^p_{eq}$ is the *equivalent flow*, which is the total flow lost due to the leaks, $\hat{Q}^p_{L_\kappa}$ is the flow lost due to the κ-th sequential leak, which is located at the position $\hat{z}_{L^p_\kappa}$ and M^p is the total number of sequential leaks.

In case of sequential leaks, the residual close to zero will indicate the section involving the *equivalent position*. Hence, the leak position of the κ-th sequential leak can be obtained through the following equation:

$$\hat{z}^p_{eq} = \frac{\sum_{\kappa=1}^{M^p} \hat{Q}^p_{L_k}(t)\hat{z}^p_{L_\kappa}}{\hat{Q}^p_{eq}(t)}, \tag{6.9}$$

6.4 Simulation Tests: Leak Diagnostic

An important component of any water supply system is the distribution network which is a pipe network used to distribute the water to consumers (such as industrial or commercial establishments and private houses) and other usage points e.g. fire hydrants. In a distribution network the product, i.e. the water, is pressurized to guarantee that it reaches all branches of the network, that a sufficient flow is available at any take-off point and to guarantee that liquid containing contaminants cannot enter the network. In this section the simple distribution network shown in Figure 6.3 is considered. It consists of a source reservoir from which the

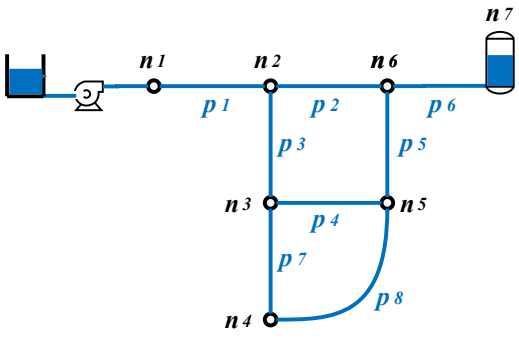

Fig. 6.3 Distribution Network

product is pumped into a two-loop pipe network. There is also a pipe leading to a storage tank. In the figure the identification labels for the various components are shown. Pipe properties are listed in Table 6.1.

Table 6.1 Network Pipe Characteristics

Pipe	Length [m]	Diameter [m]
1	914.4	0.3556
2	1524	0.3048
3	1524	0.2032
4	1524	0.2032
5	1524	0.2032
6	2133.6	0.254
7	1524	0.1524
8	2133.6	0.1524

Three scenarios regarding the application of the proposed method algorithms are presented. In the first one a single leaks scenario is considered, while in the second one a sequential leaks scenario is treated and in the third one a single leaks scenario, but with vainrying pressures head at the ends of the network, is considered. The pipeline network behavior was recreated with the commercial software PipelineStudio® from Energy Solutions, by considering as boundary conditions the upstream and downstream pressure heads $H_{n1}(t)$ and $H_{n7}(t)$ (see Figure 6.3). Thus, this simulator provides the boundary flow rates to be injected to the Liénard model (5.3), in order to compute the discrete flows for the residual generation. Table 6.2 provides the list of model parameters considered.

Table 6.2 Physical parameters

Symbol	Value	Units	Description
g	9.81	m/s^2	Gravitational acceleration
ε	1.083×10^{-3}	m	Mean height of roughness
ν	7.9822×10^{-7}	m^2/s	Kinematic viscosity

6.4.1 Single Leaks Scenario

In this section three independent single leak cases were induced in pipe branches 1, 4 and 6. Table 6.3 shows details of the leaks scenario recreated, i.e. pipe in which the leak takes place, leak position z_{leak}, leak activation and deactivation times t^{on} and t^{off}. The mean values of the boundary conditions considered were $H_{n1}(t) = 700\,[\text{m}]$ and $H_{n7}(t) = 300\,[\text{m}]$. The mean nominal flows obtained were about $\overline{Q}_{0_{p1}} = 0.6029\,[\text{m}^3/\text{s}]$, $\overline{Q}_{0_{p4}} = 0.1304\,[\text{m}^3/\text{s}]$ and $\overline{Q}_{0_{p6}} = 0.5145\,[\text{m}^3/\text{s}]$ for pipes branches 1, 4 and 6 respectively.

Table 6.3 Single Leaks Scenario

Pipe	z_{leak} [m]	t^{on} [s]	t^{off} [s]
1	300	200	400
4	762	600	800
6	533.4	1000	1200

On the other hand, the Liénard-type model (6.4) was programmed in Matlab® by fixing a space step (section size) $\Delta z_i^p = L^p/N_\ell^p = L^p/21\,[\text{m}]$, where L^p is the length of the particular pipe branch (see Table 6.1). Since $N_\ell = 21$, 20 internal flow are calculated (i.e. $n_\ell = 20$), thereby 20 residuals can be calculated ($r_1(t)$, $r_2(t)$, ..., $r_{20}(t)$).

Fig. 6.4a, Fig. 6.4b and Fig. 6.4c show the residuals calculated through (6.5) for the three leaks considered respectively. The effects of the leak on the synthetic flows is clearly observed (once a leak occurs the leak outflow is distributed as several leaks in each discretization node). Fig. 6.4d, Fig. 6.4e and Fig. 6.4f show the response of Hotelling's statistic and the results of leak position and leak flow rate estimations respectively.

The residuals with mean value closer to zero were $r_7^1(t)$, $r_{12}^4(t)$ and $r_6^6(t)$ for the leaks considered respectively. The leak positions were estimated through (5.9). Table 6.4 summarizes the estimated leak positions $\hat{z}_{leak}^p$ and the estimation errors obtained for each one of three leaks considered. Notice that the estimation errors is calculated as $e = 100\left|\frac{z_{leak}^p - \hat{z}_{leak}^p}{L^p}\right|$.

Table 6.4 Single Leaks Diagnosis Results

z_{leak}^p [m]	$\hat{z}_{leak}^p$ [m]	Error [%]
300	290.95	0.99
762	831.27	4.55
533.4	581.89	2.27

6.4.2 Sequential Leaks Scenario

In this section two sequential leak were induced in pipe branches 3 and 8. Table 6.5 shows details of the leaks scenario recreated, i.e. pipe in which the leak takes place, leak position z_{leak}, leak activation and deactivation times t^{on} and t^{off}. The mean values of the boundary conditions considered were $H_{n1}(t) = 700\,[\text{m}]$ and $H_{n7}(t) = 300\,[\text{m}]$. The mean nominal flows obtained were about $\overline{Q}_{0_{p3}} = 0.1982\,[\text{m}^3/\text{s}]$ and $\overline{Q}_{0_{p8}} = 0.0776\,[\text{m}^3/\text{s}]$ for pipes branches 3 and 8 respectively.

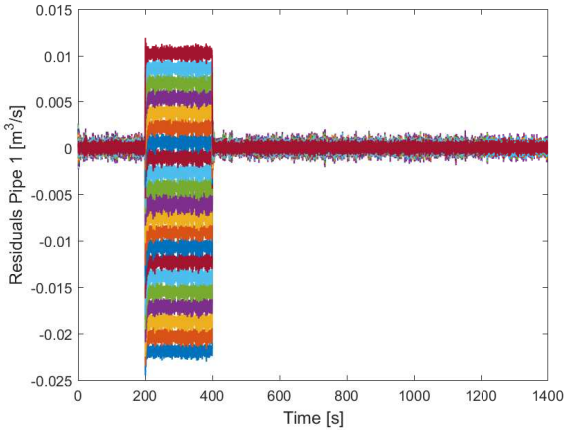

(a) Residuals for leak in pipe branch 1

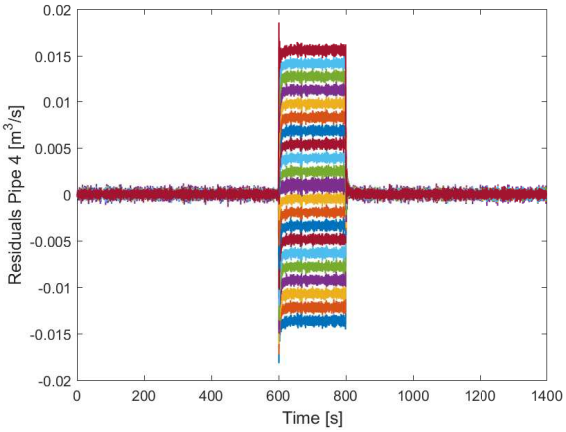

(b) Residuals for leak in pipe branch 4

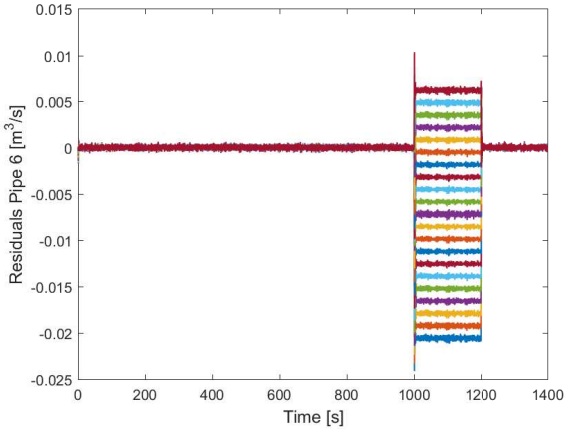

(c) Residuals for leak in pipe branch 6

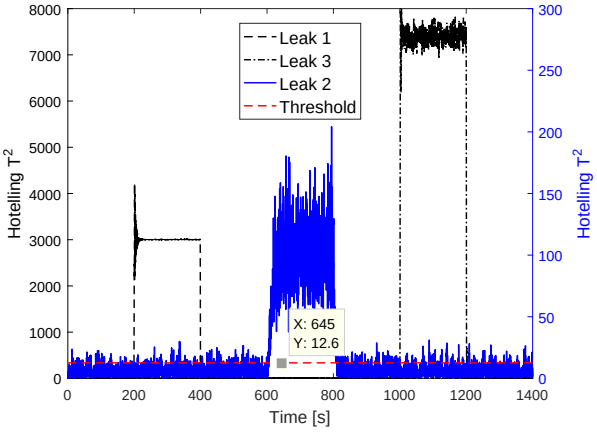

(d) Hotelling's T^2 statistic

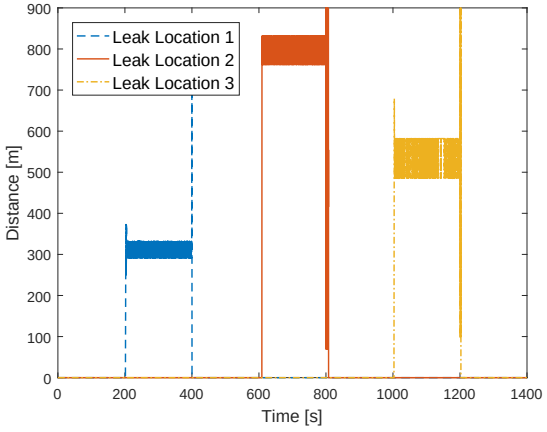

(e) Estimation of Leak Position

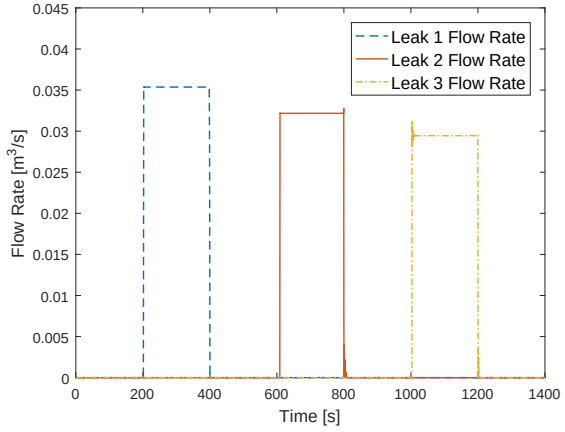

(f) Estimation of Leak Flow Rate

Fig. 6.4 Results for Simulation Test 1

Table 6.5 Sequential Leaks Scenario

Pipe	z_{leak} [m]	t^{on} [s]	t^{off} [s]
3	150	200	400
8	1600.2	300	500

As in the single leak case, the Liénard-type model (6.4) was programmed in Matlab® by fixing a space step (section size) $\Delta z_i^p = L^p/N_\ell^p = L^p/21$ [m], where L^p is the length of the particular pipe branch (see Table 6.1). Since $N_\ell = 21$, 20 internal flow are calculated (i.e. $n_\ell = 20$), thereby 20 residuals can be calculated ($r_1^p(t)$, $r_2^p(t)$, ..., $r_{20}^p(t)$). Fig. 6.5a and Fig. 6.5b show the residuals calculated through (6.5) for the two leaks considered respectively. Again the effects of the leak on the synthetic flows is clearly observed (once a leak occurs the leak outflow is distributed as several leaks in each discretization node). Fig. 6.5c, Fig. 6.5d and Fig. 6.5e show the response of Hotelling's statistic, the results of leak location and leak flow rate estimations respectively.

The residuals with mean value closer to zero were $r_2^3(t)$ and $r_{17}^8(t)$ for the leaks considered respectively. The leak positions were estimated through (6.6). Table 6.6 summarizes the estimated leak positions $\hat{z}_{leak}^p$ and the estimation errors obtained for each one of two leaks considered.Notice that the estimation errors is calculated as $e = 100\left|\frac{z_{leak}^p - \hat{z}_{leak}^p}{L^p}\right|$.

Table 6.6 Sequential Leaks Diagnosis Results

z_{leak}^p [m]	$\hat{z}_{leak}^p$ [m]	Error [%]
150	138.55	0.75
1600.2	1648.7	0.0023

6.4.3 Varying Pressures Heads

In contrast with the two previous scenarios in which constant boundary conditions were considered, in this case sine-like pressure signals were used as boundary conditions ($H_{n1}(t)$ and $H_{n7}(t)$) for the simulations in PipelineStudio®, see Figure 6.6a. Two independent single leak cases were induced in pipe branches 2 and 4. Table 6.7 shows details of the leaks scenario recreated, i.e. pipe in which the leak takes place, leak position z_{leak}, leak activation and deactivation times t^{on} and t^{off}. Figure 6.6b shows the flow rates provided by PipelineStudio® for the two leaks considered.

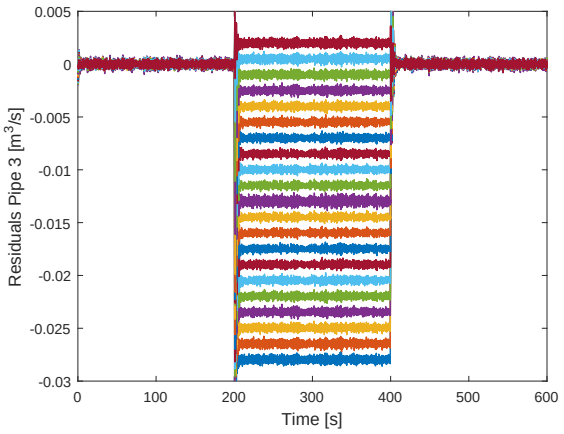

(a) Residuals for leak in pipe branch 3

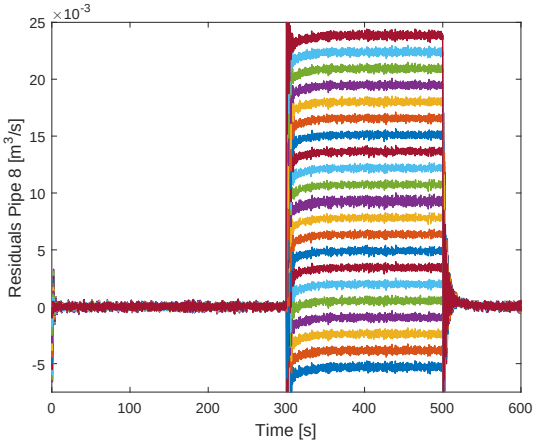

(b) Residuals for leak in pipe branch 5

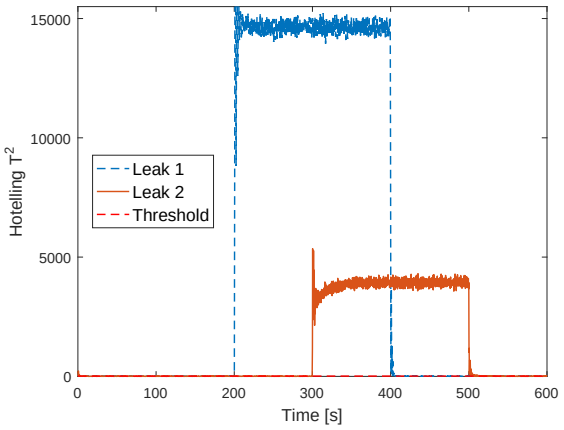

(c) Hotelling's T^2 statistic

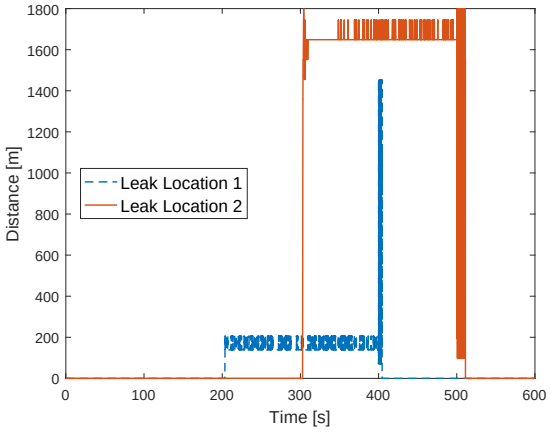

(d) Estimation of Leak Position

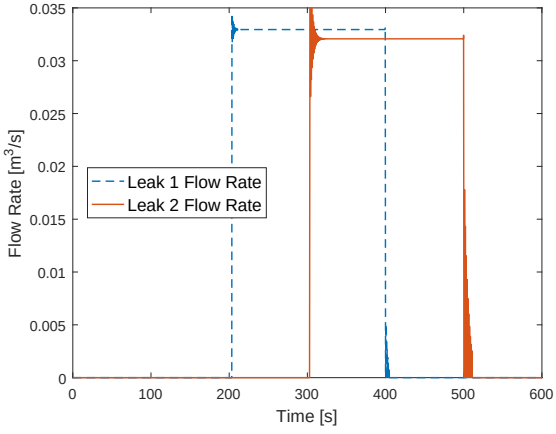

(e) Estimation of Leak Flow Rate

Fig. 6.5 Results for Simulation Test 2

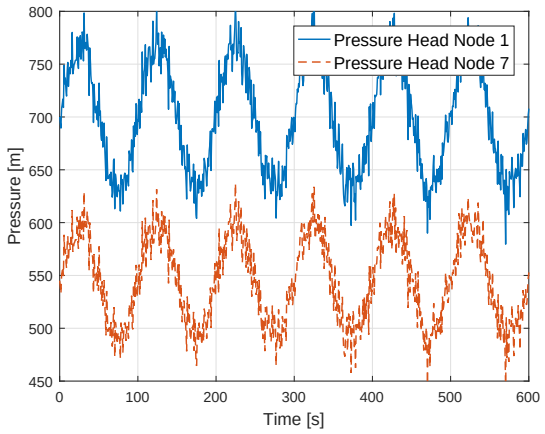

(a) Pressure Heads at the network ends

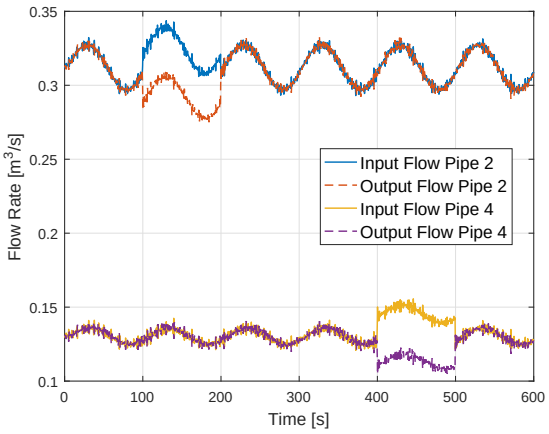

(b) Flow rates at pipes 2 and 4

Table 6.7 Varying Pressures Leaks Scenario

Pipe	z_{leak} [m]	t^{on} [s]	t^{off} [s]
2	950	100	200
4	762	400	500

The Liénard-type model (6.4) was programmed in Matlab® by fixing a space step (section size) $\Delta z_i^p = L^p/N_\ell^p = L^p/21$ [m], where L^p is the length of the particular pipe branch (see Table 6.1). Since $N_\ell = 21$, 20 internal flow are calculated (i.e. $n_\ell = 20$), thereby 20 residuals can be calculated ($r_1(t)$, $r_2(t)$, ..., $r_{20}(t)$). Fig. 6.7a and Fig. 6.7b show the residuals calculated through (6.5) for the two leaks considered respectively. The effects of the leak on the synthetic flows is clearly observed (once a leak occurs the leak outflow is distributed as several leaks in each discretization node).

The residuals with mean value closer to zero were $r_{14}^2(t)$ and $r_{12}^4(t)$ for the leaks considered respectively. The leak positions were estimated through (6.6). Table 6.8 summarizes the estimated leak positions $\hat{z}_{leak}^p$ and the estimation errors obtained for each one of three leaks considered. Notice that the estimation errors is calculated as $e = 100\left|\frac{z_{leak}^p - \hat{z}_{leak}^p}{L^p}\right|$.

Table 6.8 Varying Pressures Leaks Diagnosis Results

z_{leak}^p [m]	$\hat{z}_{leak}^p$ [m]	Error [%]
950	969.82	1.3
762	831.27	4.55

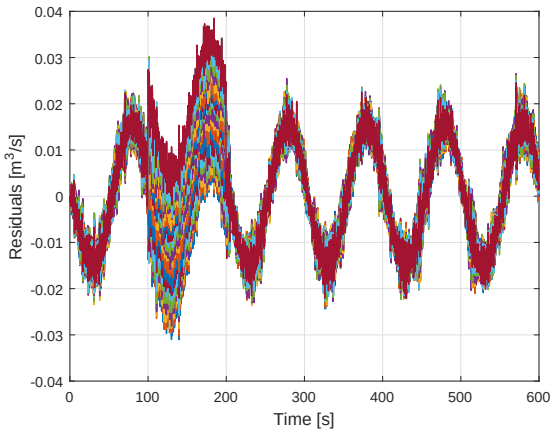

(a) Residuals for leak in pipe branch 1

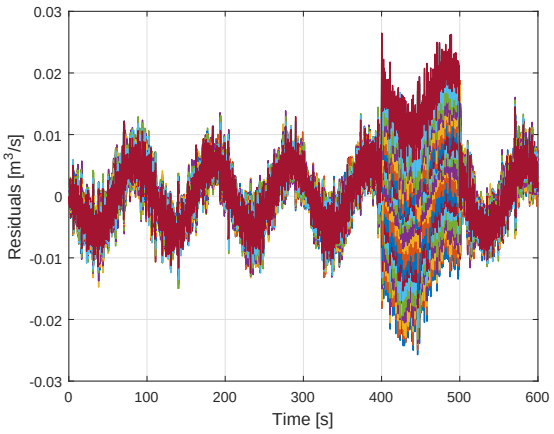

(b) Residuals for leak in pipe branch 4

6.5 Conclusions

In this chapter, we have presented a novel approach to diagnose single and sequential leaks in water distribution networks. In order to avoid the necessity of using pressure measurements, a representation of the pipeline dynamics under the form of a flow rate Liénard-type model has been considered for the formulation of the proposed method. The commercial software PipelineStudio® from Energy Solutions was used to reproduce the behavior of a distribution network, and data provided by this software were used to support the validation of the proposed approach. Provided simulations illustrated the good leak position estimation results obtained with the proposed methodology.

Chapter 7

Conclusions and Future Works

7.1 Summary

The formulation of reliable method for leak diagnosis in pipelines is an important problem to be solved in order to prevent catastrophic failures and wasting valuable resources. The scope for this thesis was the design of a liquid pipeline monitoring system that incorporates state estimators for both iteratively identifying physical parameters as well as early detection and tracing of leaks. The main contributions of this work are as follows:

- **Input Optimization Algorithms:** Optimization algorithms for calculating *regularly persistent inputs* for state affine systems that can be used to sensitize appropriate signals for parameter identification issue were presented. Two representations of pipeline dynamics under the form of Liénard-like systems and by considering of a varying friction factor were used in formulating identification problems as observers. Such observers were used to estimate pipeline parameters as wave speed and equivalent length. The approach both for input constraints and parameters' estimation was validated through simulation results as well as experimental tests.

- **Pipeline Leaks Diagnosis Algorithm:** A novel approach to detect and locate single and sequential leaks was presented. To avoid the necessity of using pressure measurements, a representation of the pipeline dynamics under the form of a flow rate Liénard-type model was used in the formulation of the proposed method. The approach was validated through simulation results as well as experimental tests. Provided simulations and, even more importantly, experimental tests illustrated the good leak position estimation results obtained with the proposed methodology. The main disadvantage of the proposed method

is that a better precision in the leak position estimation requires an increasing of the model resolution (that is a reduction of the step used in the spatial discretization) which in turn means an increment of the order of the model (a greater number of equations). However with the current computational resources, this disadvantage can easily be overcome.

- **Leaks Diagnosis Algorithm for Water Distribution Network:** The pipeline leak detection algorithm presented before is extended to water distribution networks. The commercial software PipelineStudio® from Energy Solutions was used to reproduce the behavior of a distribution network, and data provided by this software were used to support the validation of the proposed approach. Provided simulations illustrated the good leak position estimation results obtained with the proposed methodology.

7.2 Future Works

Future works derived from this research could address the following issues:

- The input optimization algorithms proposed in this study generate a variable amplitude pulse train signal. Since a sinusoidal signal have less energy that a square signal with the same amplitude and frequency, it would be interesting to generate an optimal sinusoidal like signal and to compare its performance with the once developed here.

- The pipeline leaks diagnosis algorithm proposed here was implemented on-line only for the single leak scenario, basically because the conventional PCA algorithm only allows the detection of the violation of a preset threshold and during sequential leaks various variations (over the threshold) of the statistics T^2 take place. Since, after the first leak, the threshold has already been exceeded, subsequent leakages are not detected automatically. It is suggested to work on the conditioning of the PCA algorithm such that an on-line multi-leak diagnose will be possible.

- Fixed pressures at the pipeline ends is an indispensable requirements for the operation of the proposed leaks diagnosis method. Although this can be guaranteed through a pressure control system, it would be better to overcome this limitation.

- This study only considered pipelines carrying liquids. To adapt the proposed algorithms to gas pipeline networks is strongly suggested.

References

[1] Aamo, O. M. (2016). Leak detection, size estimation and localization in pipe flows. *IEEE Transactions on Automatic Control*, 61(1):246–251.

[2] Ahmed-Ali, T., Van Assche, V., Massieu, J., and Dorleans, P. (2013). Continuous-discrete observer for state affine systems with sampled and delayed measurements. *IEEE Transactions on Automatic Control*, 58(4):1085–1091.

[3] Ali, J. M., Hoang, N. H., Hussain, M. A., and Dochain, D. (2015). Review and classification of recent observers applied in chemical process systems. *Computers & Chemical Engineering*, 76:27–41.

[4] API (1995). 1155: Evaluation methodology for software based leak detection systems.

[5] API, R. (2007). 1130: Computational pipeline monitoring for liquids.

[6] Apriliani, E., Nurhadi, H., et al. (2017). Ensemble and fuzzy kalman filter for position estimation of an autonomous underwater vehicle based on dynamical system of auv motion. *Expert Systems with Applications*, 68:29–35.

[7] Begovich, O., Navarro, A., Sanchez, E. N., and Besançon, G. (2007). Comparison of two detection algorithms for pipeline leaks. In *Control Applications, 2007. CCA 2007. IEEE International Conference on*, pages 777–782. IEEE.

[8] Begovich, O. and Valdovinos-Villalobos, G. (2010). Dsp application of a water-leak detection and isolation algorithm. In *Electrical Engineering Computing Science and Automatic Control (CCE), 2010 7th International Conference on*, pages 93–98. IEEE.

[9] Bejarano, F. J., Fridman, L., and Poznyak, A. (2007). Output integral sliding mode control based on algebraic hierarchical observer. *International Journal of Control*, 80(3):443–453.

[10] Belsito, S., Lombardi, P., Andreussi, P., and Banerjee, S. (1998). Leak detection in liquefied gas pipelines by artificial neural networks. *AIChE Journal*, 44(12):2675–2688.

[11] Benson, T. (2014). Oil spill one of the worst environmental events in Israel's history, official says.

[12] Besançon, G. (1999). Further results on high gain observers for nonlinear systems. In *Proceedings of the 38th IEEE Conference on Decision and Control*, pages 2904–2909, Phoenix, AZ, USA.

[13] Besançon, G. and Ţiclea, A. (2007). An immersion-based observer design for rank-observable nonlinear systems. *IEEE Transactions on Automatic Control*, 52(1):83–88.

[14] Besançon, G., Voda, A., and Jouffroy, G. (2010). A note on state and parameter estimation in a Van der Pol oscillator. *Automatica*, 46(10):1735–1738.

[15] Besançon, G. (2007). *Nonlinear observers and applications*, volume 363. Springer.

[16] Besançon, G., Bornard, G., and Hammouri, H. (1996). Observer synthesis for a class of nonlinear control systems. *European Journal of control*, 2(3):176–192.

[17] Besançon, G., de León-Morales, J., and Huerta-Guevara, O. (2006). On adaptive observers for state affine systems. *International journal of Control*, 79(06):581–591.

[18] Besançon, G., Guillén, M., Dulhoste, J.-F., Santos, R., and Georges, D. (2012). Finite-difference modeling improvement for fault detection in pipelines. *IFAC Proceedings Volumes*, 45(20):928–933.

[19] Bird, R. B. (2002). Transport phenomena. *Applied Mechanics Reviews*, 55(1):R1–R4.

[20] Brkić, D. (2011). Review of explicit approximations to the colebrook relation for flow friction. *Journal of Petroleum Science and Engineering*, 77(1):34–48.

[21] Brunone, B. and Ferrante, M. (2001). Detecting leaks in pressurised pipes by means of transients. *J. Hydraul. Res.*, 39(5):539–547.

[22] Campbell, D. A. (2017). An update on the united nations millennium development goals. *Journal of Obstetric, Gynecologic & Neonatal Nursing*, 46(3):e48–e55.

[23] Campbell, S. L. and Nikoukhah, R. (2015). *Auxiliary signal design for failure detection*. Princeton University Press.

[24] Campuzano-Cervantes, J., Meléndez-Pertuz, F., Núñez-Perez, B., and Simancas-García, J. (2017). Sistema de monitoreo electrónico de desplazamiento de tubos de extensión para junta expansiva. *Revista Iberoamericana de Automática e Informática Industrial {RIAI}*, 14(3):268 – 278.

[25] Cartwright, J. H., Eguíluz, V. M., Hernández-García, E., and Piro, O. (1999). Dynamics of elastic excitable media. *International Journal of Bifurcation and Chaos*, 9(11):2197–2202.

[26] Carvajal-Rubio, J., Begovich, O., and Sánchez-Torres, J. D. (2015). Real-time leak detection and isolation in plastic pipelines with equivalent control based observers. In *Electrical Engineering, Computing Science and Automatic Control (CCE), 2015 12th International Conference on*, pages 1–6. IEEE.

[27] Chaudhry, M. H. (1979). Applied hydraulic transients. Technical report, Springer.

[28] Chen, N. H. (1979). An explicit equation for friction factor in pipe. *Industrial & Engineering Chemistry Fundamentals*, 18(3):296–297.

[29] Chen, W. and Saif, M. (2006). Unknown input observer design for a class of nonlinear systems: an lmi approach. In *American Control Conference, 2006*, pages 5–pp. IEEE.

[30] Chen, W.-s., Bakshi, B. R., Goel, P. K., and Ungarala, S. (2004). Bayesian estimation via sequential monte carlo sampling: unconstrained nonlinear dynamic systems. *Industrial & engineering chemistry research*, 43(14):4012–4025.

[31] Choi, D. Y., Kim, S.-W., Choi, M.-A., and Geem, Z. W. (2016). Adaptive kalman filter based on adjustable sampling interval in burst detection for water distribution system. *Water*, 8(4):142.

[32] Churchill, S. W. (1973). Empirical expressions for the shear stress in turbulent flow in commercial pipe. *AIChE Journal*, 19(2):375–376.

[33] Colombo, A. F., Lee, P., and Karney, B. W. (2009). A selective literature review of transient-based leak detection methods. *Journal of Hydro-environment Research*, 2:212–227.

[34] Darouach, M., Zasadzinski, M., and Hayar, M. (1996). Reduced-order observer design for descriptor systems with unknown inputs. *IEEE transactions on automatic control*, 41(7):1068–1072.

[35] Davila, J., Fridman, L., and Levant, A. (2005). Second-order sliding-mode observer for mechanical systems. *IEEE transactions on automatic control*, 50(11):1785–1789.

[36] Delgado-Aguinaga, J., Begovich, O., and Besançon, G. (2016a). Exact-differentiation-based leak detection and isolation in a plastic pipeline under temperature variations. *Journal of Process Control*, 42:114–124.

[37] Delgado-Aguinaga, J., Begovich, O., and Besançon, G. (2016b). Varying-parameter modeling and extended kalman filtering for reliable leak diagnosis under temperature variations. In *System Theory, Control and Computing (ICSTCC), 2016 20th International Conference on*, pages 632–637. IEEE.

[38] Delgado-Aguiñaga, J., Besançon, G., Begovich, O., and Carvajal, J. (2016). Multi-leak diagnosis in pipelines based on extended kalman filter. *Control Engineering Practice*, 49:139–148.

[39] DESA, U. N. (2014). World urbanization prospects: the 2014 revision, highlights. *United Nations, Department of Economic and Social Affairs, Population Division (2014)*.

[40] Dochain, D. (2000). State observers for tubular reactors with unknown kinetics. *Journal of process control*, 10(2-3):259–268.

[41] Dochain, D., Couenne, F., and Jallut, C. (2009). Enthalpy based modelling and design of asymptotic observers for chemical reactors. *International Journal of Control*, 82(8):1389–1403.

[42] Dorf, R. C. and Bishop, R. H. (2011). *Modern control systems*. Pearson.

[43] DOT, U. (49). Cfr part 195, transportation of hazardous liquids by pipeline. 2004. *Washington, DC: US Dept. of Transportation*.

[44] Dulhoste, J.-F., Besançon, G., Torres, L., Begovich, O., and Navarro, A. (2011). About friction modeling for observer-based leak estimation in pipelines. In *Decision and Control and European Control Conference (CDC-ECC), 2011 50th IEEE Conference on*, pages 4413–4418. IEEE.

[45] Eleiwi, F. and Laleg-Kirati, T. M. (2017). Observer-based perturbation extremum seeking control with input constraints for direct-contact membrane distillation process. *International Journal of Control*, (just-accepted):1–21.

[46] Engel, C. (2011). Approval procedures and technical rules for pipelines in germany. In *4th Pipeline Technology Conference 2009*. EITEP Institute.

[47] Espinoza-Moreno, G., Begovich, O., and Sanchez-Torres, J. (2014). Real time leak detection and isolation in pipelines: A comparison between sliding mode observer and algebraic steady state method. In *World Automation Congress (WAC), 2014*, pages 748–753. IEEE.

[48] Eze, J., Nwagboso, C., and Georgakis, P. (2017). Framework for integrated oil pipeline monitoring and incident mitigation systems. *Robotics and Computer-Integrated Manufacturing*, 47:44–52.

[49] Factbook, C. I. A. (2010). The world factbook. *https://www.cia.gov/library/publications/the-world-factbook/fields/2117.html*.

[50] Ferrante, M. and Brunone, B. (2003). Pipe system diagnosis and leak detection by usteady-state test-1: Harmonic analysis. *Advanced Water Resousrces*, 26(1):95–105.

[51] FritzHugh, R. (1961). Impulses and physiological states in theoretical models of nerve membranes. *Biophysical Journal*, 1(6):445–466.

[52] Fuchs, H. and Riehle, R. (1991). Ten years of experience with leak detection by acoustic signal analysis. *Applied acoustics*, 33(1):1–19.

[53] Gao, Y., Brennan, M. J., Liu, Y., Almeida, F. C., and Joseph, P. F. (2017). Improving the shape of the cross-correlation function for leak detection in a plastic water distribution pipe using acoustic signals. *Applied Acoustics*, 127:24–33.

[54] Gauthier, J. P., Hammouri, H., and Othman, S. (1992). A simple observer for nonlinear systems applications to bioreactors. *IEEE Transactions on automatic control*, 37(6):875–880.

[55] Gebrekidan, S. (2013). Corrosion may have led to North Dakota pipeline leak, regulators say.

[56] Geiger, G., Werner, T., Matko, D., et al. (2003). Leak detection and locating-a survey. In *PSIG Annual Meeting*. Pipeline Simulation Interest Group.

[57] Genić, S., Aranđelović, I., Kolendić, P., Jarić, M., Budimir, N., and Genić, V. (2011). A review of explicit approximations of colebrook's equation. *FME transactions*, 39(2):67–71.

[58] Goffaux, G., Wouwer, A. V., and Bernard, O. (2009). Improving continuous–discrete interval observers with application to microalgae-based bioprocesses. *Journal of Process Control*, 19(7):1182–1190.

[59] Gonzalez, J., Fernandez, G., Aguilar, R., Barron, M., and Alvarez-Ramirez, J. (2001). Sliding mode observer-based control for a class of bioreactors. *Chemical Engineering Journal*, 83(1):25–32.

[60] Gopalakrishnan, A. and Biegler, L. T. (2013). Economic Nonlinear Model Predictive Control for periodic optimal operation of gas pipeline networks. *Computers and Chemical Engineering*, 52:90–99.

[61] Graef, J. R. (1972). On the generalized liénard equation with negative damping. *Journal of Differential Equations*, 12(1):34–62.

[62] Guercio, R. and Xu, Z. X. Z. (1995). The automatic control of flow in pipeline system. *Proceedings IEEE Conference on Industrial Automation and Control Emerging Technology Applications*, pages 87–94.

[63] Haaland, S. E. (1983). Simple and explicit formulas for the friction factor in turbulent pipe flow. *Journal of Fluids Engineering*, 105(1):89–90.

[64] Hauge, E., Aamo, O., and Godhavn, J. (2009). Model-based monitoring and leak detection in oil and gas pipelines. *SPE Projects Facilities and Construction*, 4(3):53–60.

[65] Hermann, R. and Krener, A. (1977). Nonlinear controllability and observability. *IEEE Transactions on automatic control*, 22(5):728–740.

[66] Herrán, a., de la Cruz, J. M., and de Andrés, B. (2012). Global Search Metaheuristics for planning transportation of multiple petroleum products in a multi-pipeline system. *Computers and Chemical Engineering*, 37:248–261.

[67] Heydari, A., Narimani, E., and Pakniya, F. (2015). Explicit determinations of the colebrook equation for the flow friction factor by statistical analysis. *Chemical Engineering & Technology*, 38(8):1387–1396.

[68] Hord, J. (1967). *Correlations for predicting leakage through closed valves*, volume 355. US National Bureau of Standards: for sale by the Supt. of Docs., US Govt. Print. Off.

[69] Hoshiya, M. and Saito, E. (1984). Structural identification by extended kalman filter. *Journal of Engineering Mechanics*, 110(12):1757–1770.

[70] Hotelling, H. (1947). Multivariate quality control illustrated by the air testing of sample bomb sights, techniques of statistical analysis, ch. ii.

[71] Huang, S.-C., Lin, W.-W., Tsai, M.-T., and Chen, M.-H. (2007). Fiber optic in-line distributed sensor for detection and localization of the pipeline leaks. *Sensors and Actuators A: Physical*, 135(2):570–579.

[72] Hulhoven, X., Wouwer, A. V., and Bogaerts, P. (2006). Hybrid extended luenberger-asymptotic observer for bioprocess state estimation. *Chemical engineering science*, 61(21):7151–7160.

[73] Isermann, R. (1982). Process fault detection based on modeling and estimation methods. *IFAC Proceedings Volumes*, 15(4):7–30.

[74] Isermann, R. and Münchhof, M. (2010). *Identification of Dynamic Systems: An Introduction with Applications*. Springer.

[75] Jackson, J. E. and Mudholkar, G. S. (1979). Control procedures for residuals associated with principal component analysis. *Technometrics*, 21(3):341–349.

[76] Jain, A. K. (1976). Accurate explicit equation for friction factor. *Journal of the Hydraulics Division*, 102(5):674–677.

[77] Jana, A. K. (2010). A nonlinear exponential observer for a batch distillation. In *Control Automation Robotics & Vision (ICARCV), 2010 11th International Conference on*, pages 1393–1396. IEEE.

[78] Jauberthie, C., Bournonville, F., Coton, P., and Rendell, F. (2006). Optimal input design for aircraft parameter estimation. *Aerospace science and technology*, 10(4):331–337.

[79] Jiang, B. and Braatz, R. D. (2017). Fault detection of process correlation structure using canonical variate analysis-based correlation features. *Journal of Process Control*, 58:131–138.

[80] Jiménez, J., Torres, L., Rubio, I., and Sanjuan, M. (2017). Auxiliary signal design and liénard-type models for identifying pipeline parameters. In *Modeling and Monitoring of Pipelines and Networks*, pages 99–124. Springer.

[81] Kalaba, R. and Spingarn, K. (1977). Optimal input system identification for nonlinear dynamic systems. *Journal of Optimization Theory and Applications*, 21(1):91–102.

[82] Kalman, R. E. et al. (1960). A new approach to linear filtering and prediction problems. *Journal of basic Engineering*, 82(1):35–45.

[83] Kasai, N., Tsuchiya, C., Fukuda, T., Sekine, K., Sano, T., and Takehana, T. (2011). Propane gas leak detection by infrared absorption using carbon infrared emitter and infrared camera. *NDT & E International*, 44(1):57–60.

[84] Kingdom, B., Liemberger, R., and Marin, P. (2006). The challenge of reducing non-revenue water (nrw) in developing countries.

[85] Kou, S. R., Elliott, D. L., and Tarn, T. J. (1975). Exponential observers for nonlinear dynamic systems. *Information and control*, 29(3):204–216.

[86] Kowalczuk, Z. and Gunawickrama, K. (2004). Detecting and locating leaks in transmission pipelines. In *Fault Diagnosis*, pages 821–864. Springer.

[87] Kurmer, J. P., Kingsley, S. A., Laudo, J. S., and Krak, S. J. (1992). Distributed fiber optic acoustic sensor for leak detection. In *Distributed and Multiplexed Fiber Optic Sensors*, pages 117–128. International Society for Optics and Photonics.

[88] Levadi, V. (1966). Design of input signals for parameter estimation. *IEEE Transactions on Automatic Control*, 11(2):205–211.

[89] Li, H., Shi, P., and Yao, D. (2017). Adaptive sliding-mode control of markov jump nonlinear systems with actuator faults. *IEEE Transactions on Automatic Control*, 62(4):1933–1939.

[90] Lina, W., Jian, W., Xianwen, G., and Mingshun, W. (2013). Summary of detection and location for oil and gas pipeline leak. In *Control and Decision Conference (CCDC), 2013 25th Chinese*, pages 821–826. IEEE.

[91] Lion, J. C. P. (1995). Leak Detection: A Transient Flow Simulation Approach. In *Pipeline Engineering AME Petroleum Division Publication PD V60, 1994 Proceedings of the Energy Source Technology Conference*.

[92] Liou, J. C. P. (1996). Leak detection by mass balance effective for Norman wells line. *Oil and gas journal*, 94(17).

[93] Litman, S. and Huggins, W. (1963). Growing exponentials as a probing signal for system identification. *Proceedings of the IEEE*, 51(6):917–923.

[94] Liu, M., Shi, P., Zhang, L., and Zhao, X. (2011). Fault-tolerant control for nonlinear markovian jump systems via proportional and derivative sliding mode observer technique. *IEEE Transactions on Circuits and Systems I: Regular Papers*, 58(11):2755–2764.

[95] Liu, Z., Su, L., and Ji, Z. (2017). Neural network observer-based leader-following consensus of heterogenous nonlinear uncertain systems. *International Journal of Machine Learning and Cybernetics*, pages 1–9.

[96] Lu, L. (2010). Optimal inputs and sensitivities for parameter estimation in bioreactors. *Journal of mathematical chemistry*, 47(3):1154–1176.

[97] Luenberger, D. (1966). Observers for multivariable systems. *IEEE Transactions on Automatic Control*, 11(2):190–197.

[98] Luenberger, D. (1971). An introduction to observers. *IEEE Transactions on automatic control*, 16(6):596–602.

[99] Luo, Y. and Chen, Y. (2012). Fractional order disturbance observer. *Fractional Order Motion Controls*, pages 223–236.

[100] Luo, Y., Zhang, T., Lee, B., Kang, C., and Chen, Y. (2013). Disturbance observer design with bode's ideal cut-off filter in hard-disc-drive servo system. *Mechatronics*, 23(7):856–862.

[101] Lurie, M. V. and Sinaiski, E. (2008). *Modeling of oil product and gas pipeline transportation*. Wiley Online Library.

[102] Manadili, G. et al. (1997). Replace implicit equations with signomial functions. *Chemical Engineering*, 104(8):129–129.

[103] Mashford, J., De Silva, D., Marney, D., and Burn, S. (2009). An approach to leak detection in pipe networks using analysis of monitored pressure values by support vector machine. In *Network and System Security, 2009. NSS'09. Third International Conference on*, pages 534–539. IEEE.

[104] Massari, C., Yeh, T.-C. J., Brunone, B., Ferrante, M., and Meniconi, S. (2013a). Diagnosis of pipe systems by means of a stochastic successive linear estimator. *Water resources management*, 27(13):4637–4654.

[105] Massari, C., Yeh, T.-C. J., Ferrante, M., Brunone, B., and Meniconi, S. (2013b). Diagnosis of pipe systems by the sle: first results. *Water Science and Technology: Water Supply*, 13(4):958–965.

[106] Massari, C., Yeh, T. C. J., Ferrante, M., Brunone, B., and Meniconi, S. (2014). Detection and sizing of extended partial blockages in pipelines by means of a stochastic successive linear estimator. *Journal of Hydroinformatics*, 16(2):248–258.

[107] Maykuth, A. (2014). 2,550 barrels of crude recovered from oil spill.

[108] Mazenc, F. and Bernard, O. (2011). Interval observers for linear time-invariant systems with disturbances. *Automatica*, 47(1):140–147.

[109] McIntosh, J. (2016). Pipeline leak fouls creek near grizzly bear protection area in northwestern Alberta.

[110] Mehra, R. (1974a). Optimal input signals for parameter estimation in dynamic systems–survey and new results. *IEEE Transactions on Automatic Control*, 19(6):753–768.

[111] Mehra, R. (1974b). Optimal inputs for linear system identification. *IEEE Transactions on Automatic Control*, 19(3):192–200.

[112] Miller, R. K., Pollock, A. A., Finkel, P., Watts, D. J., Carlyle, J. M., Tafuri, A. N., and Yezzi, J. J. (1999). The development of acoustic emission for leak detection and location in liquid-filled, buried pipelines. In *Acoustic Emission: Standards and Technology Update*. ASTM International.

[113] Mizuochi, S. (1977). Fluid-leak detector cable.

[114] Moody, L. F. (1947). An approximate formula for pipe friction factors. *Trans. ASME*, 69(12):1005–1011.

[115] Multikanga, H. E., Sharma, S., and Vairavamoorthy, K. (2009). Water loss management in developing countries: Challenges and prospects. *American Water Works Association. Journal*, 101(12):57.

[116] Muntakim, A. H., Dhar, A. S., and Dey, R. (2017). Interpretation of acoustic field data for leak detection in ductile iron and copper water-distribution pipes. *Journal of Pipeline Systems Engineering and Practice*, 8(3):05017001.

[117] Nagumo, J., Arimoto, S., and Yoshizawa, S. (1962). An active pulse transmission line simulating nerve axon. *Proceedings of the IRE*, 50(10):2061–2070.

[118] Navarro, A., Begovich, O., Besançon, G., and Dulhoste, J. (2011). Real-time leak isolation based on state estimation in a plastic pipeline. In *Control Applications (CCA), 2011 IEEE International Conference on*, pages 953–957. IEEE.

[119] Navarro, A., Begovich, O., Sánchez, J., and Besançon, G. (2017). Real-time leak isolation based on state estimation with fitting loss coefficient calibration in a plastic pipeline. *Asian Journal of Control*, 19(1):255–265.

[120] Navarro, A., Begovich, O., Sanchez-Torres, J. D., Besançon, G., and Murillo, J. A. P. (2012). Leak detection and isolation using an observer based on robust sliding mode differentiators. In *World Automation Congress (WAC), 2012*, pages 1–6. IEEE.

[121] Nazarov, M. and Gorodyankin, G. (2016). Oil spills into Black Sea near Russian port after pipeline leak.

[122] Negrete, M. A. and Verde, C. (2012). Multi-leak reconstruction in pipelines by sliding mode observers. *IFAC Proceedings Volumes*, 45(20):934–939.

[123] Newman, N. (2015). New integrity solutions facing many same old problems. *Pipeline & Gas Journal*, 242(10).

[124] Niklès, M., Vogel, B. H., Briffod, F., Grosswig, S., Sauser, F., Luebbecke, S., Bals, A., and Pfeiffer, T. (2004). Leakage detection using fiber optics distributed temperature monitoring. In *Smart Structures and Materials*, pages 18–25. International Society for Optics and Photonics.

[125] Nise, N. S. (2007). *CONTROL SYSTEMS ENGINEERING, (With CD)*. John Wiley & Sons.

[126] Okeya, I., Kapelan, Z., Hutton, C., and Naga, D. (2014). Online burst detection in a water distribution system using the kalman filter and hydraulic modelling. *Procedia Engineering*, 89:418–427.

[127] Patwardhan, S. C., Manuja, S., Narasimhan, S., and Shah, S. L. (2006). From data to diagnosis and control using generalized orthonormal basis filters. part ii: Model predictive and fault tolerant control. *Journal of Process Control*, 16(2):157–175.

[128] Pham, V., Georges, D., and Besançon, G. (2014). Predictive control with guaranteed stability for water hammer equations. *IEEE Trans Automatic Control*, 59(2):465–70.

[129] Pipeline101 (2016). What-do-pipelines-transport? http://www.pipeline101.com/why-do-we-need-pipelines/what-do-pipelines-transport. Accessed: 2017-10-28.

[130] Pizano-Moreno, A. and Begovich, O. (2010). Isolation of two non-concurrent leaks in water pipelines. In *Electrical Engineering Computing Science and Automatic Control (CCE), 2010 7th International Conference on*, pages 164–169. IEEE.

[131] Pizano-Moreno, A. and Begovich, O. (2012). Leak isolation with temperature compensation in pipelines. In *Electrical Engineering, Computing Science and Automatic Control (CCE), 2012 9th International Conference on*, pages 1–5. IEEE.

[132] Portnoy, I., Melendez, K., Pinzon, H., and Sanjuan, M. (2016). An improved weighted recursive pca algorithm for adaptive fault detection. *Control Engineering Practice*, 50:69–83.

[133] Rafajłowicz, E. (1989). Time-domain optimization of input signals for distributed-parameter systems identification. *Journal of optimization theory and applications*, 60(1):67–79.

[134] Rao, C. V., Rawlings, J. B., and Lee, J. H. (2001). Constrained linear state estimation—a moving horizon approach. *Automatica*, 37(10):1619–1628.

[135] Raymond, D. M. (2017). Twisted leak detection cable. US Patent 9,755,389.

[136] Reddy, S. R. (1993). System and method for detecting leaks in a vapor handling system.

[137] Reddy III, W. J. (1992). Capacitance measuring circuit and method for liquid leak detection by measuring charging time.

[138] Romeo, E., Royo, C., and Monzón, A. (2002). Improved explicit equations for estimation of the friction factor in rough and smooth pipes. *Chemical engineering journal*, 86(3):369–374.

[139] Round, G. (1980). An explicit approximation for the friction factor-reynolds number relation for rough and smooth pipes. *The Canadian Journal of Chemical Engineering*, 58(1):122–123.

[140] Salmatanis, N., Van Reet, J., Dutta-Roy, K., Shaw, D., et al. (2015). The api 1149 update, model-based leak detection uncertainty assessment. In *PSIG Annual Meeting*. Pipeline Simulation Interest Group.

[141] Sandberg, C., Holmes, J., McCoy, K., and Koppitsch, H. (1989). The application of a continuous leak detection system to pipelines and associated equipment. *IEEE Transactions on Industry applications*, 25(5):906–909.

[142] Scola, I. R., Besançon, G., and Georges, D. (2013). Input optimization for observability of state affine systems. *Proc. 5th IFAC Symposium on System Structure and Control*, 46(2):737–742.

[143] Shafer, M. F. (1984). Flight investigation of various control inputs intended for parameter estimation.

[144] Sheets, C. (2016). EPA says it is 'not known' how long Alabama pipeline leaked gas prior to discovery of break. *Al.com*.

[145] Sinha, N. K. and Kuszta, B. (1983). *Modelling and identification of dynamic systems*. Springer.

[146] Souza, A., Cruz, S., and Pereira, J. (2000). Leak detection in pipelines through spectral analysis of pressure signals. *Brazilian Journal of Chemical Engineering*, 17(4-7):557–564.

[147] Spirin, V. V., Shlyagin, M. G., Miridonov, S. V., Jimenez, F. J. M., and Gutierrez, R. M. L. (1999). Fiber Bragg grating sensor for petroleum hydrocarbon leak detection. *Optics and Lasers in Engineering*, 32(5):497–503.

[148] Staff (2016). Alberta pipeline spilled about 250K litres of oil and water: Trilogy. Technical report.

[149] Standard, C. (2003). Oil and gas pipeline systems: Z662-03. *Canadian Standard Association, Etobicoke, Canada*.

[150] Sun, L. and Chang, N. (2014). Integrated-signal-based leak location method for liquid pipelines. *Journal of Loss Prevention in the Process Industries*, 32:311–318.

[151] Swamee, P. K. (1993). Design of a submarine oil pipeline. *Journal of transportation Engineering*, 119(1):159–170.

[152] Swamee, P. K. and Jain, A. K. (1976). Explicit equations for pipe-flow problems. *Journal of the Hydraulics*, 102(5):657–664.

[153] Swarz, R. S. (2017). The trans-alaska pipeline system: A systems engineering case study. In *Complex Systems Design & Management*, pages 17–27. Springer.

[154] Ţiclea, A. and Besançon, G. (2009). State and parameter estimation via discrete-time exponential forgetting factor observer. *IFAC Proceedings Volumes*, 42(10):1370–1374.

[155] Torres, L., Aguiñaga, J. A. D., Besançon, G., Verde, C., and Begovich, O. (2016). Equivalent Liénard-type models for a fluid transmission line. *Comptes Rendus Mécanique*, 344(8):582–595.

[156] Torres, L., Astorga, C. M., Targui, B., and Quintero-Marmol, E. (2004). On-line monitoring and modelling of multivariable nonlinear systems : methanol/ethanol distillation. In *2nd IFAC Symposium on System, Structure and Control*, Oaxaca, Mexico.

[157] Torres, L., Besançon, G., and Georges, D. (2008). A collocation model for water-hammer dynamics with application to leak detection. In *Proceedings of the 47th IEEE Conference on Decision and Control*, Cancun, Mexico.

[158] Torres, L., Besançon, G., and Georges, D. (2009a). Collocation modeling with experimental validation for pipeline dynamics and application to transient data estimations. In *European Control Conference*, Budapest, Hungary.

[159] Torres, L., Besançon, G., and Georges, D. (2009b). Multi-leak estimator for pipelines based on an orthogonal collocation model. In *Proceedings of the 48th IEEE Conference on Decision and Control*, Shanghai, China.

[160] Torres, L., Besançon, G., Navarro, A., Begovich, O., and Georges, D. (2011a). Examples of pipeline monitoring with nonlinear observers and real-data validation. In *8th International Multi-Conference on Systems, Signals and Devices, Sousse, Tunisia*.

[161] Torres, L., Besançon, G., and Verde, C. (2015). Liénard type model of fluid flow in pipelines: Application to estimation. In *12th International Conference on Electrical Engineering, Computing Science and Automatic Control*, pages 148–153, Mexico City, Mexico. IEEE.

[162] Torres, L., Besançon, G., Navarro, A., Begovich, O., Georges, D., et al. (2011b). Examples of pipeline monitoring with nonlinear observers and real-data validation. In *8th IEEE International Multi-Conf on Signals Systems and Devices, Sousse, Tunisia*.

[163] Torres, L., Verde, C., Besançon, G., and Gonzalez, O. (2014). High-gain observers for leak location in subterranean pipelines of liquefied petroleum gas. *International Journal of Robust and Nonlinear Control*, 24(6):1127–1141.

[164] Tsal, R. (1989). Altshul-tsal friction factor equation. *Heating, Piping and Air Conditioning*, 8:30–45.

[165] Tubb, R. (2017). P&gj's 2017 worldwide pipeline construction report. *Pipeline & Gas Journal*.

[166] U.S. Department of Transportation (2016). Pipeline and Hazardous Materials Safety Administration: Serious Pipeline Incidents Report.

[167] Van Der Pol, B. and Van Der Mark, J. (1928). Lxxii. the heartbeat considered as a relaxation oscillation, and an electrical model of the heart. *The London, Edinburgh, and Dublin Philosophical Magazine and Journal of Science*, 6(38):763–775.

[168] Van Loan, C. (1977). Computing integrals involving the matrix exponential. Technical report, Cornell University.

[169] Vanaei, H., Eslami, A., and Egbewande, A. (2017). A review on pipeline corrosion, in-line inspection (ili), and corrosion growth rate models. *International Journal of Pressure Vessels and Piping*, 149:43–54.

[170] Vargas-Guzmán, J. and Yeh, T.-C. J. (2002). The successive linear estimator: a revisit. *Advances in Water Resources*, 25(7):773–781.

[171] Verde, C. (2001). Multi-leak detection and isolation in fluid pipelines. *Control Engineering Practice*, 9(6):673–682.

[172] Verde, C., Molina, L., and Torres, L. (2014). Parameterized transient model of a pipeline for multiple leaks location. *Journal of Loss Prevention in the Process Industries*, 29:177–185.

[173] Verde, C., Morales-Menendez, R., Garza, L., Vargas, A., Velasquez-Roug, P., Rea, C., Aparicio, C., and De la Fuente, J. (2008). Multi-leak diagnosis in pipelines a comparison of approaches. In *Artificial Intelligence, 2008. MICAI'08. Seventh Mexican International Conference on*, pages 352–357. IEEE.

[174] Verde, C., Torres, L., and González, O. (2016). Decentralized scheme for leaks' location in a branched pipeline. *Journal of Loss Prevention in the Process Industries*, 43:18–28.

[175] Verde, C., Visairo, N., and Gentil, S. (2007). Two leaks isolation in a pipeline by transient response. *Adv. Water Resour.*, 30(8):1711–1721.

[176] (WHO, W. H. O., UNICEF, et al. (2000). Global water supply and sanitation assessment 2000 report. Technical report, World Health Organization (WHO).

[177] Wiener, N. (1949). *Extrapolation, interpolation, and smoothing of stationary time series*, volume 7. MIT press Cambridge, MA.

[178] Wood, D. J. (1966). An explicit friction factor relationship. *Civil Eng*, 36(12):60–61.

[179] Xia, Q., Rao, M., Ying, Y., and Shen, X. (1994). Adaptive fading kalman filter with an application. *Automatica*, 30(8):1333–1338.

[180] Xiong, Y. and Saif, M. (2001). Sliding mode observer for nonlinear uncertain systems. *IEEE transactions on automatic control*, 46(12):2012–2017.

[181] Xu, S., Ma, Q., Yang, X.-F., and Wang, S.-D. (2017). Design and fabrication of a flexible woven smart fabric based highly sensitive sensor for conductive liquid leakage detection. *RSC Advances*, 7(65):41117–41126.

[182] Yang, J., Wen, Y., and Li, P. (2008). Leak location using blind system identification in water distribution pipelines. *Journal of Sound and Vibration*, 310(1):134–148.

[183] Yunus, A. C. and Cimbala, J. M. (2006a). Fluid mechanics fundamentals and applications. *International Edition, McGraw Hill Publication*, 185201.

[184] Yunus, A. C. and Cimbala, J. M. (2006b). Fluid mechanics fundamentals and applications. *McGraw-Hill Publication*.

[185] Zecchin, A. C., White, L. B., Lambert, M. F., and Simpson, A. R. (2013). Parameter identification of fluid line networks by frequency-domain maximum likelihood estimation. *Mechanical Systems and Signal Processing*, 37(1):370–387.

[186] Zeghdoudi, H., Bouchahed, L., and Dridi, R. (2013). A complete classification of lienard equation. *European Journal of Pure and Applied Mathematics*, 6(2):126–136.

[187] Zeitz, M. (1987). The extended luenberger observer for nonlinear systems. *Systems & Control Letters*, 9(2):149–156.

[188] Zhang, T., Tan, Y., Zhang, X., and Zhao, J. (2015). A novel hybrid technique for leak detection and location in straight pipelines. *Journal of Loss Prevention in the Process Industries*, 35:157–168.

[189] Zigrang, D. and Sylvester, N. (1982). Explicit approximations to the solution of colebrook's friction factor equation. *AIChE Journal*, 28(3):514–515.

[190] Zlotnik, A., Chertkov, M., and Backhaus, S. (2015). Optimal control of transient flow in natural gas networks. In *54th IEEE Conference on Decision and Control, Osaka, Japan*.

[191] Zwick, W. R. and Velicer, W. F. (1986). Comparison of five rules for determining the number of components to retain. *Psychological bulletin*, 99(3):432.